ABSTRACT

DONG, YUHAN. MIMO Beamforming with Mutual Coupling, Limited Feedback and Coordination. (Under the direction of Dr. Brian L. Hughes).

Multi-input, multi-output (MIMO) techniques use multiple antennas at both the transmitter and receiver to improve the performance of wireless communications systems over multipath fading channels. In recent years, MIMO techniques that employ transmit beamforming have been adopted in several new and emerging standards for situations where channel state knowledge is available at the transmitter. Most existing studies of MIMO beamforming assume that perfect channel knowledge is available at both the transmitter and receiver, and that the antenna elements in both the transmit and receive arrays are spaced sufficiently far apart so as to be essentially uncoupled. In practice, however, constraints on the physical size of antenna arrays may require elements to be spaced close together, leading to antenna coupling and signal correlation. The capacity of the feedback link from the receiver to the transmitter may also be limited, so that channel knowledge is necessarily imperfect at the transmitter. These challenges become all the more difficult in multiuser scenarios, when efficient coordination among several transmitters is required.

In this dissertation, we consider the analysis and design of MIMO beamforming techniques with antenna mutual coupling, limited feedback and multiuser coordination. We begin by introducing a circuit model of a compact wireless MIMO transceiver that incorporates the effects of antenna mutual coupling. We then use this model to derive new MIMO beamforming strategies appropriate for both single-user and multiuser systems. Through numerical examples, we illustrate the performance

of the proposed beamforming techniques and their dependence on the properties of the antenna arrays, matching networks, channel estimation errors, and channel state feedback. Finally, we propose new asymmetric-rate coordinated beamforming strategies which improve both the individual rates of each user and the sum-rate subject to zero-interference constraints. These asymmetric-rate strategies can also be combined using time-division to create new, higher-rate symmetric beamforming strategies.

MIMO Beamforming with Mutual Coupling, Limited Feedback and Coordination

by
Yuhan Dong

A dissertation submitted to the Graduate Faculty of
North Carolina State University
in partial fullfillment of the
requirements for the Degree of
Doctor of Philosophy

Electrical Engineering

Raleigh, North Carolina

2009

APPROVED BY:

Dr. Mihail L. Sichitiu	Dr. Kazufumi Ito
Dr. Brian L. Hughes Chair of Advisory Committee	Dr. J. Keith Townsend

DEDICATION

To my dearest parents and fiancee

BIOGRAPHY

Yuhan Dong received his Bachelor of Science degree in July 2002 and Master of Science degree in July 2005, both in Electronic Engineering from Tsinghua University. In August 2005, he started work towards the Ph.D. in Electrical Engineering at North Carolina State University under the supervision of Dr. Brian L. Hughes. His research focuses on the design and analysis of MIMO wireless communication systems in the presence of mutual coupling.

ACKNOWLEDGMENTS

First and foremost, I would like to express my deepest gratitude to my advisor, Dr. Brian L. Hughes, for his guidance and continuous support throughout my PhD study. I have benefited tremendously from his wisdom, vision, technical insight, illuminating instruction, professionalism and assiduous work. He will be a truly inspiring role model for my future career.

I am grateful to the professors serving in my PhD committee: Dr. J. Keith Townsend, Dr. Mihail L. Sichitiu and Dr. Kazufumi Ito for their valuable comments and feedback. I would like to extend my sincere thanks to Dr. Gianluca Lazzi, who served as my former committee member, and is co-author of some of my papers. My gratitude is also given to Dr. Huaiyu Dai who provided useful knowledge in the general area of wireless communications in the courses he taught.

I am thankful to all colleagues from Wireless Systems Engineering (WiSE) lab for making a friendly and fruitful research environment. Carlo Domizioli and Pawandeep Singh have always been great partners for enlightening discussions. I would like to thank all my friends, here at Raleigh and elsewhere, for making my life enjoyable.

Finally, I dedicate this thesis to my parents and my fiancee and I would like to express my deepest appreciation to my entire family for their love and encouragement.

TABLE OF CONTENTS

LIST OF TABLES

LIST OF FIGURES

Chapter 1

Introduction

1.1 Motivation

Over the past few decades, the need for reliable, high data-rate, wireless communications has dramatically increased due to the growing demand for broadband mobile access to the Internet. In recent years, a wide variety of transmission schemes have been proposed that use multiple antennas at the transmitter and receiver to improve the performance of wireless systems. These schemes are collectively known as multiple-input multiple-output (MIMO) techniques.

The concept of MIMO can be traced back more than 20 years. In 1987, Winters [95] showed that multiple antennas with well designed transmit/receive processing could transmit more independent data streams through wireless multipath fading channels than a corresponding single-antenna system. Telatar [87] and Foschini and Gans [34] independently showed that the ergodic capacity of a MIMO channel scales with array size in proportion to the minimum of the number of transmit and receive

antennas. These pioneering works predicted that MIMO techniques can achieve large spectral efficiencies, which ignited much interest in this area [40]. Over the past decade, MIMO communication techniques have been adopted in new standards for wireless local area networks (IEEE 802.11n [47]), metropolitan area networks (e.g. IEEE 802.16e [48] and 802.16m[1]), and cellular telephony (W-CDMA [44], HSPA [45] and LTE[2] [1]).

When channel knowledge is available at both the transmitter and receiver, beamforming techniques are a relatively simple and effective way to exploit the diversity benefits of the MIMO channel. These techniques seek to transmit data along the dominant eigenmodes of the MIMO channel. Single-user MIMO beamforming was first considered by Lo [62]. Later, Tse *et al.* [90] and Dighe *et al.* [24] optimized MIMO beamformer design by using maximum-ratio transmission (MRT) and maximum-ratio combining (MRC). Kang and Alouini [55] evaluated the outage probability and ergodic capacity of this optimal MIMO beamforming scheme. MIMO beamforming has also been considered for multiuser scenarios to improve the capacity and reliability. Some specific MIMO beamforming techniques that use transmit/receive coordination to eliminate multiuser interference and improve the sum-rate are presented in [33], [97] and [14].

The ability of MIMO beamforming to adapt to changing fading conditions make it a promising technique to mitigate fading and enhance the performance over

[1]IEEE 802.11n and IEEE 802.16e modify the physical (PHY) and medium access control (MAC) layers of Wi-Fi (IEEE 802.11) and WiMAX (IEEE 802.16), respectively, to provide higher throughput using OFDM and MIMO technologies. IEEE 802.16m is the latest version of 802.16e and still in progress.

[2]W-CDMA defines the air interface for UMTS which, together with WiMAX, are the members of 3G mobile telecommunication technologies. HSPA extends and improves the existing W-CDMA protocols and LTE is a set of enhancements to UMTS and represents one of the 4G standards.

slowly-varying channels. For this reason, MIMO beamforming has been adopted as an optional advanced transmission strategy in the wireless cellular standards mentioned earlier. Most existing studies of MIMO beamforming, however, assume that perfect channel knowledge is available at both the transmitter and receiver, and that the antenna elements in both the transmit and receive arrays are spaced sufficiently far apart so as to be essentially uncoupled. In practice, however, constraints on the physical size of antenna arrays may require elements to be spaced close together, leading to antenna coupling and signal correlation. The capacity of the feedback link from the receiver to the transmitter may also be limited, so that channel knowledge is necessarily imperfect at the transmitter. These challenges become all the more difficult in multiuser scenarios, when efficient coordination among several transmitters is required.

In this dissertation, we consider the analysis and design of MIMO beamforming techniques with antenna mutual coupling, limited feedback and multiuser coordination. We begin by introducing a circuit model of a compact wireless MIMO transceiver that incorporates the effects of antenna mutual coupling. We then use this model to derive new MIMO beamforming strategies appropriate for both single-user and multiuser systems. Through numerical examples, we illustrate the performance of the proposed beamforming techniques and their dependence on the properties of the antenna arrays, matching networks, channel estimation errors, and channel state feedback. Finally, we propose new asymmetric-rate coordinated beamforming strategies which improve both the individual rates of each user and the sum-rate subject to zero-interference constraints. These asymmetric-rate strategies can also be combined using time-division to create new, higher-rate symmetric beamforming strategies.

1.1.1 Mutual Coupling in Compact Antenna Arrays

An antenna is a transducer designed to convert electromagnetic waves into electrical currents and vice versa. However, when antenna elements are placed in close proximity, a current in one antenna will induce voltages across its neighbors [22]. This phenomenon is called *mutual coupling*.

Many compact wireless transceivers, such as cellular telephones and wireless LAN cards, are severely constrained in physical size. When MIMO antennas are brought close together, the electric fields detected by different elements become correlated, the radiation patterns of each element may become distorted, mutual coupling occurs between the antennas, and power may radiated or captured less efficiently. It is therefore important to determine how close the elements of an array may be placed and still enjoy the benefits of MIMO beamforming.

When the receive antennas are coupled due to the small inter-element spacing, the noise from each receive chain may no longer be spatially white [71], [25]. Moreover, the statistics of the signal and noise will depend in general on detailed aspects of the receiver design. To optimize performance in such scenarios, it is necessary to develop realistic models of RF front-ends with coupled antenna arrays as well as new MIMO beamforming techniques that exploit these models to improve the performance.

1.1.2 Channel State Information

In wireless communications, the radio signal may travel to the receiving antennas by multiple paths. These paths may combine constructively at some times and destructively at other times, resulting in signal attenuation and distortion. This

phenomenon is called *multipath fading*. When fading is frequency-nonselective, the impact of fading on the transmitted signal in a single-antenna system can be represented by the *fading path gain,* a complex number that reflects the change in amplitude and phase of the received signal due to fading. In a MIMO channel, fading conditions may be different between each pair of transmit and receive elements, so the current *channel state* is represented by a matrix $\mathbf{H}$ which consists of the fading path gains between each pair of transmit and receive elements.

In a MIMO beamforming system, channel state information (CSI) allows the transmitter and receiver to communicate data along the dominant eigenmode of the MIMO channel, thereby mitigating the damaging effects of fading and maximizing the output signal-to-noise ratio (SNR) of the channel. By the dominant eigenmode, we mean the singular vector of the channel state matrix $\mathbf{H}$ that corresponds to the largest singular value, based on the singular-value decomposition (SVD).

The receiver can acquire CSI by MIMO channel estimation. One approach to performing MIMO channel estimation at the receiver is to employ known pilot symbols (also referred to as training sequences) to estimate the channel state matrix $\mathbf{H}$ from the received signal [8], [106]. In some two-way channels, transmitter CSI can easily be obtained from the reciprocity of the channel. In other systems, such as frequency-division duplexing (FDD), the transmitter and receiver do not employ reciprocal channels and thus CSI must be conveyed to the transmitter via a feedback link. In a practical system, however, errors may arise in the channel estimates, due to the time or frequency separation between the pilot and the signal [35]. These imperfect channel estimates can significantly degrade the performance of MIMO beamforming systems [89].

Perfect CSI at the transmitter can also be difficult to achieve when the capacity of the feedback link is low. One approach to performing MIMO beamforming in the presence of this impairment is to employ limited feedback (also known as finite-rate feedback) techniques [65], [98], [14]. Limited feedback techniques can significantly reduce the required capacity of the feedback link by transmitting only quantized or compressed versions of the CSI or beamforming vectors. This area of research has been very active recently due to its relevance to implementing MIMO beamforming techniques in practical settings, such as WiMAX and LTE.

1.1.3 Coordination and Interference Mitigation

For single-user MIMO (SU-MIMO) scenarios, such as point-to-point communication links, MIMO beamforming can improve system reliability and maximize the output SNR over fading multipath channels. In the literature, optimal SU-MIMO beamforming is also known as MIMO maximal ratio combining (MRC) [55], [103]. In multiuser MIMO (MU-MIMO) scenarios, such as the MIMO broadcast channel (BC),[3] MIMO beamforming techniques can also can be used to increase the number of users supported by the system, or to increase overall throughput.

When CSI is available at the transmitter, it is well known that the sum-capacity of the MIMO BC can be achieved by dirty-paper coding (DPC). However, DPC is difficult to implement in practice due to its high complexity [11], [94]. A simpler suboptimal method of sharing the MIMO broadcast channel is linear MIMO

[3]In a MU-MIMO broadcast system, the base station communicates with multiple mobile users, which is also known as downlink communication. MU-MIMO multiple access systems use multiple access channel (MAC) and correspond to the uplink scenario, which is beyond the scope of this dissertation.

beamforming [20], [77]. In linear MIMO beamforming, the data symbols intended for each mobile receiver are modulated onto distinct beamforming vectors at the transmitter. The mobiles then separate these symbols by applying distinct linear combiners at the receiver. Since the design of these beamforming vectors and combiners generally requires coordination among the users, this type of linear beamforming is also called *coordinated beamforming (CBF)* [14]. Most existing studies of CBF have considered the case of symmetric rates and uncoupled antennas. It is natural to ask how these techniques generalize to the asymmetric rate situations, and how the performance of these techniques is affected by the presence of antenna mutual coupling.

1.2 Contributions

As noted earlier, this dissertation considers the analysis and design of MIMO beamforming techniques with antenna mutual coupling, limited feedback and multiuser coordination. The main contributions may be summarized as follows.

Single-User MIMO MRC with Mutual Coupling: First, we consider the impact of fading correlation, mutual coupling, matching networks and channel estimation on single-user MIMO MRC systems. We start by introducing a circuit model with transmitter coupling, correlation and matching networks. We then consider three possible measures of input power used in the literature. For each input power metric, we present optimal transmission strategies as well as the outage formulas for different matching networks. Numerical examples show the range of inter-element spacing at which the antenna array can be closely placed and preserve the benefits of SU-MIMO MRC. The performance degradation in the presence of channel estimation error and

the impact of SNR and the length of pilot symbols is also addressed.

We then assume perfect channel estimation at the receiver and consider the design of finite-rate codebooks of possible beamforming vectors for three input power metrics. The receiver, who has full CSI, can then select the vector in the codebook that maximizes the output SNR and communicate the index of this vector to the transmitter via the feedback channel. The performance of limited feedback and its dependence on matching, coupling and number of feedback bits is evaluated through numerical examples. We also analyze the performance degradation for actual system when codebooks are mismatched.

Coordinated Beamforming with Mutual Coupling: Second, we consider the impact of receiver correlation, antenna coupling, matching and noise on the performance of downlink MU-MIMO coordinated beamforming systems. We first present a new coordinated beamforming technique for two receivers that is suitable for MIMO broadcast channels with signal and noise correlation at the receiver. We then apply this technique to the specific type of signal and noise correlation that occurs in the presence of receiver mutual coupling by introducing a more realistic model for a multi-antenna receiver front-end. Numerical examples demonstrate how different noise sources and matching networks may impact performance in different ways. We also consider the design and performance of limited feedback techniques for coordinated beamforming systems and how performance is affected by receiver coupling, correlation, matching networks and noise.

New Coordinated Beamforming Techniques: Third, we consider the design of new coordinated beamforming methods for MIMO broadcast channels which seek to improve the overall sum-rate performance. We first consider the design of symmet-

ric methods for coordinated beamforming for two receivers and the MIMO broadcast channel. By changing the design order of the transmit beamforming vectors and receive combining vectors, we develop a new *symmetric coordinated beamforming (SCBF)* scheme that is linear and non-iterative. We then relax the symmetry restriction and propose a new *asymmetric coordinated beamforming (ACBF)* method. In this method, the first user employs single-user MIMO MRC, while the second user attempts to maximize his rate of transmission subject to zero-interference constraints.

Finally, we consider the maximization of sum-rate over all these coordinated beamforming strategies. We propose a *parameterized asymmetric coordinated beamforming (P-ACBF)* method that achieves a better tradeoff between the rates of the two users than existing methods. Numerical examples illustrate the advantage of introducing time-division policy into ACBF and P-ACBF, respectively, by changing the priorities of two users. A simple upper bound of the sum-rate is derived to facilitate the comparison of performance.

1.3 Outline

This dissertation is organized as follows. Chapter 2 gives an overview of existing SU-MIMO and MU-MIMO BC beamforming methods, with and without limited feedback. Chapter 3 presents optimal transmission strategies for SU-MIMO MRC systems with antenna mutual coupling at the transmitter. Chapter 4 considers the design and performance of limited feedback techniques for SU-MIMO MRC systems with transmitter mutual coupling and quantifies the performance loss due to channel estimation error. Chapter 5 analyzes CBF design for MU-MIMO broadcast systems

with correlated fading and noise, and Chapter 6 proposes asymmetric CBF structures and analyzes the maximization of sum-rate using appropriate parameter and time-division policy. Finally, conclusions and future work are presented in Chapter 7.

Chapter 2

MIMO Beamforming over Rayleigh Fading Channels

In wireless communications, signals are transmitted through radio propagation channel which determines crucially the characteristics of the entire MIMO system [75]. There are a variety of different approaches used for modeling the MIMO wireless channel to capture the realistic properties or facilitate spatial-temporal signal processing.

In this chapter, we begin our study by introducing a stochastic MIMO fading channel model used for point-to-point wireless communications and discussing the optimal design for beamforming. The main purpose of this chapter is to demonstrate the impact of fading and its correlation on the system design and performance. We then extend this MIMO channel model to a broadcast setting where the base station communicates with multiple mobile terminals simultaneously. In the next section, we present a most recent non-iterative coordinated beamforming scheme subject to the

zero-interference constraints.

Both the MIMO beamforming strategies, i.e. SU-MIMO MRC and downlink MU-MIMO CBF, are close-loop technique and require channel state information at transmitter. In some one-way communication systems, CSI can be feed back from the receiver to the transmitter via feedback link, i.e. control channel, which is practically constrained in capacity. The effective approaches to implement limited feedback are addressed in the last section of this chapter.

2.1 MIMO Channel Model

In this section, we present a MIMO channel model to understand the nature of MIMO radio channels. Consider a system employed N antennas at the transmitter and M antennas at the receiver, denoted as $N \times M$ MIMO system and shown in Figure 2.1. In a rich scattering environment with a delay spread that is small compared to the inverse signal bandwidth[1], a linear time-variant MIMO channel may be represented as an $M \times N$ matrix [5]

$$\mathbf{H}(t) = \begin{bmatrix} h_{11}(t) & h_{12}(t) & \cdots & h_{1N}(t) \\ h_{21}(t) & h_{22}(t) & \cdots & h_{2N}(t) \\ \vdots & \vdots & \ddots & \vdots \\ h_{M1}(t) & h_{M2}(t) & \cdots & h_{MN}(t) \end{bmatrix}, \tag{2.1}$$

where $h_{mn}(t)$ denotes the time-variant impulse response between the m-th receive antenna and n-th transmit antenna pair due to multipath phenomenon, which is also known as fading path gain for *single-input single-output (SISO)* channel. At a time

[1]The fading is frequency-flat over the signal bandwidth, which represents a *narrowband* system.

instant, we denote each individual fading path gain and channel matrix as h_{mn} and $\mathbf{H}$, respectively. Therefore, the discrete-time input-output relation over a symbol period can be expressed in a matrix form as

$$\mathbf{r} = \mathbf{H}\mathbf{x} + \mathbf{n} \ , \tag{2.2}$$

where $\mathbf{x}$ is the complex baseband transmitted signal vector, $\mathbf{r}$ is the received signal vector, and $\mathbf{n}$ represents additive Gaussian noise with zero-mean and covariance $\mathbf{R}_{\mathrm{n}} = \mathsf{E}\left[\mathbf{n}\mathbf{n}^H\right]$, here $\mathsf{E}[\cdot]$ is the expectation. We denoted the noise distribution by $\mathbf{n} \sim \mathcal{CN}(\mathbf{0}, \mathbf{R}_{\mathrm{n}})$. A reasonable model for the noise is additive white Gaussian noise (AWGN) and therefore the covariance matrix is $\mathbf{R}_{\mathrm{n}} = N_0\mathbf{I}$ where $\frac{N_0}{2}$ is the power spectral density of the noise in single branch and $\mathbf{I}$ is the identity matrix. The total transmit power is $P = \mathrm{tr}\left(\mathsf{E}\left[\mathbf{x}\mathbf{x}^H\right]\right)$ where $\mathrm{tr}(\cdot)$ is the trace and superscript H denotes conjugate-transpose.

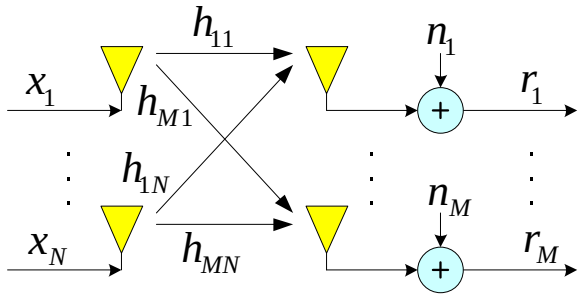

Figure 2.1: A channel model for $N \times M$ MIMO systems.

As for the case of SISO channels, the individual fading path gains comprising the MIMO channel are commonly modeled as zero-mean circularly symmetric complex Gaussian (ZMCSCG) variables with unit variance [7], we denote this by

$h_{mn} \sim \mathcal{CN}(0,1)$. Since the amplitudes $|h_{mn}|$ are Rayleigh-distributed random variables, the multipath fading is also referred to as *Rayleigh fading*[2]. Then the channel matrix $\mathbf{H}$ can be fully represented by a zero-mean multivariate complex normal (MCN) distribution and completely characterized by the covariance matrix $\mathbf{R}$ with covariance matrix $\mathbf{R}$

$$\mathbf{R} = \mathsf{E}\left[\mathrm{vec}(\mathbf{H})\mathrm{vec}(\mathbf{H})^H\right] \ , \tag{2.3}$$

where $\mathrm{vec}(\mathbf{A})$ denotes the vectorization of the matrix $\mathbf{A}$ by stacking the columns of $\mathbf{A}$ into a single column vector. We denote this distribution by $\mathbf{H} \sim \mathcal{CN}(\mathbf{0}, \mathbf{R})$. The *spatial correlation* of the MIMO channel can be completely characterized by the $MN \times MN$ matrix $\mathbf{R}$.

When the spatial Tx and Rx fading correlation are assumed to be separable, the full covariance matrix can be written as *Kronecker product*

$$\mathbf{R} = \mathbf{R}_{\mathrm{T}}^T \otimes \mathbf{R}_{\mathrm{R}} \tag{2.4}$$

with the Tx and Rx correlation matrices

$$\mathbf{R}_{\mathrm{T}} = (1/M)\mathsf{E}\left[\mathbf{H}^H\mathbf{H}\right], \quad \mathbf{R}_{\mathrm{R}} = (1/N)\mathsf{E}\left[\mathbf{H}\mathbf{H}^H\right], \tag{2.5}$$

respectively. Then the MIMO channel matrix can be further simplified as widely-used *Kronecker MIMO channel model* [39], [56],

$$\mathbf{H} = \mathbf{R}_{\mathrm{R}}^{1/2}\mathbf{H}_{\mathrm{w}}\mathbf{R}_{\mathrm{T}}^{1/2} \ , \tag{2.6}$$

where $\mathbf{H}_{\mathrm{w}}$ is the channel matrix with independent and identically distributed (i.i.d.) entries $\mathcal{CN}0, 1$. Though it may lead to modeling inaccuracy with a large number of

[2]We restrict ourselves to Rayleigh fading, i.e., only consider non line-of-sight (LOS) multipath component. The multipath fading with LOS component can be modeled as *Rician fading*.

antennas [74], the Kronecker MIMO channel model is quite popular by its simplicity and separability of Tx and Rx which allows for independent array optimization [5].

Now let us consider some special cases of the Kronecker MIMO channel model. When Tx side fading of the MIMO channel is spatially uncorrelated, then $\mathbf{R}_{\mathrm{T}} = \mathbf{I}$ and the columns of $\mathbf{H}$ are independent $\mathcal{CN}(\mathbf{0}, \mathbf{R}_{\mathrm{R}})$ random vectors. Similarly, when Rx side fading is spatially uncorrelated, the $\mathbf{R}_{\mathrm{R}} = \mathbf{I}$ and the rows of $\mathbf{H}$ are independent $\mathcal{CN}(\mathbf{0}, \mathbf{R}_{\mathrm{T}})$ random vectors. When both Tx and Rx side fading are spatially uncorrelated, i.e., the whole MIMO channel is spatially uncorrelated, then $\mathbf{H} = \mathbf{H}_{\mathrm{w}}$.

2.2 SU-MIMO MRC

In wireless communications, *diversity* is an effective way to reduce fading and increase the link reliability. Contrast to receive diversity only systems such as single-input multiple-output (SIMO) system using maximum-ratio combining (MRC) [10], MIMO systems using beamforming and combining employ the diversity at both the transmitter and receiver and improve the performance by jointly designing the beamforming vector and combining vector. When channel knowledge is available at the transmitter, this scheme seeks to transmit data along the largest eigenmode and maximize the output signal-to-noise ratio SNR. This attractive scheme has been called variously *maximum-ratio transmission (MRT)* [62], [90], [24], *MIMO transmit beamforming* [79], [98], and *MIMO MRC* [55], [103].

2.2.1 System Design

Now consider a $N \times M$ SU-MIMO system using beamforming and combining shown in Figure 2.2.

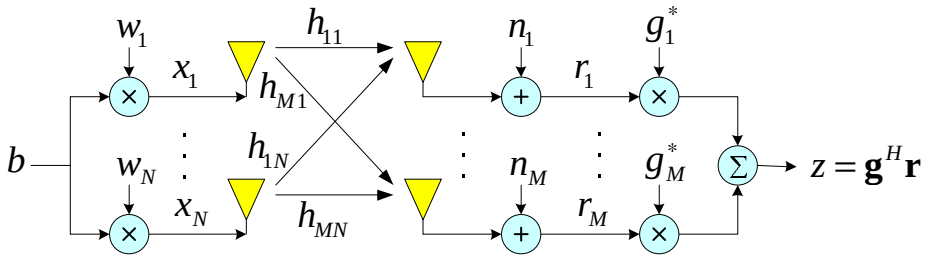

Figure 2.2: A$N \times M$ SU-MIMO system using beamforming and combining.

In this system, the transmit signal vector is of the form

$$\mathbf{x} = b\mathbf{w} = [bw_1, bw_2, \ldots, bw_N]^T \tag{2.7}$$

where b is a transmitted symbol with power $\mathsf{E}\left[|b|^2\right] = P$, $\mathbf{w}$ is a beamforming vector with unit-norm $||\mathbf{w}||_2 = 1$, and superscript T denotes transpose.

The receiver employs a combiner of the form

$$z = \mathbf{g}^H\mathbf{r} = \tilde{h}b + \tilde{n} \ , \tag{2.8}$$

where $\tilde{h}b$ represents the signal component and $\tilde{n}$ represents noise. Then the instantaneous SNR at the receiver is [90]

$$\gamma(\mathbf{w}, \mathbf{g}) = \frac{|\tilde{h}|^2}{\mathsf{E}\left[|\tilde{n}|^2\right]} = \frac{P}{N_0}\frac{|\mathbf{gHw}|^2}{\mathbf{g}^H\mathbf{g}} \ . \tag{2.9}$$

The aim of SU-MIMO MRC is to choose the unit-norm beamformer $\mathbf{w} \in \mathbb{C}^{N\times 1}$ and combiner $\mathbf{g} \in \mathbb{C}^{M\times 1}$ to maximize (2.9) given an input power P.

Cauchy-Schwarz inequality implies the maximization of SNR by using MRC principle[3] $\mathbf{g} = \mathbf{H}\mathbf{w}$. The optimal instantaneous SNR is therefore given by [90]

$$\gamma^o \equiv \max_{\mathbf{w}:||\mathbf{w}||_2=1} \gamma(\mathbf{w}, \mathbf{H}\mathbf{w}) = \max_{\mathbf{w}:||\mathbf{w}||_2=1} \Gamma \mathbf{w}^H \mathbf{H}^H \mathbf{H}\mathbf{w} = \Gamma \Lambda_{\max} \ , \tag{2.10}$$

where $\Gamma = (P/N_0)$ is the average input SNR, $\Lambda_{\max}$ is the largest eigenvalue of $\mathbf{H}^H\mathbf{H}$, and the last equality is achieved if and only if $\mathbf{w}$ is an orthonormal eigenvector associated with $\Lambda_{\max}$, which is implied by Rayleigh-Ritz inequality (cf. [24]). In some literature, $\Lambda_{\max}$ is referred to as *array gain* of dominant eigenmode [52].

As noted in [24] or [55], this largest eigenvalue problem can be solved equivalently by letting $\mathbf{w} = \mathbf{H}^H\mathbf{g}/||\mathbf{H}^H\mathbf{g}||_2$ and $\mathbf{g}$ be the eigenvector associated with the largest eigenvalue of $\mathbf{H}\mathbf{H}^H$ exactly the same as $\Lambda_{\max}$, or letting $\mathbf{g}$ and $\mathbf{w}$ be the left and unit-norm right singular vector associated with the largest singular value of $\mathbf{H}$ denoted as $\sigma_{\max} = \sqrt{\Lambda_{\max}}$.

2.2.2 Outage Probability

The outage probability of SU-MIMO MRC is

$$P_{\text{out}}(\tau) = \Pr\{\gamma^o \leq \tau\} = \Pr\{\Lambda_{\max} \leq \tau/\Gamma\} \ , \tag{2.11}$$

where τ is a non-negative threshold. Note that the outage probability can be evaluated by the cumulative density function (cdf) of the largest eigenvalue of $\mathbf{H}^H\mathbf{H}$.

For i.i.d. Rayleigh fading, i.e., $\mathbf{H} = \mathbf{H}_{\text{w}}$, the cdf of $\Lambda_{\max}$ is given by Khatri's result [57, eq. (6)] (see also [24, eq. (18)-(19)] and [54, eq. (9)]).

$$F_{\Lambda_{\max}}(y) \ = \ \frac{\det[\Psi(y)]}{\prod_{k=1}^{s} \Gamma(t-k+1)\Gamma(s-k+1)} \tag{2.12}$$

[3]Though the MRC principle takes the general form $\mathbf{g} \propto \mathbf{H}\mathbf{w}$, the performance does not depend on the norm of $\mathbf{g}$

where $s = \min\{N, M\}$, $t = \max\{N, M\}$, $\Gamma(n) = (n-1)!$ is the Gamma function, and $\Psi(y)$ is an $s \times s$ matrix

$$[\Psi(x)]_{i,j} = p(t - s + i + j - 1, x), \quad i, j = 1, \ldots, s \tag{2.13}$$

and $p(n, y) = \int_0^y x^{n-1} e^{-x} dx$ is the lower incomplete gamma function.

For semi-correlated Rayleigh fading, i.e., one of $\mathbf{R}_{\mathrm{T}}$ and $\mathbf{R}_{\mathrm{R}}$ but not both is identity matrix. The outage probability is studied by Kang and Alouni [55][4]

$$F_{\Lambda_{\max}}(y) \;=\; \frac{\det[\boldsymbol{\Delta}(y)]}{\det[\mathbf{V}] \cdot \prod_{i=1}^{s}(m-i)!} \tag{2.14}$$

where $s = \min\{M, N\}$, $\boldsymbol{\Delta}(y)$ is the $n \times n$ matrix

$$[\boldsymbol{\Delta}(y)]_{ij} \;=\; \begin{cases} \lambda_j^{m-i+1}\gamma(m-i+1, y/\lambda_j) & 1 \le i \le s \\ (-\lambda_j)^{i-n} & s < i \le n \end{cases}$$

$$\det[\mathbf{V}] \;=\; \left(\prod_{i=1}^{n} \lambda_i^m\right) \prod_{1 \le l < k \le n} \left(\frac{1}{\lambda_k} - \frac{1}{\lambda_l}\right) \;,$$

where $0 < \lambda_1 < \ldots < \lambda_n$ are the distinct eigenvalues of $\boldsymbol{\Sigma}$. If $\mathbf{R}_{\mathrm{R}} = \mathbf{I}$ then $\boldsymbol{\Sigma} = \mathbf{R}_{\mathrm{T}}$, $n = N$ and $m = M$; else if $\mathbf{R}_{\mathrm{T}} = \mathbf{I}$ then $\boldsymbol{\Sigma} = \mathbf{R}_{\mathrm{R}}$, $n = M$ and $m = N$.

For double-correlated Rayleigh fading, McKay *et al.* studied this extremely complicated case and derived the closed-form expression of the outage probability for $N \le M$ [69, eq. (6)].

Note that semi-correlated Rayleigh fading is quite common in cellular communications such as transmitter correlation in uplink and receiver correlation in downlink. The base station in these scenarios have large enough antenna spacings and

[4]This simplified version of [55, eqs. (25)-(29)] is obtained by interchanging $\Psi_{2A}(x)$ and $\Delta_{2B}(x)$ in eq. (28), which changes $\det[\Delta_2(x)]$ by a factor of $(-1)^{s(t-s)}$.

therefore less fading correlation. In this dissertation, we mainly focus on the i.i.d. and semi-correlated Rayleigh fading without loss of generality (WLOG).

Using (2.12) and (2.14), the outage probability for SU-MIMO MRC is

$$P_{\text{out}}(\tau) = F_{\Lambda_{\max}}(\tau/\Gamma) \tag{2.15}$$

2.2.3 Limited Feedback

In Section 2.2.1, we assumed the transmitter has full channel state information (CSI) and considered the problem of choosing $\mathbf{w}$ to maximize $\gamma(\mathbf{w}, \mathbf{Hw})$ in (2.10). In this section, we assume no CSI is available at transmitter but there exists a low-rate, error-free, zero-delay, feedback link. In this limited feedback scenario [64], one attractive approach is that the receiver (who has full CSI) may choose a beamforming vector $\mathbf{w}_i$ from a finite codebook $\mathcal{W} = \{\mathbf{w}_1, \ldots, \mathbf{w}_K\}$ and then communicate the index i to the transmitter via the feedback link. The main problem then is to design the codebook $\mathcal{W}$ so as to maximize $\gamma(\mathbf{w}, \mathbf{Hw})$, where $K = 2^B$ and B is the number of feedback bits determined by the bandwidth of feedback link. This scheme represent the whole beamformer space $\mathbb{C}^{N\times 1}$ by its quantized version, finite codebook, which is also known as *finite rate feedback* [72], [105] or *limited-rate feedback* [98].

Codebook design techniques derived in [64] and [72] take the codebook vectors as points in the Grassmann manifold. This connection allows us to construct a codebook on the results of optimal Grassmannian line packing from literature to maximize

$$d_{\text{Grass}}(\mathcal{W}) = \min_{1\le k<l\le N} \sqrt{1 - |\mathbf{w}_k^H \mathbf{w}_k|^2}\ , \tag{2.16}$$

where $d_{\text{Grass}}(\mathcal{W})$ is so called minimum distance of codebook $\mathcal{W}$. Some example code-

books for different (N, M) are given in [64, Appendix A].

Alternatively, by thinking of the codebook vectors as the points in a unit sphere, Xia and Giannakis [98] applied sphere vector quantization (SVQ) technique using generalized Lloyd algorithm to design the a codebook which minimizes the average distortion

$$d_{\text{Lloyd}}(\mathcal{W}) = \mathsf{E}\left[||\mathbf{H}||_2^2 - \max_{1\leq i\leq N} |\mathbf{H}\mathbf{w}_i|^2\right] \ . \tag{2.17}$$

Compared with Grassmannian method, Lloyd algorithm is fairly simple and is now a standard tool in feedback codebook design [65]. Note that both schemes can be used to generate optimal codebook offline for uncorrelated Rayleigh fading channels. However, the codebooks may degrade the SNR performance for spatially correlated Rayleigh fading channels.

Subsequently, Love *et al.* [65] and Xia *et al.* [98] propose that a good codebook $\mathcal{U} = \{\mathbf{u}_1, \ldots, \mathbf{u}_K\}$ for correlated Rayleigh fading channel denoted by $\mathbf{H} \sim (\mathbf{0}, \mathbf{R}_{\text{T}} \otimes \mathbf{R}_{\text{R}})$ can be designed via the construction

$$\mathbf{u}_i = \frac{\mathbf{R}_{\text{T}}^{H/2}\mathbf{w}_i}{||\mathbf{R}_{\text{T}}^{H/2}\mathbf{w}_i||_2}, \quad i = 1, \ldots, K \ , \tag{2.18}$$

where $\mathcal{W} = \{\mathbf{w}_1, \ldots, \mathbf{w}_K\}$ is a codebook optimized for the uncorrelated fading channel using either criterion in (2.16) and (2.17). Note that the codebook design does not depend on spatial correlation at Rx side.

2.2.4 Performance

In previous sections, we present the optimal transmission for SU-MIMO MRC systems with full CSI as well as the limited feedback design. In this section, we give numerical examples to illustrate the corresponding outage performance.

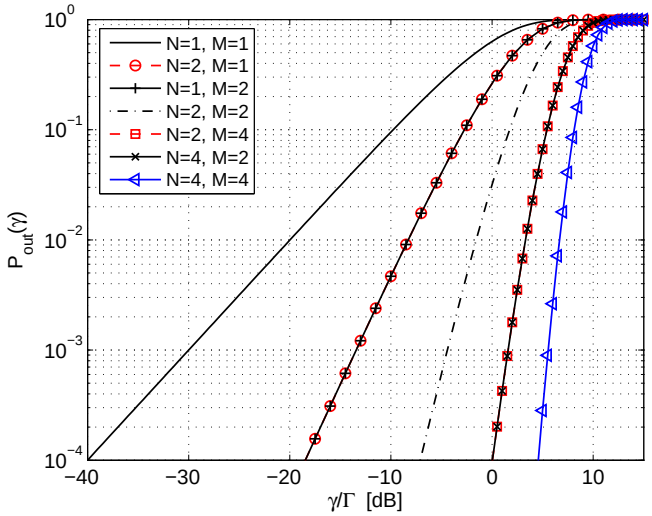

Figure 2.3: Outage probability of $N \times M$ SU-MIMO MRC systems with i.i.d. Rayleigh fading.

Figure 2.3 shows a plot of outage probability (2.12) of $N \times M$ SU-MIMO MRC systems with i.i.d. Rayleigh fading channels. Also shown for comparison are the cases of SISO with $N = M = 1$, MISO with $N = 2$ and $M = 1$ and SIMO with $N = 1$ and $M = 2$. It is seen that at 1% outage level (equals the value of 10^{-2}), i.e., 99% reliability, MIMO MRC provides 27 dB savings in power with 4×4, 23 dB savings with 4×2 and 2×4, 18.5 dB savings with 2×2 and 12 dB savings with 2×1 and 1×2. These savings in power compared with the SISO case are also referred to as *diversity gain*. Hence, MIMO systems offers more diversity and outperforms the MISO or SIMO systems which outperforms no diversity system (SISO). More antennas is promising to improve the outage performance. Another key observation is the duality of MIMO MRC system, i.e., $N \times M$ is the dual system of $M \times N$ in the sense of achieving the same outage performance. This is intuitive since $\mathbf{H}$ and

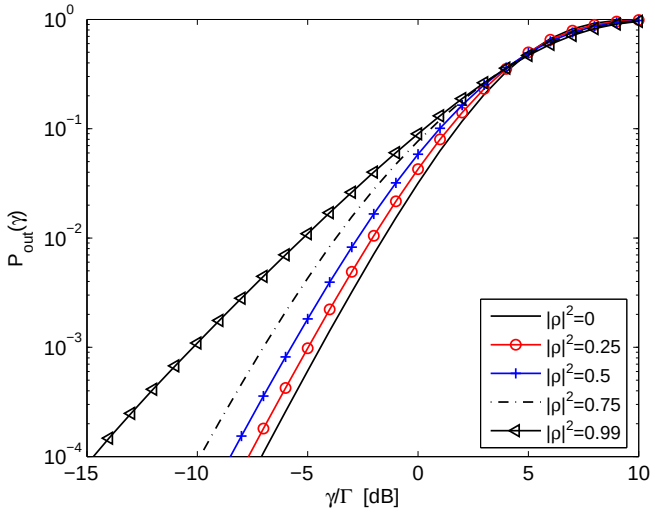

Figure 2.4: Outage probability of 2×2 SU-MIMO MRC systems with transmitter correlation.

$\mathbf{H}^T$ have the same largest eigenmode.

Figure 2.4 shows the outage probability of 2×2 SU-MIMO MRC system with transmitter correlation given by

$$\mathbf{R}_{\mathrm{T}} = \begin{bmatrix} 1 & \rho \\ \rho & 1 \end{bmatrix} \tag{2.19}$$

for some correlation coefficient $\rho \in [0, 1)$ and envelop correlation is approximated by $|\rho|^2$. Compared with Figure 2.3, we can see that outage curves of 2×2 system with correlation lie in between 2×1 and 2×2 systems without correlation. Larger correlation causes worse performance, which is due to the fact that correlation between antenna branches reduces the effective diversity and then degrades the outage performance.

Finally, performance of limited feedback (LF) is shown in Figure 2.5 and 2.6

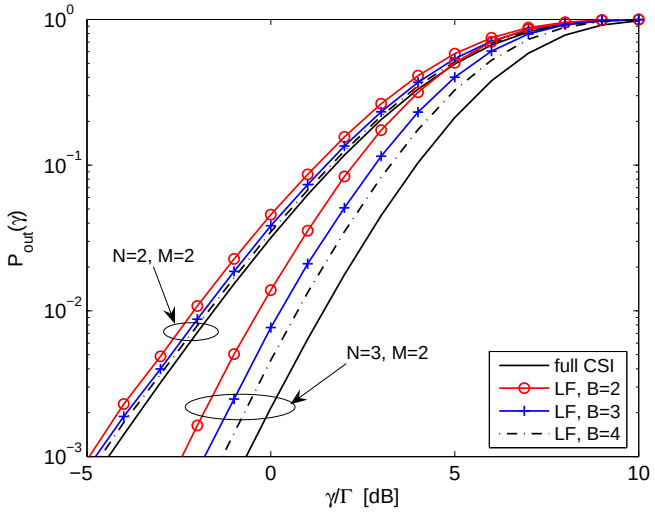

Figure 2.5: Outage probability of $N \times M$ SU-MIMO MRC systems with limited feedback and i.i.d. Rayleigh fading.

for i.i.d. and correlated Rayleigh fading, respectively. It can be seen in 2.5 that the performance degradation caused by limited feedback can be reduced by using more feedback bits denoted by B. When using the same number of feedback bits, 3×2 system suffers more than 2×2 system. This is intuitive since more antennas increases the dimension of beamformer space which therefore needs to be quantized by more vectors (codewords).

In Figure 2.6(a), though crossings occur around 1% outage level for the outage probabilities with limited feedback using codebook rotated for correlated Rayleigh fading and the one optimized for i.i.d. Rayleigh fading, the rotated codebook still achieves a better overall performance, i.e., in the most outage range from 0 to 1. This can be observed more clearly in Figure 2.6(b) that limited feedback using rotated codebook performs closely to full CSI scenario for both 2×2 and 3×2 systems. Note

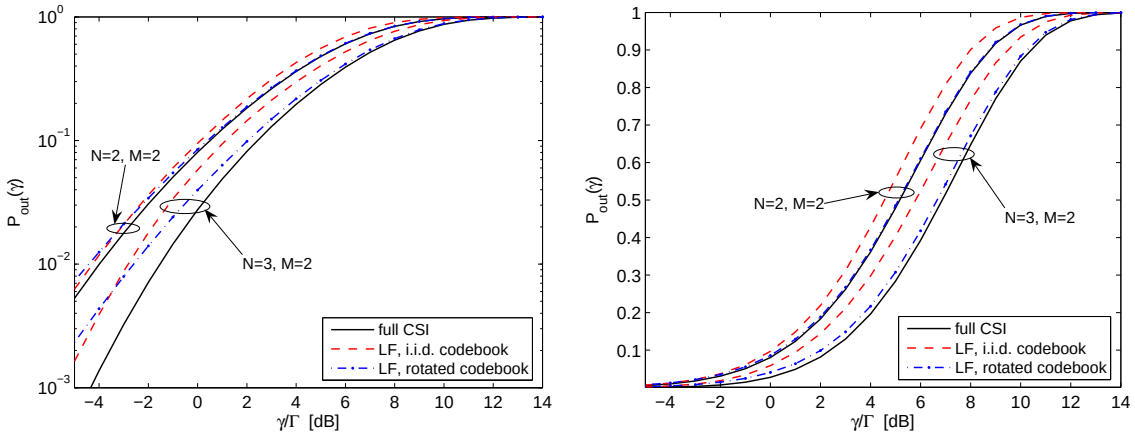

(a) $\log_{10} P_{\text{out}}(\gamma)$ vs. γ/Γ (b) $P_{\text{out}}(\gamma)$ vs. γ/Γ

Figure 2.6: Outage probability of $N \times M$ SU-MIMO MRC systems with limited feedback $B = 3$ and correlated Rayleigh fading $|\rho|^2 = 0.8$.

that, for the purpose of simulation, a simple *exponential correlation model* [3] is used for seme-correlated Rayleigh fading channel when more than two transmit antennas are used

$$[\mathbf{R}_{\text{T}}]_{ij} = \rho^{|i-j|}. \tag{2.20}$$

The correlation matrix in (2.19) is a special case of this model. More realistic correlation model such as the classic Clarke's 2D model and the model incorporated with mutual coupling will be discussed in Chapter 3. The codebook used in this numerical example is derived from a codebook $\mathcal{W}$ optimized for i.i.d. Rayleigh fading channel. As noted earlier, $\mathcal{W}$ can be designed by several different methods. The impact of different choice of $\mathcal{W}$ on the outage probability is investigated in Chapter 4.

2.3 MIMO Broadcast Channel Model

The previous section considered the design of beamforming for MIMO systems operating as single-user systems. In this section we present a basic model for multiuser MIMO broadcast channel, through which system throughput can be improved significantly. In a MIMO broadcast channel, one multiple-antenna transmitter sends information to many multiple-antenna receivers. In cellular-type architectures (e.g. cellular networks or WLAN/WMAN as noted in Chapter 1), broadcast channel models the downlink channel from the base station to mobile users [7].

We now consider a multiuser MIMO system in which a base station (transmitter) with N antennas sends data to K active users (receivers) with M_k antennas at the k-th user over the wireless broadcast channel. In the same propagation environment as in Section 2.1, the multipath channel between the base station and the k-th user can be modeled as a Rayleigh fading MIMO channel denoted by a channel matrix $\mathbf{H}_k \in \mathbb{C}^{M_k \times N}$, $k = 1, \ldots, K$. Similar to (2.2), we have following input-output relationship,

$$\mathbf{r}_k = \mathbf{H}_k \mathbf{x} + \mathbf{n}_k, \quad k = 1, \ldots, K \tag{2.21}$$

where $\mathbf{x} \in \mathbb{C}^{N \times 1}$ is the transmitted signal vector with input power $P = \mathrm{tr}\left(\mathsf{E}\left[\mathbf{x}\mathbf{x}^H\right]\right)$, $\mathbf{r}_k \in \mathbb{C}^{M_k \times 1}$ and $\mathbf{n}_k \in \mathbb{C}^{M_k \times 1}$ are the received signal vector and noise (AWGN) vector at user k, respectively. Note that the base station may have independent message for each of the users.

Network information theory predicts the emergence of many new elements: interference, cooperation and feedback when multiple transmitters and receivers are involved in this communication problem [23]. In the next section, we will introduce

a multiuser MIMO beamforming technique which is suitable for MIMO broadcast channels.

2.4 Downlink MU-MIMO CBF

As noted in Chapter 1, dirty paper coding (DPC) achieves the capacity region for the MIMO broadcast channels but is hard to implement in practice due to its non-linearity and high complexity [11], [94]. The linear beamforming techniques then have received considerable attention due to the lower complexity and the capability of sending data in good beam directions. Prior studies on linear beamforming, such as zero-forcing beamforming [20], [84], [77] and [101], employ only beamforming at the transmitter and suffer from the dimensionality constraint which requires specific number of antennas for one or both ends. Another approaches extend these work by applying both the transmit beamforming and receive combining, i.e., MIMO beamforming, and introducing transmit-receive coordination [33], [76] and [13], which however requires iterative calculation and may not converge. More recently, some non-iterative linear MIMO beamforming algorithms have been proposed for MU-MIMO broadcast systems and referred variously as *generalized zeroforcing (GZF)* [33], [97], and *coordinated beamforming (CBF)* [14]. MU-MIMO CBF is effective to mitigate the inter-user interference and improve the sum-rate by jointly design of beamforming vector and all the combining vectors.

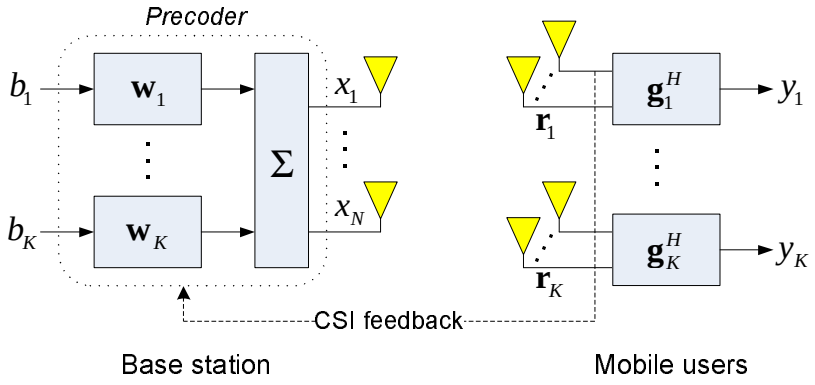

Figure 2.7: A MIMO broadcast channel with coordinated beamforming.

2.4.1 System Design

Consider a MIMO broadcast system with N antennas at the base station and K active users shown in Figure 2.7. Without loss of generality (WLOG), all K users are assumed to have M receive antennas each[5]. In this scheme, the base station sends one symbol[6] to each user via linear beamforming, so that $\mathbf{x} = \sum_{k=1}^{K} \mathbf{w}_k b_k$ is transmitted, where b_k is the symbol intended for the k-th user and $\mathbf{w}_k$ is a unit-norm beamformer. This transmitter design as well as the one for SU-MIMO MRC is a special case of MIMO *precoding* strategies [81] and the corresponding structure is called *precoder*.

The k-th user applies a unit-norm combiner $\mathbf{g}_k$ on the received signal vector

[5]Coordinated beamforming design can be easily extend to the scenario that mobile users are equipped with unequal number of receive antennas.

[6]We adopt the same resource allocation policy as in [97] and [14] by restricting one data stream per use.

(2.21) and outputs the signal

$$y_k = \mathbf{g}_k^H \mathbf{H}_k \mathbf{w}_k b_k + \mathbf{g}_k^H \mathbf{H}_k \sum_{l=1, l\leq k}^{K} \mathbf{w}_l b_l + \mathbf{g}_k^H \mathbf{n}_k \ , \tag{2.22}$$

where $\mathbf{H}_k \in \mathbb{C}^{M\times N}$ is the channel matrix between the transmitter and the k-th user, and $\mathbf{n}_k \sim (\mathbf{0}, N_0\mathbf{I})$ represents noise. The coordinated beamforming is aim to choose the beamformers and combiners such that no inter-user interference is experienced at each user, i.e.,

$$\mathbf{g}_k^H \mathbf{H}_k \sum_{l=1, l\leq k}^{K} \mathbf{w}_l = 0, \quad k = 1, \ldots, K \ . \tag{2.23}$$

As noted earlier, the prior studies in [33], [76] and [13] work for arbitrary number of active users but requires iterative computation and may not converge. Being restricted to $K = 2$ users case, [97] and [14] proposed non-iterative coordinated beamforming schemes. The decision statistics are therefore given by

$$\begin{aligned} y_1 = \mathbf{g}_1^H \mathbf{r}_1 &= \mathbf{g}_1^H \mathbf{H}_1 \mathbf{w}_1 b_1 + \mathbf{g}_1^H \mathbf{H}_1 \mathbf{w}_2 b_2 + \mathbf{g}_1^H \mathbf{n}_1 \ , \\ y_2 = \mathbf{g}_2^H \mathbf{r}_2 &= \mathbf{g}_2^H \mathbf{H}_2 \mathbf{w}_1 b_1 + \mathbf{g}_2^H \mathbf{H}_2 \mathbf{w}_2 b_2 + \mathbf{g}_2^H \mathbf{n}_2 \ . \end{aligned} \tag{2.24}$$

And the zero-interference constraints (2.23) imply

$$\mathbf{g}_1^H \mathbf{H}_1 \mathbf{w}_2 = \mathbf{g}_2^H \mathbf{H}_2 \mathbf{w}_1 = 0 \ , \tag{2.25}$$

in which case the sum-rate of the resulting system is given by

$$C(\mathbf{w}_1, \mathbf{w}_2, \mathbf{g}_1, \mathbf{g}_2) = \log_2(1 + \gamma_1) + \log_2(1 + \gamma_2) \ , \tag{2.26}$$

where $P_k = E[|b_k|^2]$ is the transmit power allotted to user k and

$$\gamma_k = \frac{P_k}{N_0} \frac{|\mathbf{g}_k^H \mathbf{H}_k \mathbf{w}_k|^2}{\mathbf{g}_k^H \mathbf{g}_k} \tag{2.27}$$

is the output SNR of the k-th receiver. We assume full channel state information is available, so $\mathbf{H}_1$ and $\mathbf{H}_2$ are known at the transmitter; the case of limited feedback is considered in Section 2.4.2. The optimization problem is therefore to maximize (2.26) over all unit-norm vectors $\mathbf{w}_1, \mathbf{w}_2, \mathbf{g}_1, \mathbf{g}_2$ that satisfy (2.25). Note that we can relax the assumption that $\mathbf{g}_1$ and $\mathbf{g}_2$ have unit norm, since (2.26) does not depend on the norms of the combiners.

For $M \geq N = 2$, Wong asserts that MRC[7] is the optimal receiver processing given the beamformers,

$$\mathbf{g}_1 = \mathbf{H}_1\mathbf{w}_1 \ , \quad \mathbf{g}_2 = \mathbf{H}_2\mathbf{w}_2 \ .$$

in which case the zero-interference constraints (2.25) become

$$\mathbf{w}_1^H\mathbf{H}_1^H\mathbf{H}_1\mathbf{w}_2 = \mathbf{w}_2^H\mathbf{H}_2^H\mathbf{H}_2\mathbf{w}_1 = 0 \ . \tag{2.28}$$

Assuming MRC is used at the receiver, Chae *et al.* [14] showed for $M \geq N \geq 2$ that any beamformers $\mathbf{w}_1$ and $\mathbf{w}_2$ that satisfy (2.25) must be generalized eigenvectors of the matrices[8]

$$\mathbf{F}_1 = \mathbf{H}_1^H\mathbf{H}_1 \ , \quad \mathbf{F}_2 = \mathbf{H}_2^H\mathbf{H}_2 \ , \tag{2.29}$$

or equivalently, eigenvectors of the matrix $\mathbf{F}_2^{-1}\mathbf{F}_1$ if $\mathbf{F}_2$ is nonsingular.

Based on this result, Chae *et al.* proposed the following approach to coordinated beamforming. First we compute a set $\mathcal{W}$ of generalized eigenvectors of $\mathbf{F}_1$ and

[7]Each user only knows its own CSI does not has the capability to estimate the beamformers which is determined by the CSIs from both users. This problem can be solved by so called feedforward scheme [15] in which each beamformer is transmitted to the corresponding user to facilitate the receive combining. In this dissertation, we omit this problem and assume each user can always obtain its corresponding beamformer perfectly.

[8]The optimal beamformers in [14] are expressed in a slightly different form, as generalized eigenvectors of the normalized matrices $\bar{\mathbf{F}}_1 = \mathbf{F}_1/\mathrm{tr}(\mathbf{F}_1)$ and $\bar{\mathbf{F}}_2 = \mathbf{F}_2/\mathrm{tr}(\mathbf{F}_2)$. Clearly, the generalized eigenvectors of $\bar{\mathbf{F}}_1$ and $\bar{\mathbf{F}}_2$ are the same as those of $\mathbf{F}_1$ and $\mathbf{F}_2$.

$\mathbf{F}_2$. We then choose beamformers from this set so as to maximize the sum-rate when MRC combining is used:

$$\{\mathbf{w}_1^o, \mathbf{w}_2^o\} \;=\; \arg \max_{\mathbf{w}_1,\mathbf{w}_2 \in \mathcal{W}, \mathbf{w}_1 \neq \mathbf{w}_2} C(\mathbf{w}_1, \mathbf{w}_2, \mathbf{H}_1\mathbf{w}_1, \mathbf{H}_2\mathbf{w}_2) \; . \tag{2.30}$$

2.4.2 Limited Feedback

The coordinated beamforming scheme in Section 2.4.1 requires the matrices $\mathbf{F}_1$ and $\mathbf{F}_2$ to be fed back by the users to the transmitter. When feedback is limited, the transmitter's estimates of these matrices may be imprecise and the resulting performance degraded. In particular, we consider a scenario in which no CSI is available at the transmitter but there exists a low-rate, error-free, zero-delay feedback link. Since the complete matrices $\mathbf{F}_1$ and $\mathbf{F}_2$ not just their subspace information are required at the transmitter, then the limited feedback design for SU-MIMO MRC in Section 2.2.3 cannot be directly applied here. In the simulations and analysis of this dissertation, we adopt the simple limited feedback method proposed in [14], in which the entries of the normalized matrices

$$\mathbf{G}_k = \frac{\mathbf{F}_k}{\mathrm{tr}(\mathbf{F}_k)} \; , \quad k = 1, 2$$

are uniformly quantized and fed back to the transmitter[9]. As shown in [14], these matrices are Hermitian, preserve the generalized eigenvectors, and the entries have well-defined ranges. For example, for $N = 2$ we have $[\mathbf{G}_k]_{11} \in [0, 1]$, $[\mathbf{G}_k]_{22} = 1 - [\mathbf{G}_k]_{11}$ and $\mathrm{Re}\{[\mathbf{G}_k]_{12}\}, \mathrm{Im}\{[\mathbf{G}_k]_{12}\} \in [-0.5, 0.5]$. To quantize all of the real scalars in these matrices using Q bits requires a total of $(N^2 - 1)Q$ bits for each user.

[9]Non-uniform quantization can be used to minimize the quantization error when the distribution of each of the entries in these two matrices is known[14], which is not considered in this dissertation.

When beamformers (2.30) are designed using quantized versions of the channel matrices $\mathbf{H}_1$ and $\mathbf{H}_2$, the multiuser interference in the decision statistics (2.24) may not be completely canceled. As a consequence, to evaluate the performance of limited-feedback beamformers, we must replace the SNRs (2.27) in the sum-rate (2.26) with the signal-to-interference-and-noise ratios (SINRs)

$$\gamma_k = \frac{P_k|\mathbf{g}_k^H \mathbf{H}_k \mathbf{w}_k|^2}{P_l|\mathbf{g}_k^H \mathbf{H}_k \mathbf{w}_l|^2 + N_0 \mathbf{g}_k^H \mathbf{g}_k} \tag{2.31}$$

where $l = 1$ if $k = 2$ and $l = 2$ when $k = 1$.

2.4.3 Performance

In previous sections, we present the coordinated beamforming strategy for multiuser MIMO broadcast systems with full CSI as well as the limited feedback design. In this section, we evaluate the system performance by several numerical examples. We assume the transmitter allocates equal power to each of two identical users, so $P_1 = P_2 = P/2$ where P is the total transmit power.

Figure 2.8 plots the sum-rates versus SNR ($= P/N_0$, which is more precisely called average input SNR in [16]) for MU-MIMO broadcast systems for $N = 2$, $M = 2$ or 4 with perfect CSI over i.i.d. Rayleigh fading channel. We compare four different strategies: sum-capacity by DPC [53], non-iterative CBF [14], non-iterative GZF [97] and iterative CBF with maximum 50 iterations [33], [13]. For $N = M = 2$ system, the three sum-rates are close to each other and slightly worse than sum-capacity. By showing the facts: (1) the iterative CBF converges to CBF if it converges; (2) GZF is a subset of CBF, Chae *et al.* claims that CBF outperforms both iterative CBF and GZF and GZF is the worst[14, Fig. 3]. The advantages of larger receive array is

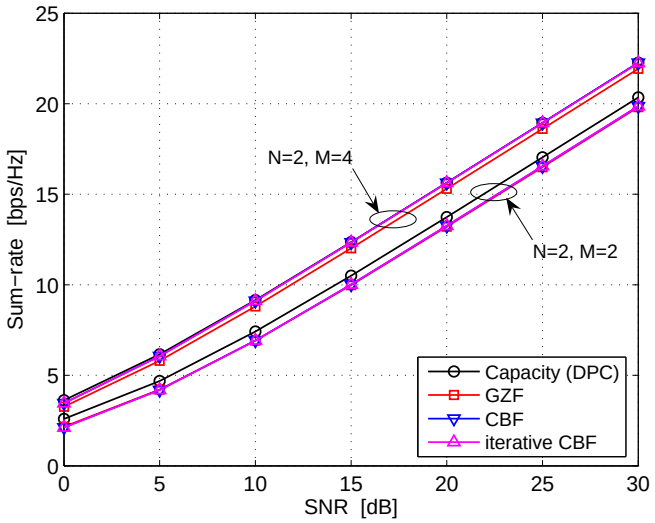

Figure 2.8: Sum-rates vs. SNR for $N = 2$, $M = 2$ or 4 with perfect CSI.

illustrate by $N = 2$ and $M = 4$ system which improves the sum-rates about $1.4 - 2.5$ bps/Hz for all the four strategies relative to $N = M = 2$ system. In particular, both CBF and iterative CBF perform close to DPC and better than GZF.

Figure 2.9 demonstrates the dependence of sum-rate performance using CBF scheme on the numbers of transmit and receive antennas. From Figure 2.9(a), we can see that the achievable sum-rate increases continuously as $N = M$ increases. Since the system is restricted to one data stream per user, the full multiplexing gain cannot be achieved [14]. Note that both $\mathbf{F}_1$ and $\mathbf{F}_2$ have rank $s = \min\{N, M\}$ and therefore have s generalized eigenvectors corresponding to non-zero eigenvalues, referred as candidate generalized eigenvectors. Since any set of generalized eigenvectors of $\mathbf{F}_1$ and $\mathbf{F}_2$ satisfy the zero-interference condition [14, Theorem 3], then the CBF algorithm is not necessarily constrained by $M \geq N = 2$ which is not noticed by the authors.

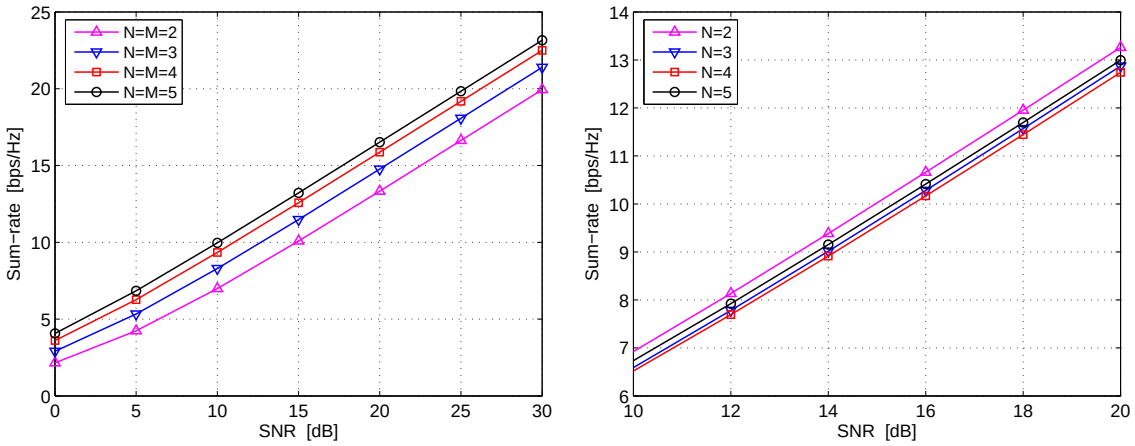

(a) $N = M$ (b) $N \geq M$

Figure 2.9: Sum-rates vs. SNR for various N and M with perfect CSI.

Figure 2.9(b) plots the sum-rate versus SNR for $M = 2$ and various N. Interestingly, the largest sum-rate is achieved by $N = 2$, the second largest is by $N = 5$, the third largest is by $N = 3$ and $N = 4$ is the lowest. This is not surprised since the candidate generalized eigenvectors may not represent a good beam direction when both $\mathbf{F}_1$ and $\mathbf{F}_2$ are singular. Thus there is a tradeoff between the large transmit array and the beam direction when the number of receive antenna is small and fixed.

Performance of limited feedback design is illustrated in Figure 2.10 which plots the average sum-rate of CBF for $N = 2$, $M = 2$ or 4 systems and different feedback scenarios. For full CSI, the larger array provides a constant 4.7 dB power saving relative to the $M = 2$ case. The power savings of limited feedback (LF) scenarios decreases as SNR increases, particular for small Q. Limited feedback scenarios perform pretty well and close to full CSI case in low SNR regime and however degrade

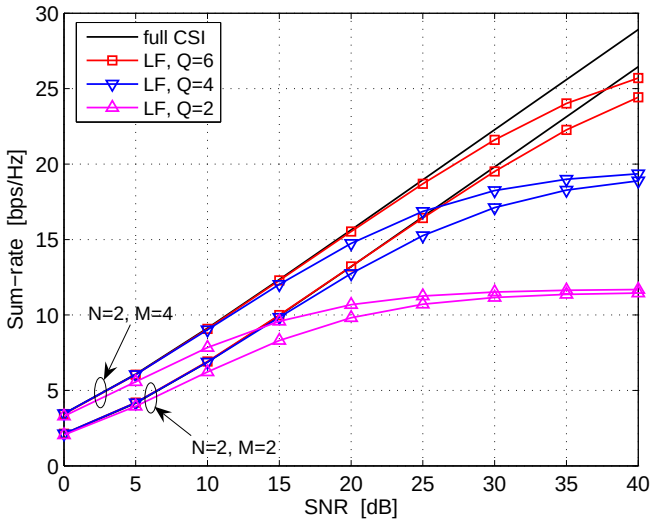

Figure 2.10: Sum-rates vs. SNR for $N = 2$, $M = 2$ or 4 with limited feedback.

performance in high SNR regime. This is intuitive since limited feedback as noted in Section 2.4.2 introduces multiuser interference which may be amplified by the power allocated to the interferers.

2.5 Summary and Discussion

In this chapter, we present the beamforming design for both SU-MIMO systems and MU-MIMO broadcast systems as well as the design of limited feedback from the viewpoint of communication theory. This is however not complete yet.

First, we only consider the impact of transmitter correlation (exponential model) on SU-MIMO MRC system. More realistic correlation model such as Clarke's model and the model incorporated antenna coupling is studied in [28] and [29]. In practice, the receiver may experience correlated fading due to several reasons such as

angular spread, antenna coupling, etc. And the noise at different receive branch may also be correlated. This interesting topic is parallelly studied in [25] - [27].

Second, there is no consideration of correlated fading and noise paid on downlink MU-MIMO CBF systems. The coordinated beamforming strategy discussed in the previous sections can still be applied for correlated fading which is full contained in matrices $\mathbf{F}_1$ and $\mathbf{F}_2$ and can be fed back to the transmitter. However, similar to SU-MIMO MRC, the correlated noise may affect the output SNR and needs to be taken into account for the actual beamforming design. This problem is originally addressed in [30] and will be covered with details in Chapter 5.

Chapter 3

SU-MIMO MRC with Compact Transmitter

As noted in Section 1.1.1, antennas packed in a close proximity may cause electromagnetic coupling. Then the transceived signal at the coupled antenna array is no longer independent, but experiences spatial correlation which may influence the performance of single-user MIMO beamforming, see Chapter 2 for details. There is also an interchange of energy among the antennas, e.g., some of the energy radiated from one antenna will be captured and re-radiated by neighboring antenna. In many cases mutual coupling complicates the analysis and design of antenna array, and is important to be taken into account especially when inter-element spacings are small. One way to incorporate the presence of mutual coupling is by means of an impedance matrix[1]. The use of impedance matrix will be most convenient for wire type of antennas [50]. In this chapter we first introduce a circuit model for a transmit

[1]Scattering matrix is another parameter (*S-parameter*) describing the electrical behavior of coupled antenna array (see [92], [93] and references therein).

array with mutual coupling and matching network using impedance parameter (*Z-parameter*), we then present the optimal transmissions for SU-MIMO MRC system in the presence of mutual coupling and validate the design by numerical examples. The main purpose of this study is to understand how mutual couple affect the system performance and how close we can place the antenna elements and still enjoy the benefits of MIMO beamforming.

3.1 Transmitter Model with Mutual Coupling

Consider a single-user MIMO MRC system equipped with N transmit and M receive antennas that communicates through a narrowband Rayleigh block-fading channel. We assume the transmit antennas are placed close together, which leads to mutual coupling. Due to the interchange of energy among couple antennas, the power may be radiated less efficiently and however can be increased by the use of matching networks. Thus, the performance of SU-MIMO MRC system depends not only on the correlation between the path gains that connect each pair of transmit and receive antennas, but also depends on the impedances of the source, antennas and matching networks used in the coupled multi-antenna transmitter.

A circuit model for this compact transmitter with a uniform linear array (ULA) of N closely spaced dipoles [59] is shown in Figure 3.1. Both the antenna array, matching network and source are treated as completely linear networks and represented by equivalent circuit models. More detailed discussion of these circuit models are offered as below.

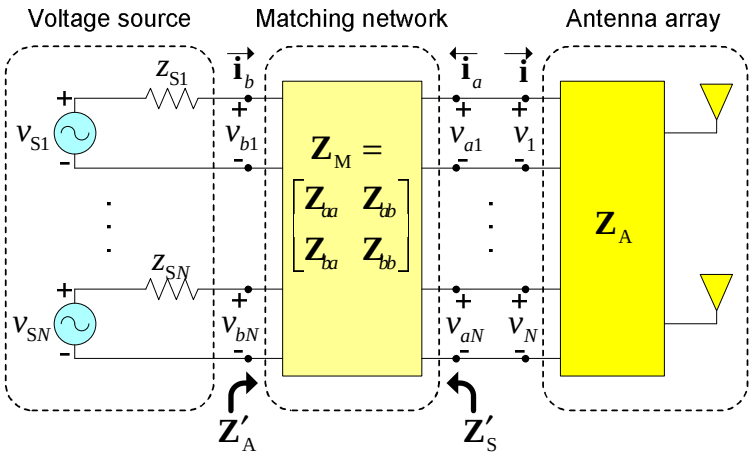

Figure 3.1: Circuit model of a transmit array with mutual coupling.

3.1.1 Antenna Array

For coupled array, the currents flowing through antenna elements will induce voltages across neighboring elements. The relationship between the complex currents and voltages of the array, arranged in column vectors $\mathbf{v}$, $\mathbf{i} \in \mathbb{C}^{N\times 1}$, respectively, is given by

$$\mathbf{v} = \mathbf{Z}_\mathrm{A}\mathbf{i} \ , \tag{3.1}$$

where $\mathbf{Z}_\mathrm{A}$ is an $N \times N$ impedance matrix. Here $[\mathbf{Z}_\mathrm{A}]_{nn}$ is the *self-impedance* of antenna n, and $[\mathbf{Z}_\mathrm{A}]_{mn}$ is the *mutual impedance* between antennas n and m. These impedances can be estimated by numerical techniques (more on this in Section 3.5). For thin dipoles, approximate formulas are given in [6, eq. (8-71)]. The closed-form expressions for these impedances for two side-by-side dipoles were given in [86].

The antenna array is driven by a bank of N voltage sources, where the n-th source has internal impedance $z_{\mathrm{S}n}$. Without matching network, the voltage driving

the array is related to the source voltages $\mathbf{v}_{\mathrm{S}}$ by

$$\mathbf{v} = \mathbf{Z}_{\mathrm{A}} \left(\mathbf{Z}_{\mathrm{A}} + \mathbf{Z}_{\mathrm{A}} \right)^{-1} \mathbf{v}_{\mathrm{S}} \ , \tag{3.2}$$

where $\mathbf{Z}_{\mathrm{S}} = \mathrm{diag}(z_{\mathrm{S}1}, \ldots, z_{\mathrm{S}N})$ is the source impedance matrix.

3.1.2 Matching Networks

When antenna array is connected to the source, strong reflection can result if the antenna array impedances differ from the source impedances [17, sec. 2.13]. In order to reduce the reflection, i.e., transfer power efficiently, a impedance matching network is placed between the array and the source [42]. Ideally a matching network is formed with passive, reactive and isotropic elements so it is noiseless, lossless, and reciprocal. Consider a $2N$-port matching network shown in Figure 3.1 with impedance

$$\mathbf{Z}_{\mathrm{M}} = \begin{bmatrix} \mathbf{Z}_{aa} & \mathbf{Z}_{ab} \\ \mathbf{Z}_{ba} & \mathbf{Z}_{bb} \end{bmatrix} \ , \tag{3.3}$$

where each block is an $N \times N$ matrix. Let $\mathbf{v}_b$, $\mathbf{i}_b$, $\mathbf{v}_a$, $\mathbf{i}_a$ denote the voltages and currents at the input and output of the network. For a network to be lossless, none of the power is dissipated (converted to heat or radiated) within it, so that the network impedance is pure imaginary: $\mathrm{Re}\{\mathbf{Z}_{\mathrm{M}}\} = 0$. Thus $\mathbf{Z}_{aa} = -\mathbf{Z}_{aa}^{H}$, $\mathbf{Z}_{ab} = -\mathbf{Z}_{ba}^{H}$ and $\mathbf{Z}_{bb} = -\mathbf{Z}_{bb}^{H}$ [42, eq. (2.4)–(2.5)]. If the network is reciprocal then it satisfies another condition that its impedance matrix is symmetric: $\mathbf{Z}_{\mathrm{M}} = \mathbf{Z}_{\mathrm{M}}^{T}$ [78, pp. 171-172]. Some specific forms of matching networks used in this study are described in Section 3.5.

From elementary circuit theory, the voltage driving the array is then related to the source voltage by

$$\mathbf{v} = \mathbf{C}_{\mathrm{T}} \mathbf{v}_{\mathrm{S}} \ , \tag{3.4}$$

where $\mathbf{C}_{\mathrm{T}} = \mathbf{Z}_{\mathrm{A}}(\mathbf{Z}_{aa} + \mathbf{Z}_{\mathrm{A}})^{-1}\mathbf{Z}_{ab}(\mathbf{Z}_{\mathrm{S}} + \mathbf{Z}'_{\mathrm{A}})^{-1}$ is the transmitter coupling matrix and

$$\mathbf{Z}'_{\mathrm{A}} = \mathbf{Z}_{bb} - \mathbf{Z}_{ba}(\mathbf{Z}_{aa} + \mathbf{Z}_{\mathrm{A}})^{-1}\mathbf{Z}_{ab} \tag{3.5}$$

is the effective impedance of the matching network and antenna array, as seen from the source. Note that another equivalent way is to examine the effective source voltage $\mathbf{v}'_{\mathrm{S}}$ and the effective source impedance $\mathbf{Z}'_{\mathrm{S}}$ of the matching network and source as seen from the antenna array:

$$\mathbf{v}'_{\mathrm{S}} = \mathbf{Z}_{ab}(\mathbf{Z}_{bb} + \mathbf{Z}_{\mathrm{S}})^{-1}\mathbf{v}_{\mathrm{S}} \tag{3.6}$$

$$\mathbf{Z}'_{\mathrm{S}} = \mathbf{Z}_{aa} - \mathbf{Z}_{ab}(\mathbf{Z}_{bb} + \mathbf{Z}_{\mathrm{S}})^{-1}\mathbf{Z}_{ba} \tag{3.7}$$

Note that the MIMO system performance depends on how well the antenna impedances are matched to the source impedances by matching networks and vice versa.

3.1.3 Power Measures

We would like to examine MIMO system performance subject to a constraint on input power. This task is complicated by the lack of a consensus definition of input power in the presence of mutual coupling. We therefore consider several measures of power introduced in previous works: Janaswamy [51] defines input power to be the power delivered by the source when connected to a bank of uncoupled 1 Ω resistors. In our notation, this yields

$$P_1 \triangleq (1/2)\mathbf{v}_{\mathrm{S}}^H\mathbf{v}_{\mathrm{S}} \ , \tag{3.8}$$

which is mathematically equivalent to the input power used in the MIMO literature. Since (3.8) does not correspond to any actual power delivered in Figure 3.1, others

(e.g. [93], [59]) have defined the input power to be the power radiated by the transmit array. If the antennas are lossless, so that all power absorbed by the antennas is radiated, then the radiated power is given by[2]

$$P_2 \triangleq (1/2)\mathrm{Re}\{\mathbf{i}^H\mathbf{v}\} = (1/2)\mathbf{v}_\mathrm{S}^H\mathbf{C}_\mathrm{T}^H\mathrm{Re}\{\mathbf{Z}_\mathrm{A}^{-1}\}\mathbf{C}_\mathrm{T}\mathbf{v}_\mathrm{S}\ . \tag{3.9}$$

Similarly, it is natural to also consider the actual power delivered by the source, which is

$$P_3 \triangleq (1/2)\mathrm{Re}\{\mathbf{i}^H\mathbf{v}_\mathrm{S}\} = (1/2)\mathbf{v}_\mathrm{S}^H\mathrm{Re}\{(\mathbf{Z}_\mathrm{S}+\mathbf{Z}_\mathrm{A})^{-1}\}\mathbf{v}_\mathrm{S}\ . \tag{3.10}$$

For simplicity, all these three power measures can be unified as,

$$P_i = (1/2)\mathbf{v}_\mathrm{S}^H\mathbf{A}_i\mathbf{v}_\mathrm{S}, \quad i = 1,2,3 \tag{3.11}$$

where $\mathbf{A}_1 = \mathbf{I}$, $\mathbf{A}_2 = \mathbf{C}_\mathrm{T}^H\mathrm{Re}\{\mathbf{Z}_\mathrm{A}^{-1}\}\mathbf{C}_\mathrm{T}$ and $\mathbf{A}_3 = \mathrm{Re}\{(\mathbf{Z}_\mathrm{S}+\mathbf{Z}_\mathrm{A})^{-1}\}$. Note that the optimal MRC transmission strategy will differ for these three constraints.

3.2 MIMO Channel and Noise

In a rich scattering environment with negligible delay spread, the complex baseband signal detected at the receiver can be modeled as [51]

$$\mathbf{r} = \mathbf{H}\mathbf{v} + \mathbf{n} \tag{3.12}$$

where $\mathbf{H} \in \mathbb{C}^{M\times N}$ is the channel matrix and $\mathbf{n} \in \mathbb{C}^{M\times 1}$ represents noise. Due to close spacing of the transmit antennas, the entries of $\mathbf{H}$ are generally correlated. We assume the M receive antennas are spaced far enough apart so as to be essentially

[2]The terms "input power" and "radiated power" are somewhat misleading here since both terms implicitly include the average path loss.

uncoupled and uncorrelated, so the rows of $\mathbf{H}$ are independent zero-mean, circularly-symmetric complex Gaussian vectors with covariance $\mathbf{R}_{\mathrm{T}}$. We denote this distribution by $\mathcal{CN}(\mathbf{0}, \mathbf{R}_{\mathrm{T}})$. The noise is also modeled as AWGN, $\mathbf{n} \sim \mathcal{CN}(\mathbf{0}, N_0\mathbf{I})$.

As noted in Chapter 2, $\mathbf{H}$ can also be expressed in the form of semi-correlated Kronecker model,

$$\mathbf{H} = \mathbf{H}_{\mathrm{w}}\mathbf{R}_{\mathrm{T}}^{1/2} \ , \tag{3.13}$$

where $\mathbf{H}_{\mathrm{w}}$ is a matrix with independent and identically distributed (i.i.d.) $\mathcal{CN}(0,1)$ entries. As in [51], the path gains at transmitter side can be assumed to be correlated to Clarke's 2D model [21]

$$[\mathbf{R}_{\mathrm{T}}]_{nm} \ = \ J_0(2\pi d_{nm}/\lambda) \tag{3.14}$$

where d_{nm} is the distance between antennas n and m, λ is the signal wavelength, and $J_0(\cdot)$ is the zero order Bessel function of the first kind. More precisely, the correlation matrix $\mathbf{R}_{\mathrm{T}}$ depends on not only the spatial distribution of the multipath but also the radiation patterns of the antenna arrays.

In SU-MIMO MRC, the source voltage is of the form

$$\mathbf{v}_{\mathrm{S}} = \mathbf{w}b = [w_1 b, w_2 b, \ldots, w_N b]^T \tag{3.15}$$

where b is a transmitted symbol with $\mathsf{E}[|b|^2]$=1, $\mathbf{w}$ is a beamforming vector to be specified later. Combining (3.4), (3.13) and (3.15), we can rewrite the channel (3.12) as

$$\mathbf{r} = \mathbf{H}_{\mathrm{mc}}\mathbf{w}b + \mathbf{n} \ , \tag{3.16}$$

where $\mathbf{H}_{\mathrm{mc}} = \mathbf{H}_{\mathrm{w}}\mathbf{R}_{\mathrm{T}}^{1/2}\mathbf{C}_{\mathrm{T}}$ is a new channel matrix which reflects the combined effects of matching, coupling and path gain correlation. For simplicity, the path loss due to separation of the transmitter and receiver is lumped into the variable $\mathbf{w}$.

3.3 SU-MIMO MRC with Mutual Coupling

Consider now the application of single-user MIMO maximum-ratio combining to channel (3.16), subject to the input power constraint 3.11. The receiver employs a combiner of the form $z = \mathbf{w}^H \mathbf{H}_{\text{mc}}^H \mathbf{r}$, if the receive antennas are uncoupled, then the instantaneous SNR at the receiver is

$$\gamma(\mathbf{w}) = (1/N_0)\mathbf{w}^H \mathbf{H}_{\text{mc}}^H \mathbf{H}_{\text{mc}} \mathbf{w} \tag{3.17}$$

We assume the transmitter has full channel knowledge, then the aim of SU-MIMO MRC is to choose the beamforming vector $\mathbf{w}$ to maximize (3.17) subject to an input power constraint. For the power measure (3.11), we can form a beamforming vector of power P_i from any arbitrary vector $\mathbf{u}_i \in \mathbb{C}^{N\times 1}$ by

$$\mathbf{w} = \sqrt{P_i} \cdot \frac{\mathbf{u}_i}{\sqrt{(1/2)\mathbf{u}_i^H \mathbf{A}_i \mathbf{u}_i}} \ . \tag{3.18}$$

The instantaneous SNR (3.17) can be written as

$$\gamma_i(\mathbf{u}_i) = \Gamma_i \frac{\mathbf{u}_i^H \mathbf{H}_{\text{mc}}^H \mathbf{H}_{\text{mc}} \mathbf{u}_i}{\mathbf{u}_i^H \mathbf{A}_i \mathbf{u}_i} \ , \tag{3.19}$$

where $\Gamma_i = 2P_i/N_0$ is the average input SNR with respect to the power metric P_i. Since $\mathbf{A}_i$ is a positive-definite Hermitian matrix, it has Hermitian positive-definite square root $\mathbf{A}_i^{1/2}$. Substituting $\mathbf{u}_i = \mathbf{A}_i^{-1/2}\mathbf{y}_i$, we obtain

$$\gamma_i(\mathbf{y}_i) = \Gamma_i \frac{\mathbf{y}_i^H \mathbf{A}_i^{-1/2} \mathbf{H}_{\text{mc}}^H \mathbf{H}_{\text{mc}} \mathbf{A}_i^{-1/2} \mathbf{y}_i}{\mathbf{y}_i^H \mathbf{y}_i}. \tag{3.20}$$

The optimal instantaneous SNR is therefore given by

$$\gamma_i^o \equiv \max_{\mathbf{w}:(1/2)\mathbf{w}^H \mathbf{A}_i \mathbf{w} = P_i} \gamma(\mathbf{w}) = \max_{\mathbf{u}_i} \gamma_i(\mathbf{u}_i) = \max_{\mathbf{y}_i} \gamma_i(\mathbf{y}_i) = \Gamma_i \Lambda_{\max,i} \ , \tag{3.21}$$

with the equality if $\mathbf{y}_i$ is the eigenvector associated with $\Lambda_{\max,i}$, where $\Lambda_{\max,i}$ is the largest eigenvalue of $\mathbf{A}_i^{-1/2}\mathbf{H}_{\rm mc}^H\mathbf{H}_{\rm mc}\mathbf{A}_i^{-1/2}$ and represents the effective array gain in the presence of mutual coupling. Since $\mathbf{AB}$ and $\mathbf{BA}$ have the same eigenvalues, we can also take $\Lambda_{\max,i}$ to be the largest eigenvalue of $\mathbf{H}_{\rm mc}^H\mathbf{H}_{\rm mc}\mathbf{A}_i^{-1}$.

For power metric P_1, the optimal transmission scheme can be simplified using the fact that $\mathbf{A}_1 = \mathbf{I}$. Then the optimal instantaneous SNR is

$$\gamma_1^o \equiv \max_{\mathbf{w}:(1/2)\mathbf{w}^H\mathbf{w}=P_1} \gamma(\mathbf{w}) = \Gamma_1\Lambda_{\max,1} \ , \tag{3.22}$$

where $\Lambda_{\max,1}$ is the largest eigenvalue of $\mathbf{H}_{\rm mc}^H\mathbf{H}_{\rm mc}$, and the optimal $\mathbf{w}$ is similar in form to the uncoupled case (2.10), performance however may be quite different due to differences in the statistical distribution of $\mathbf{H}_{\rm mc}$. Note that the conventional MRC transmission strategies in [24] and [90] are no longer optimal for the power measures P_2 and P_3.

3.4 Outage Probability

In this section, we derive outage probabilities of the optimal instantaneous SNRs γ_i^o, $i = 1, 2, 3$. We consider not only the MIMO system with multi-antenna receiver but also the MISO system with single-antenna receiver. Both system are assumed to employe coupled transmit antenna array.

3.4.1 One Receive Antenna

For one receive antenna ($M = 1$), observe that $\mathbf{H}_{\rm mc}^H \mathbf{H}_{\rm mc} \mathbf{A}_i^{-1}$ has only one non-zero eigenvalue is given by the quadratic form

$$\Lambda_{{\rm max},i} = \mathbf{H}_{\rm mc} \mathbf{A}_i^{-1} \mathbf{H}_{\rm mc}^H = \mathbf{H}_{\rm w} \mathbf{\Sigma}_i \mathbf{H}_{\rm w}^H \quad (M = 1) \tag{3.23}$$

where $\mathbf{\Sigma}_i = \mathbf{R}_{\rm T}^{1/2} \mathbf{C}_{\rm T} \mathbf{A}_i^{-1} \mathbf{C}_{\rm T}^H \mathbf{R}_{\rm T}^{1/2}$ and $\mathbf{H}_{\rm w} \sim \mathcal{CN}(\mathbf{0}, \mathbf{I})$. The pdfs of random quadratic forms of this type were derived in [91]: When the non-zero eigenvalues $\lambda_1, \ldots, \lambda_N$ of $\mathbf{\Sigma}_i$ are identical and denoted as λ, $\Lambda_{{\rm max},i}$ follows the Gamma distribution with cdf

$$F_{\Lambda_{\rm max}}^{(1)}(y) = \frac{p(N, y/\lambda)}{(N-1)!} \tag{3.24}$$

where $p(n, y)$ is the lower incomplete gamma function (2.13).

When the non-zero eigenvalues $\lambda_1, \ldots, \lambda_N$ of $\mathbf{\Sigma}_i$ are distinct, the cdf of $\Lambda_i^{\rm max}$ is given as [91],

$$F_{\Lambda_{\rm max}}^{(1)}(y) \;=\; \sum_{n=1}^{N} \frac{\lambda_n^{N-1}}{\prod_{k \neq n} (\lambda_n - \lambda_k)} \left(1 - e^{-y/\lambda_n}\right) \tag{3.25}$$

Using (3.24) and (3.25), the outage probability for power metric P_i, $i = 1, 2, 3$, is given by

$$P_{\rm out}(\tau) \stackrel{\triangle}{=} \Pr\{\gamma_i^o < \tau\} = F_{\Lambda_{\rm max}}^{(1)}(\tau/\Gamma_i) \tag{3.26}$$

where τ is a non-negative threshold. We may again take $\mathbf{\Sigma}_i = \mathbf{C}_{\rm T}^H \mathbf{R}_{\rm T} \mathbf{C}_{\rm T} \mathbf{A}_i^{-1}$ above, since it has the same non-zero eigenvalues as $\mathbf{R}_{\rm T}^{1/2} \mathbf{C}_{\rm T} \mathbf{A}_i^{-1} \mathbf{C}_{\rm T}^H \mathbf{R}_{\rm T}^{1/2}$.

Finally, we note that $\mathbf{A}_2 = \mathbf{C}_{\rm T}^H {\rm Re}\{\mathbf{Z}_{\rm A}^{-1}\} \mathbf{C}_{\rm T}$ will yield $\mathbf{\Sigma}_2 = \mathbf{R}_{\rm T} ({\rm Re}\{\mathbf{Z}_{\rm A}^{-1}\})^{-1}$ if the coupling matrix $\mathbf{C}_{\rm T}$ is invertible. This observation suggests that the outage performance for power measure P_2 does not depend on the matching networks.

3.4.2 Multiple Receive Antennas

Formulas for outage become significantly more complex for $M \geq 1$. Nevertheless, we can still obtain closed-form expressions using the results of [54, 55, 57]. When matrix $\mathbf{\Sigma}_i$ has identical eigenvalues as $\lambda_1 = \ldots = \lambda_N = \lambda$ and $\mathbf{\Sigma}_i = \lambda \mathbf{I}$, the cdf of $\Lambda_{\max,i} = \Lambda$ reduces to the result of SU-MIMO MRC over i.i.d. Rayleigh fading channel (2.12):

$$F^{(2)}_{\Lambda_{\max}}(y) \;=\; \frac{\det[\Psi(y)]}{\prod_{k=1}^{s} \Gamma(t-k+1)\Gamma(s-k+1)} \;. \tag{3.27}$$

When $0 < \lambda_1 < \ldots < \lambda_N$ are the distinct eigenvalues of $\mathbf{\Sigma}_i$, the cdf of $\Lambda_{\max,i}$ is equivalent to the result of SU-MIMO MRC over semi-correlated Rayleigh fading channel (2.14)

$$F^{(2)}_{\Lambda_{\max}}(y) \;=\; \frac{\det[\mathbf{\Delta}(y)]}{\det[\mathbf{V}] \cdot \prod_{i=1}^{s}(m-i)!} \tag{3.28}$$

Details of these two cdf expressions are given in Section 2.2.2. Using (3.27) and (3.28), the outage probability for power P_i is similar to (3.26),

$$P_{\text{out}}(\tau) = F^{(2)}_{\Lambda_{\max}}(\tau/\Gamma_i) \tag{3.29}$$

where $\lambda_1, \ldots, \lambda_N$ are the non-zero eigenvalues of $\mathbf{\Sigma}_i = \mathbf{C}_{\text{T}}^H \mathbf{R}_{\text{T}} \mathbf{C}_{\text{T}} \mathbf{A}_i^{-1}$. As noted above, the outages for power measure P_2 does not depend on the matching networks if the coupling matrix $\mathbf{C}_{\text{T}}$ is invertible.

3.5 Numerical Results

In the previous sections, we presented the optimal MRC transmission strategies for three different input power constraints as well as formulas for the resulting outage

probabilities. In this section, we give numerical examples which illustrate the behavior of these formulas.

We consider a transmit array consisting of N half-wavelength dipoles spaced a distance d apart. Each dipole has radius $10^{-3}\lambda$, where λ is the signal wavelength. For each d, the array impedance $\mathbf{Z}_{\rm A}$ and signal correlation matrix $\mathbf{R}_{\rm T}$ were evaluated numerically, as described in [25]. Briefly, the array impedance $\mathbf{Z}_{\rm A}$ and radiation pattern were estimated using the *Numerical Electromagnetics Code* (NEC) [2], a program based on the Method of Moments. The radiation pattern was then used to estimate $\mathbf{R}_{\rm T}$ numerically for a superposition of 32 equal-power multipath components equally spaced about the array. Further details may be found in [25].

The signal is received by $M = 1$ or 2 receive antennas spaced far enough apart so as to be uncoupled and uncorrelated. The source impedances are also uncoupled, so $\mathbf{Z}_{\rm S}$=diag$(z_0, \ldots, z_0)$ where $z_0 = 50\Omega$ is the characteristic impedance.

As noted earlier, a matching network is used to efficiently transfer power from the source to the transmit antennas. Here we consider two different choices of matching. In the *multiport match* [59] and [93], also known as *Hermitian match* [42] , a network $\mathbf{Z}_{\rm M}$ is chosen $\mathbf{Z}'_{\rm A}$ in (3.5) conjugate-matched to the source impedance: $\mathbf{Z}'_{\rm A} = \mathbf{Z}_{\rm S}^H$, which leads to maximum power transfer to the antennas. A reciprocal network that implements this match is

$$\mathbf{Z}_{\rm M}^{\rm mm} = -\begin{bmatrix} j\mathbf{X}_{\rm A} & j\sqrt{z_0}\mathbf{R}_{\rm A}^{1/2} \\ j\sqrt{z_0}\mathbf{R}_{\rm A}^{1/2} & \mathbf{0} \end{bmatrix} \tag{3.30}$$

where $r_0 = {\rm Re}\{z_0\} = 50\Omega$, $\mathbf{X}_{\rm A} = {\rm Im}\{\mathbf{Z}_{\rm A}\}$ and $\mathbf{R}_{\rm A} = {\rm Re}\{\mathbf{Z}_{\rm A}\}$ are the reactance and resistance matrices of antenna array, respectively. From a equivalent viewpoint, multiport match also satisfies the condition $\mathbf{Z}'_{\rm S} = \mathbf{Z}_{\rm A}^H$.

While the Hermitian match is optimal, it can be difficult to realize in practice. We therefore also consider a simpler, suboptimal type of matching, called *self-matching* [59], in which each source is connected to a single dipole using the matching that is optimal for uncoupled antennas: $[\mathbf{Z}'_{\mathrm{S}}] = \mathrm{diag}([\mathbf{Z}_{\mathrm{A}}]^*)$. A reciprocal network that implements this match is

$$\mathbf{Z}_{\mathrm{M}}^{\mathrm{sm}} = -\begin{bmatrix} j\mathbf{X}_{\mathrm{AS}} & j\sqrt{r_0}\mathbf{R}_{\mathrm{AS}}^{1/2} \\ j\sqrt{r_0}\mathbf{R}_{\mathrm{AS}}^{1/2} & \mathbf{0} \end{bmatrix} \tag{3.31}$$

where $\mathbf{Z}_{\mathrm{AS}} = \mathrm{diag}(\mathbf{Z}_{\mathrm{A}})$, $\mathbf{R}_{\mathrm{AS}} = \mathrm{Re}\{\mathbf{Z}_{\mathrm{AS}}\}$ and $\mathbf{X}_{\mathrm{AS}} = \mathrm{Im}\{\mathbf{Z}_{\mathrm{AS}}\}$. From the circuit point of view, the $2N$-port self-matching network is formed by N parallel 2-port networks. Note that these two matching are equivalent, i.e., $\mathbf{Z}_{\mathrm{M}}^{\mathrm{mm}} = \mathbf{Z}_{\mathrm{M}}^{\mathrm{sm}}$ when antennas are uncoupled since $[\mathbf{Z}_{\mathrm{A}}]_{mn} = 0$ implies $\mathbf{R}_{\mathrm{A}} = \mathbf{R}_{\mathrm{AS}}$.

Figure 3.2 shows the outage probabilities (3.26) for $M = 1$ and (3.29) for $M = 2$ with antenna spacing $d = 0.3\lambda$ for each of the three input power constraints. Also shown for comparison are the case of i.i.d. fading path gains and path gains with spatial correlation (3.14) but no coupling (obtained by setting $[\mathbf{Z}_{\mathrm{A}}]_{mn} = 0$ for $m \neq n$). From Figure 3.2(a), the two outages with coupling lie on the right of both the i.i.d. case and the no-coupling case. Thus coupling tends to improve performance at this spacing relative to the other two uncoupled cases. This occurs because the coupling matrix $\mathbf{C}_{\mathrm{T}}$ in (3.26) and (3.29) tends to whiten the Clarke covariance $\mathbf{R}_{\mathrm{T}}$; a similar phenomenon has been observed in MRC receive diversity [85]. This improvement is also achieved for radiated power P_2 in Figure 3.2(b) and for the actual power P_3 in Figure 3.2(c). Another key observation is that multiport-matching outperforms self-matching constantly about 0.5 dB for power measure P_1 and P_3. This is intuitive since self-matching may not transfer power to the antennas for small d as efficiently

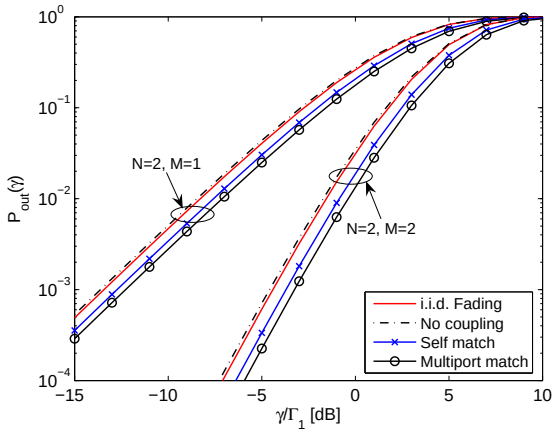

(a) Power measure P_1

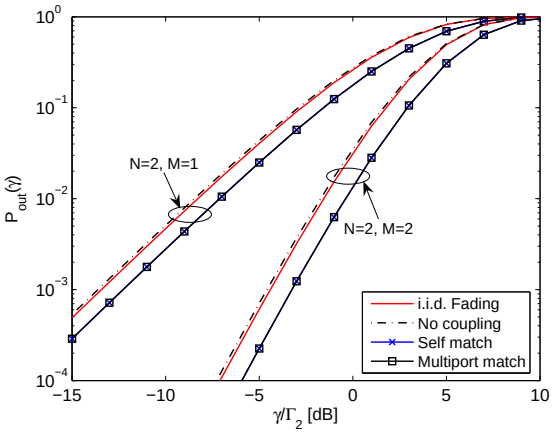

(b) Power measure P_2

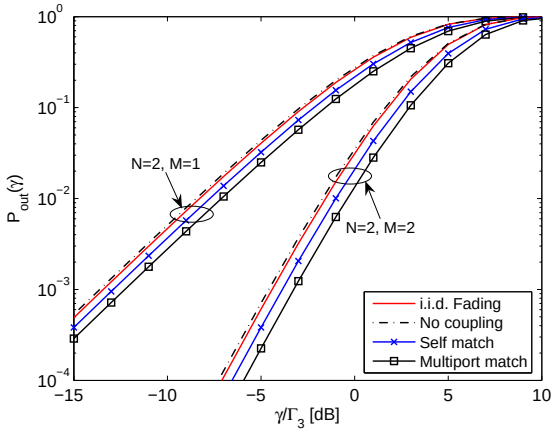

(c) Power measure P_3

Figure 3.2: Outage probabilities vs. normalized SNR with $N = 2$, $M = 1$ or 2 and spacing $d = 0.3\lambda$ for three different power measures.

as multiport-matching. However, these two achieve the same outage for P_2 as expected. Effects of different matching networks are not distinguishable on the system performance since P_2 is measured after the matching network in Figure 3.1 and does not reflect how efficiently the power is transferred to the antenna array.

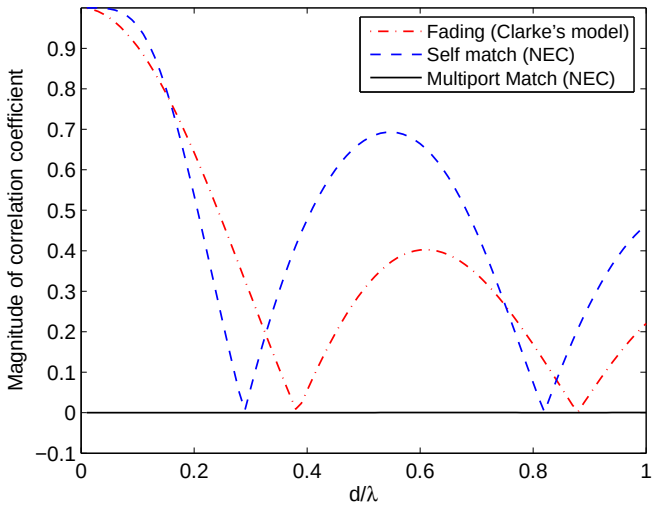

Figure 3.3: Magnitude of correlation coefficients vs. antenna spacing d/λ.

The correlation coefficient between two correlated and/or coupled antennas versus the antenna spacing from 0.01 λ to 1 λ are shown in Figure 3.3. The correlation for no coupling case is obtained by Clarke's model (3.14), which may be altered by coupling matrix $\mathbf{C}_{\mathrm{T}}$ using different matching networks. From this figure, we can see that self-matching tends to decorrelate the Clarke covariance when antenna spacing is near 0.3λ while multiport-matching can completely decorrelate the antenna array at any spacings. This is due to the fact that the multiport-matching is chosen such that $\mathbf{Z}'_{\mathrm{A}} = \mathbf{Z}_{\mathrm{S}} = z_0\mathbf{I}$, which means the coupled antenna array can be perfectly decoupled. This result suggests that mutual coupling does not simply result in spatial correlation. In fact, mutual coupling and spatial correlation tend to cancel each other at certain antenna spacings and not others.

Further insights can be gained by examining the effect of transmit antenna

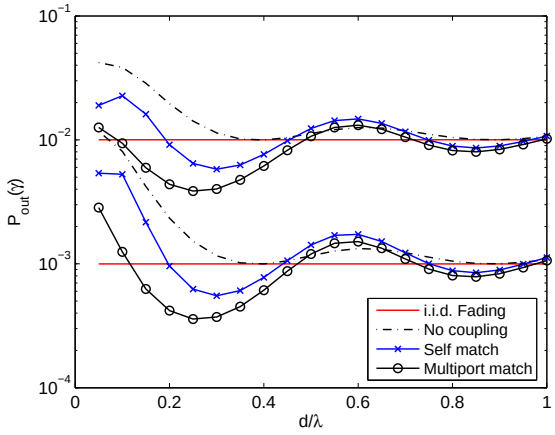

(a) Power measure P_1

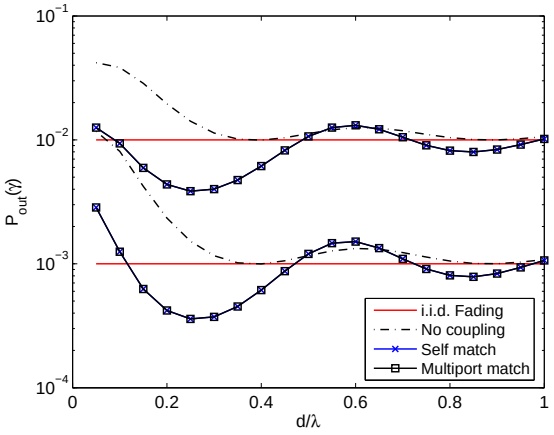

(b) Power measure P_2

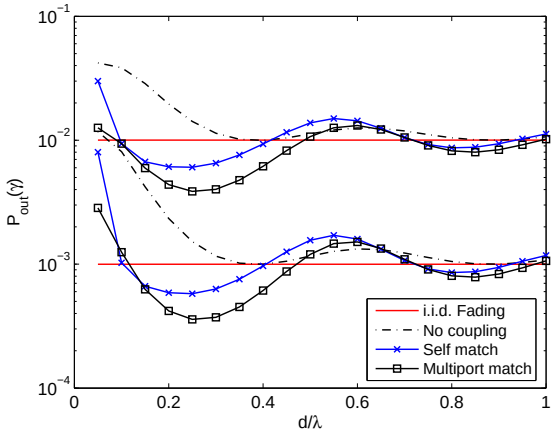

(c) Power measure P_3

Figure 3.4: Outage probabilities vs. antenna spacings d/λ with $N = 2$, $M = 2$ at two outage level for three different power measures.

spacing on the outage probability. Figure 3.4 plots the outage probability versus spacing d/λ for fixed SNR and each of the three power metrics. Each plot displays *two* different SNRs which are chosen such that the outage of the i.i.d. case is close to the values 10^{-2} and 10^{-3}, respectively. In Figure 3.4(a), we see that the coupled

system with power P_1 outperforms the i.i.d. and no-coupling systems for all spacings $0.2\lambda \leq d \leq 0.45\lambda$ with self-matching and $0.15\lambda \leq d \leq 0.45\lambda$ with multiport-matching. The improvement is again similar for the radiated power P_2, as shown in Figure 3.4(b), and for the delivered power P_3, as shown in Figure 3.4(c). In particular, we note that, for all power measures considered here, coupling improves the outage for all $0.2\lambda \leq d \leq 0.45\lambda$, with the greatest improvement occurring around $d \approx 0.25\lambda - 0.3\lambda$.

Wallace and Jensen [93] suggested the explanation that closely-spaced antennas can actually radiate or collect more power than widely separated ones (i.i.d.) because part of the power scattered by each transmit antenna can be recaptured and re-radiated by the adjacent antenna, especially when appropriate matching is implemented. However, this benefit may be dismissed when antennas are extremely strongly coupled which can be observed at $d \leq 0.1\lambda$. At this spacing, higher outage (i.e., lower reliability) occurs in the SU-MIMO MRC system and should be avoided in the practical use. Both the coupling and no-coupling cases tend to converge to the i.i.d. case as antenna spacing increases, which is due to the following fact. When antennas are placed far apart enough, both the correlation coefficient in (3.14) and the mutual impedance of antenna array tend to be zero, which means uncorrelated and uncoupled.

SU-MIMO MRC is one of MIMO diversity techniques and normally adopts the diversity gain as one of the performance metrics. Here diversity gain is defined as the SNR difference between diversity system and non-diversity system (e.g. SISO system with $N = M = 1$) at a 1% probability of outage, which indicates the power savings without a performance loss. Figure 3.5 shows the diversity gain as a function of antenna spacing $0.5\lambda \leq d \leq \lambda$ for $N = M = 2$ system with each of the three power

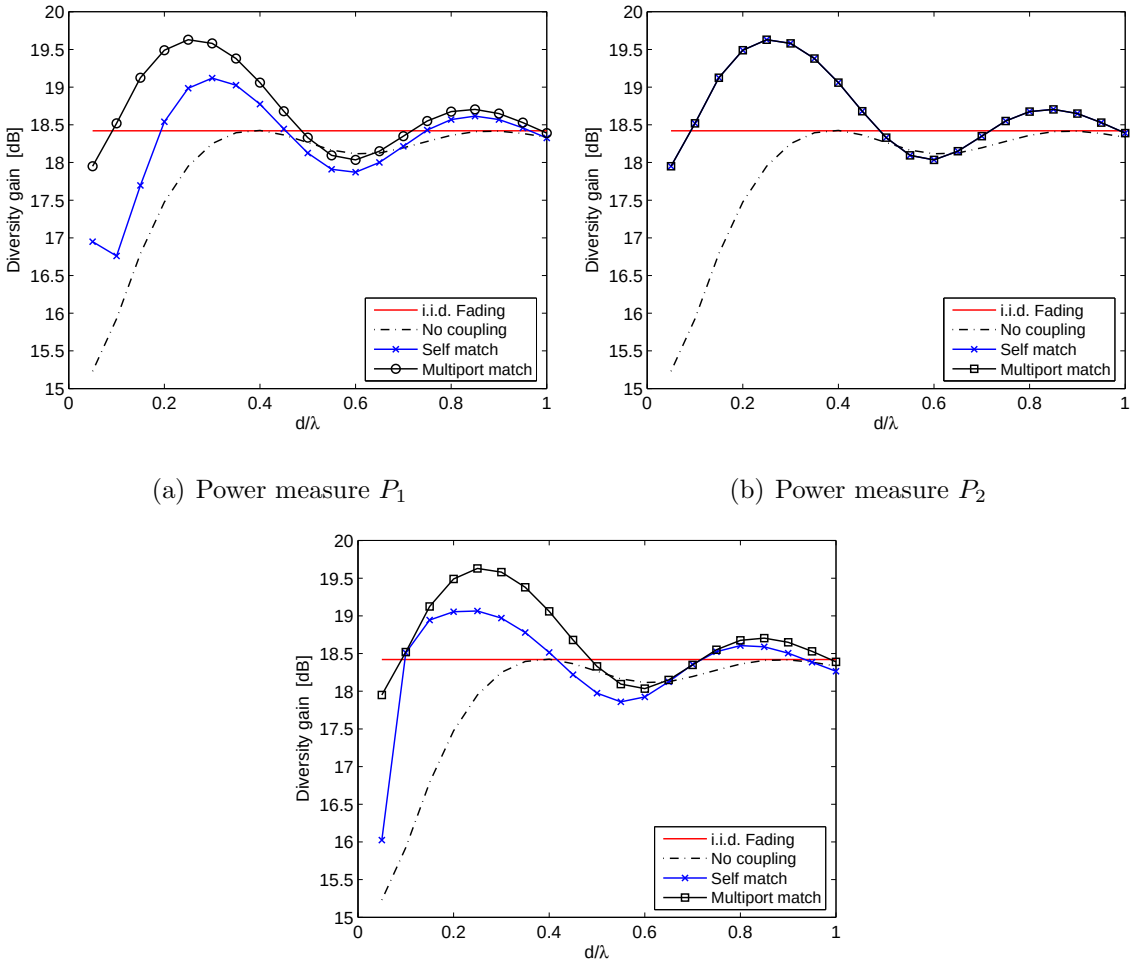

(a) Power measure P_1

(b) Power measure P_2

(c) Power measure P_3

Figure 3.5: Diversity gain vs. antenna spacings d/λ with $N = 2$, $M = 2$ at 1% outage level for three different power measures.

metrics. It can be observed similarly to Figure 3.4 that coupling achieves even higher diversity all $0.2\lambda \leq d \leq 0.45\lambda$ compared with the other two uncoupled cases, with the highest gain occurring around $d \approx 0.25\lambda - 0.3\lambda$ about 1.2 dB higher than i.i.d. case. The results suggest large power savings by using appropriate matching networks in

the presence of mutual coupling.

3.6 Conclusion and Discussion

A model for a compact diversity transmitter is presented with coupled dipole antenna array, matching network and voltage sources. Using this model, we investigated the effect of transmitter correlation, mutual coupling and matching network on SU-MIMO MRC systems. We presented optimal MRC transmission schemes for three input power metrics widely used in the literature as well as the formulas for the resulting outage probabilities. Numerical results we shown in the previous section suggest the following findings:

First, regardless of the power measure considered and matching networks used, most of the performance benefits of SU-MIMO MRC can be obtained with transmit antennas spaced as close as $0.2\lambda - 0.3\lambda$ apart. In this range, spatial correlation and mutual coupling tend to cancel each other, so that performance close to (or better than) the i.i.d. case can be obtained even when the antenna elements are strongly coupled.

Second, matching performance should be evaluated according to the specified power measure. For traditional power metric P_1 and actual power metric P_3, optimal multiport-matching outperforms suboptimal self-matching throughout the whole range of antenna spacings. Since the radiated power metric P_2 is measured posterior to the matching networks, then both self-matching and multiport matching are not distinguishable for the outage performance. Thus, appropriate power measure and matching network are helpful in the design of compact SU-MIMO MRC systems.

There may exist a large family of matching networks which are noiseless, lossless and reciprocal impedance networks. Multiport matching and self-matching are two specific forms and suitable for narrow-band systems. Multiport matching has the capability of completely decoupling the antenna array whose impedance may vary with frequency, which makes system bandwidth extremely narrow at small antenna separations [59]. Thus, from a practical point of view, we need to consider the bandwidth issue when designing a good matching network for wide-band compact MIMO systems, which may be one of future directions in our work.

Note that $0.2\lambda - 0.3\lambda$ corresponds to $3.0 - 4.5$ cm at 2 GHz[3] and $1.2 - 1.8$ cm at 5 GHz[4], which seems plausible even within the size constraints of a mobile handset or a wireless LAN card.

[3]Some mobile communication systems are designed to operate at or near 2 GHz, such as UMTS.

[4]A wireless LAN antenna/card which can transmit/receive RF signals in a high frequency band (e.g., 5 GHz) and a low frequency band (e.g., 2.4 GHz).

Chapter 4

Imperfect CSI for SU-MIMO MRC with Compact Transmitter

Multiple antennas packed in compact transceiver may cause mutual coupling and result in system impairment. In Chapter 3, we investigated the effects of mutual coupling on single-user MIMO maximum-ratio combining systems and presented optimal beamforming schemes when assuming full channel knowledge available at both the transmitter and receiver. As noted in Chapter 1, another impairment related with availability and accuracy of channel state information may degrade the system performance, which motives our study on the effects of imperfect channel estimation and limited feedback. In this chapter, by relaxing the assumption of perfect CSI for the system, we consider two separated problems:

First, the limited feedback design for SU-MIMO MRC system with mutual coupling by assuming perfect CSI at the receiver, i.e., perfect channel estimation;

Second, the effect of channel estimation error on the same system with the

assumption of perfect feedback.

4.1 Limited Feedback for SU-MIMO MRC

The optimal instantaneous SNR at the receiver output for a input power constraint P_i, $i = 1, 2, 3$, is given by (3.21)

$$\gamma_i^o \equiv \max_{\mathbf{w}:(1/2)\mathbf{w}^H\mathbf{A}_i\mathbf{w}=P_i} \gamma(\mathbf{w}) = \max_{\mathbf{u}_i} \gamma_i(\mathbf{u}_i) = \max_{\mathbf{y}_i} \gamma_i(\mathbf{y}_i) = \Gamma_i \Lambda_{\max,i} \ , \qquad (4.1)$$

with the last equality if the signal is transmitted through the largest eigenmode of effective channel $\mathbf{H}_{\text{mc}}$ associated with eigenvalue $\Lambda_{\max,i}$. From (4.1), we know that the optimal transmission is completely determined by two mutually dependent amounts: channel state information and beamforming vector, which results in two consequent approaches for limited feedback. In the first approach, the quantized channel is fed back to help the transmitter design the beamforming scheme [73]. Since the SU-MIMO MRC strategy [90], [24] allows the receiver to directly design the beamforming vectors, then the problem could be approached differently by feeding back quantized beamforming vector. The receiver now, in some sense, controls how the signal is adapted to the channel. This makes sense because the receiver will nearly always have higher quality CSI than the transmitter [66].

In this section, following the idea of finite codebook design correlated Rayleigh channels [65] and [98], we present the codebook design for SU-MIMO MRC systems with mutual coupling.

4.1.1 Codebook Design

Consider a SU-MIMO MRC system with N coupled transmit antennas and M uncorrelated and uncoupled receive antennas in a narrow-band Rayleigh fading environment. The same system models for coupled transmitter, wireless MIMO channel, receiver and noise in Chapter 3 is used in this study. Then transmitter coupling, matching and correlation are lumped into the effective channel matrix $\mathbf{H}_{\text{mc}} = \mathbf{H}_{\text{w}}\mathbf{R}_{\text{T}}^{1/2}\mathbf{C}_{\text{T}}$ where $\mathbf{H}_{\text{w}} \in \mathbb{C}^{M\times N}$ is the channel matrix with i.i.d. entries $\mathcal{CN}(0,1)$, $\mathbf{R}_{\text{T}}$ and $\mathbf{C}_{\text{T}}$ are the transmitter correlation and coupling matrices, respectively. We assume the receiver has the full knowledge of $\mathbf{H}_{\text{mc}}$.

Let $\mathcal{C} = \{\mathbf{c}_1, \ldots, \mathbf{c}_K\}$ denote the codebook optimized for the uncorrelated fading channel using either criterion in (2.16), (2.17) and etc, where $K = 2^B$ and B is the number of feedback bits. For input power constraint P_i, $i = 1, 2, 3$, the rows of $\mathbf{H}_{\text{mc}}$ are independent complex Gaussian vectors and distributed as $\mathcal{CN}(\mathbf{0}, \mathbf{\Sigma}_i)$ where

$$\mathbf{\Sigma}_i = \mathbf{A}_i^{-1/2}\mathbf{C}_{\text{T}}^H\mathbf{R}_{\text{T}}\mathbf{C}_{\text{T}}\mathbf{A}_i^{-1/2} \ .$$

Similar to [65] and [98], a good codebook $\mathcal{Y}_i = \{\mathbf{y}_1, \ldots, \mathbf{y}_K\}$ for this correlated channel can be designed via the construction

$$\mathbf{y}_k = \frac{\mathbf{\Sigma}_i^{H/2}\mathbf{c}_k}{||\mathbf{\Sigma}_i^{H/2}\mathbf{c}_k||_2}, \quad k = 1, \ldots, K \ . \tag{4.2}$$

Note that this codebook is designed for the interim unit-norm beamforming vector $\mathbf{y}$ used in (3.20). Using the relationship between $\mathbf{y}$ and $\mathbf{w}$ in Section 3.3, the codebook $\mathcal{W}_i = \{\mathbf{w}_1, \ldots, \mathbf{w}_K\}$ for the final beamformer $\mathbf{w}$ can be designed by

$$\mathbf{w}_k = \sqrt{P_i} \cdot \frac{\mathbf{A}_i^{-1/2}\mathbf{y}_k}{\sqrt{(1/2)\mathbf{y}_k^H\mathbf{y}_k}} = \sqrt{2P_i}\mathbf{A}_i^{-1/2}\mathbf{y}_k, \quad k = 1, \ldots, k \ . \tag{4.3}$$

At this point, it is worthwhile to pause and consider the different assumptions that underlie the design of codebooks $\mathcal{W}_i$, $i = 1, 2, 3$. Most studies of mutual coupling in MIMO systems assume that coupling alters only the correlation of the fading path gains and not the transmitted power. Here this assumption leads to codebook $\mathcal{W}_1$, which is designed for the conventional power P_1. However, coupling can profoundly alter the power radiated or captured by an array (see Chapter 3 for details), and P_1 does not correspond to any actual power in the transmitter. Note that changing the power metric alters the mathematics of the SU-MIMO MRC optimization, which seeks to maximize the SNR at the receiver. The codebooks $\mathcal{W}_2$ and $\mathcal{W}_3$ are intended to address this problem, by optimizing performance as a function of the actual power radiated by the transmitter P_2 or the power delivered by the source P_3 [28].

4.1.2 Codebook Performance

In the last section, we considered the design of codebooks for SU-MIMO MRC systems with limited feedback for three different input power metrics. In this section, we give numerical examples which illustrate the behavior of these codebooks.

We consider a transmit array consisting of $N = 2$ or 3 half-wavelength dipoles spaced a distance d apart. Each dipole has radius $10^{-3}\lambda$ where λ is the signal wavelength. For each d, the array impedance $\mathbf{Z}_{\mathrm{A}}$ and signal correlation matrix $\mathbf{R}_{\mathrm{T}}$ were evaluated numerically, as described in [25]. We assume the M receive antennas are spaced far enough apart so as to be uncoupled and uncorrelated. The source impedances are also uncoupled with impedance matrix $\mathbf{Z}_{\mathrm{S}} = \mathrm{diag}(50, \ldots, 50)\ \Omega$.

For the power metric P_i, $i = 1, 2, 3$, the performance of SU-MIMO MRC with

the codebook $\mathcal{W}_i$ is measured by the outage probability

$$P_{\text{out}}(\tau) = \Pr\left\{\max_{\mathbf{w}\in\mathcal{W}_i} \gamma(\mathbf{w} < \tau)\right\} \ , \tag{4.4}$$

where $\gamma(\mathbf{w})$ is given in (3.17). To contrast, the outage probability for full CSI at both the transmitter and receiver is defined in (3.26) and (3.29) as

$$P_{\text{out}} = \Pr\left\{\gamma^o \leq \tau\right\} \ . \tag{4.5}$$

The fact that $\max_{\mathbf{w}\in\mathcal{W}_i} \gamma(\mathbf{w} < \gamma^0$ implies the performance degradation due to limited feedback.

In Figure 4.1, these outage probabilities are plotted versus antenna spacing d/λ for $N = M = 2$ SU-MIMO system at a fixed SNR for each of three power measures. The SNR has been chosen so that the outage of the i.i.d. case with full CSI (i.e unlimited feedback) is 10^{-2} (1% outage). The figure plots the performance of codebooks $\mathcal{W}_i$ for $B = 2$ and 3 feedback bits, both constructed as described in Section 4.1.1 from codes $\mathcal{C} = \{\mathbf{c}_1, \ldots, \mathbf{c}_K\}$ optimized for the *uncorrelated* channel using Grassmannian line packing [64]. Also shown for comparison is the optimal outage probability of the full CSI case (4.1) with correlation and coupling; closed-form formulas for this outage probability were given in Section 3.4. Finally, observe that each curve is plotted for both multiport and self-matching. From the figure for all three power measures, we see that SU-MIMO MRC with limited feedback (LF) can achieve performance comparable to the i.i.d. case even when the transmit antennas are strongly coupled ($0.2\lambda \leq d \leq 0.3\lambda$). Not surprisingly, limited feedback leads to a small loss in performance relative to the full CSI case, and the loss is greatest when the antennas are close together. Further note that multiport matching outperforms self-matching for all codebooks and all antenna spacings when power metrics P_1 and

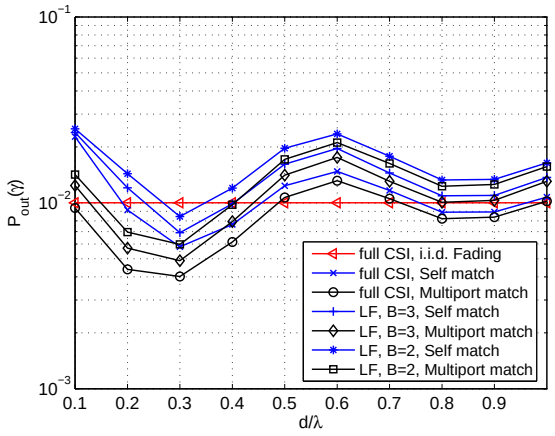

(a) Power measure P_1

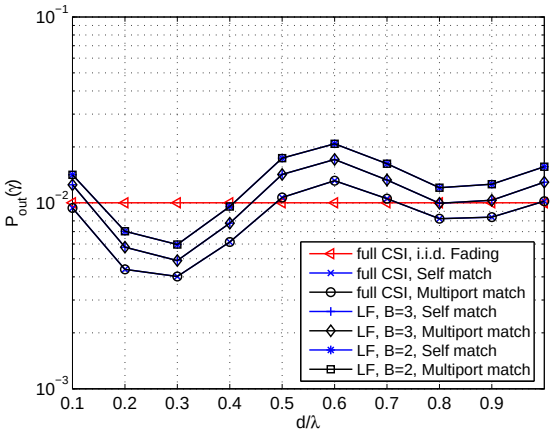

(b) Power measure P_2

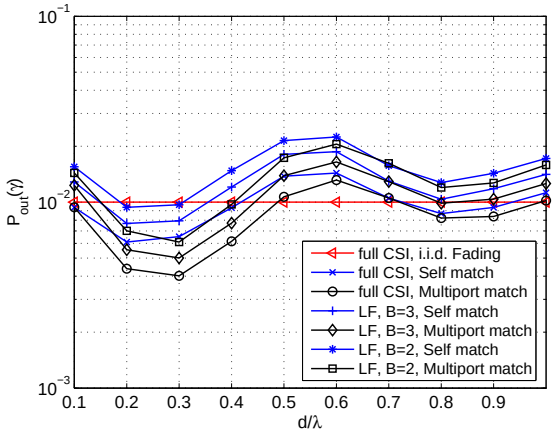

(c) Power measure P_3

Figure 4.1: Outage probabilities vs. antenna spacings d/λ for $N = M = 2$ SU-MIMO MRC system with different feedback scenarios and power measures.

P_3 are considered. However, type of matching used has little impact on performance for power metric P_2. This is intuitive, since P_2 measures only the power radiated by the antennas and not how efficiently the power is delivered by the source. We conclude that performance close to (or better than) the i.i.d. case can be achieved

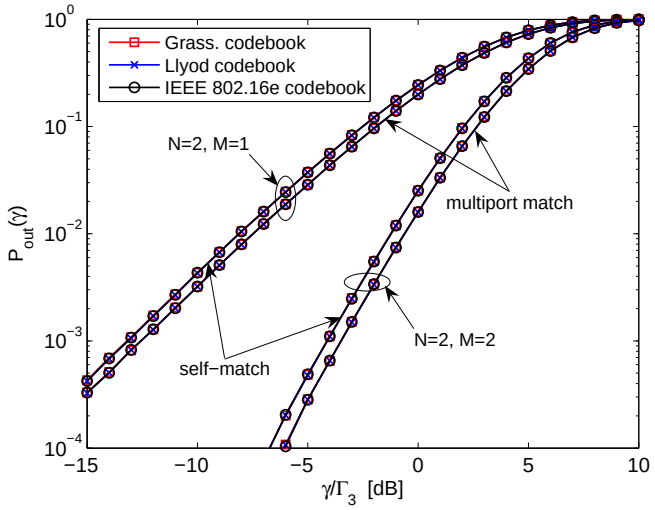

Figure 4.2: Outage probabilities for codebooks generated by three methods with power measure P_3, $B = 3$ and $d = 0.3\lambda$

Table 4.1: Grassmannian codebook for $N = 2$, $B = 3$ and $K = 8$

0.8393 - 0.2939i -0.1677 + 0.4256i	-0.3427 + 0.9161i 0.0498 + 0.2019i	-0.2065 + 0.3371i 0.9166 + 0.0600i	0.3478 - 0.3351i 0.2584 + 0.8366i
0.1049 + 0.6820i 0.6537 + 0.3106i	0.0347 - 0.2716i 0.0935 - 0.9572i	-0.7457 + 0.1181i -0.4553 - 0.4719i	-0.7983 + 0.3232i 0.5000 + 0.0906i

with $B = 2$ bits and antennas as close as 0.2λ apart.

Each codebook considered in this paper is derived from a codebook $\mathcal{C}$ optimized for the uncorrelated fading channel. As noted earlier, $\mathcal{C}$ can be designed by several different methods. Figure 4.2 investigates the impact of different choices of $\mathcal{C}$ on the outage probability of $\mathcal{W}_g$ for power measure P_3 and antenna spacing 0.3λ. The codebooks $\mathcal{W}_3$ are generated by three methods: Grassmannian line packing [64, Table III], Vector Quantization using Lloyd's algorithm [98] and the codebook $V(2, 1, 3)$

Table 4.2: Llyod (vector quantization) codebook for $N = 2$, $B = 3$ and $K = 8$

0.3918 + 0.4725i 0.7894	0.3086 - 0.2204i 0.9253	-0.2472 + 0.0029i 0.9690	0.9932 -0.0126 - 0.1156i
0.8489 0.5065 + 0.1510i	0.7915 -0.5965 + 0.1328i	0.7123 -0.3405 - 0.6137i	0.7580 -0.0739 + 0.6480i

Table 4.3: IEEE 802.16e-2005 codebook for $N = 2$, $B = 3$ and $K = 8$

1.0000 0	0.7940 -0.5801 + 0.1818i	0.7940 0.0576 + 0.6051i	0.7941 -0.2978 - 0.5298i
0.7941 0.6038 + 0.0689i	0.3289 0.6614 + 0.6740i	0.5112 0.4754 - 0.7160i	0.3289 -0.8779 - 0.3481i

listed in IEEE standard 802.16e-2005 [48, Table 298m], which are listed in Table 4.1, 4.2 and 4.3. Note the performances of these different codebooks are virtually indistinguishable over the range of this plot for both self-matching and multiport matching. Similar results were obtained for the power measures P_1 and P_2.

Finally, we consider the impact of using a codebook designed for the conventional power metric P_1, when the transmitted power is actually given by P_3. In Figure 4.3, we plot the outage of codebooks $\mathcal{W}_1$ and $\mathcal{W}_3$ with respect to the power generated by the source P_3. Both codebooks are derived from the $B = 2$ bits uncorrelated Grassmannian codebook [64, Table IV]. At 1% outage, $\mathcal{W}_1$ is about 1.0 dB worse than $\mathcal{W}_3$ for a 3×1 SU-MIMO system with self-matching, and about 0.5 dB worse for a 3×2 system. Larger performance differences occur at 0.1% outage. By contrast, note that $\mathcal{W}_1$ and $\mathcal{W}_3$ yield the same performance for the multiport matching. This is due to the fact that the multiport matching leads to a diagonal $\mathbf{A}_3 = a\mathbf{I}$,

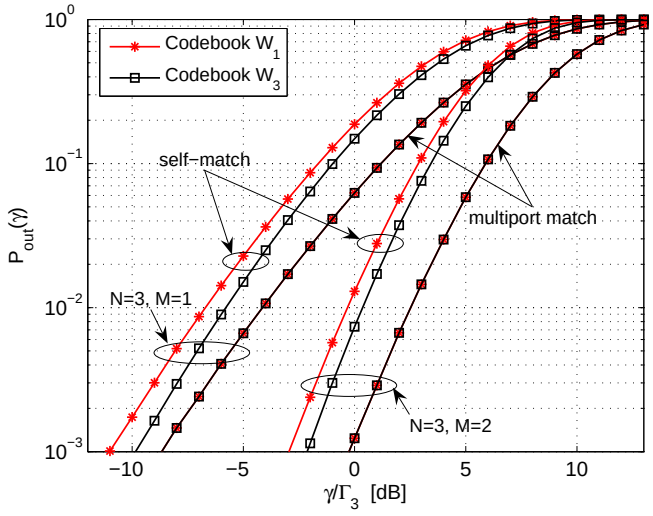

Figure 4.3: Outage probabilities for codebooks $\mathcal{W}_1$ and $\mathcal{W}_3$ with power measure P_3, $B = 2$ and $d = 0.2\lambda$

so that the power measures P_1 and P_3 are proportional.

Our results suggest the proposed codebooks can achieve near optimal performance with low computational complexity and relatively little feedback [65], [98]. The proposed codebooks can be constructed easily from codebooks designed for i.i.d. Rayleigh fading channels for any antenna spacing and correlation structure. For each power measure, numerical results suggest that most of the performance benefits of SU-MIMO MRC can be obtained with transmit antennas spaced as close as $0.2\lambda - 0.3\lambda$ using as few as $B = 2$ bits of feedback.

4.2 Imperfect Channel Estimation for SU-MIMO MRC

It has been shown in previous chapters that the channel knowledge is important to characterize the performance of MIMO beamforming systems. However, the performance will degrade if the channel state information is not perfect. Since perfect CSI is difficult to obtain in MIMO systems due to the large number of channel parameters to estimate at the receiver and to be fed back to the transmitter [102]. Section 4.1 introduced the limited feedback method to facilitate CSI at the transmitter when feedback link is restricted in bandwidth. In this section, we focus the accuracy of CSI and the way CSI is obtained at the receiver. CSI at the receiver (CSIR) is typically obtained via channel estimation. There is a rich literature on the performance of SU-MIMO MRC system in the presence of imperfect channel estimation [18], [80], [67] and [83]. Most of these prior studies, however, are limited to the uncorrelated Rayleigh fading channels and simply treated the signal component related with the channel estimation error as self-interference. We proceed our study by introducing a more realistic model of channel estimation of correlated fading channels. Then we consider the joint effect of channel correlation, estimation error and mutual coupling on SU-MIMO MRC system.

4.2.1 Channel Estimation

One of the most popular and widely used approaches to the MIMO channel estimation is the pilot or training based scheme which estimates the MIMO channels by the received data and the knowledge of training symbols [8], [41].

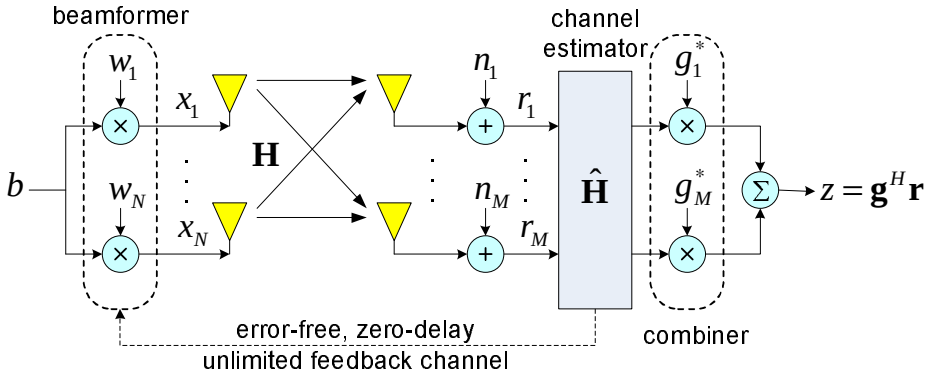

Figure 4.4: A $N \times M$ SU-MIMO MRC system in the presence of channel estimation error.

Once again, we consider a SU-MIMO MRC system with N coupled transmit antennas and M uncorrelated and uncoupled receive antennas in a narrow-band Rayleigh block-fading environment shown in Figure 4.4.

Assume the block fading duration is T symbols. During each transmission block, transmit antennas send L pilot symbols (usually $L > N$), followed by $T - L$ data symbols. Then the receiver uses the received symbols and the prior knowledge of pilot symbols to perform channel estimation. Combining the first L receive symbols in a $M \times L$ matrix, we have

$$\mathbf{Y} = \mathbf{H}\mathbf{X} + \mathbf{N} \ , \tag{4.6}$$

where $\mathbf{X} = [\mathbf{x}_1 \dots \mathbf{x}_L] \in \mathbb{C}^{N \times L}$ is the pilot matrix contains L pilot symbols $\{\mathbf{x}_l\}_{l=1}^{L}$, $\mathbf{H} = \mathbf{H}_{\mathrm{w}}\mathbf{R}_{\mathrm{T}}^{1/2} \in \mathbb{C}^{M \times N}$ is the channel matrix with transmit correlation $\mathbf{R}_{\mathrm{T}}$, and $\mathbf{N} = [\mathbf{n}_1 \dots \mathbf{n}_L] \in \mathbb{C}^{M \times L}$ is the noise matrix with each column modeled as independent AWGN $\mathsf{E}\left[\mathbf{n}_l\mathbf{n}_l^H\right] = N_0\mathbf{I}$, $l = 1, \dots, L$, and N_0 is the noise power spectral density.

Assuming the channel spatial correlation and the number of pilot symbols are

known at the receiver. The linear minimum mean square error (LMMSE) channel estimator is both unbiased and computationally efficient [83], which gives the channel estimation $\widetilde{\mathbf{H}}$ and estimation error $\mathbf{E}$ as [8],

$$\widetilde{\mathbf{H}} = \mathbf{Y}\left(\mathbf{X}^H\mathbf{R}_{\mathrm{T}}\mathbf{X} + N_0\mathbf{I}\right)^{-1}\mathbf{X}^H\mathbf{R}_{\mathrm{T}} \tag{4.7}$$

$$\mathbf{E} = \mathbf{H} - \widetilde{\mathbf{H}}\,. \tag{4.8}$$

Similar to the original channel matrix, both the channel estimation and error are zero-mean Gaussian random matrices and can be denoted as

$$\widetilde{\mathbf{H}} = \widetilde{\mathbf{H}}_{\mathrm{w}}\mathbf{R}_{\widetilde{\mathbf{H}}}^{1/2}, \quad \mathbf{E} = \mathbf{E}_{\mathrm{w}}\mathbf{R}_{\mathbf{E}}^{1/2} \tag{4.9}$$

where $\widetilde{\mathbf{H}}_{\mathrm{w}}$ and $\mathbf{E}_{\mathrm{w}}$ are uncorrelated with i.i.d. $\mathcal{CN}(0,1)$ entries, and correlation matrix of each is given by

$$\mathbf{R}_{\mathbf{E}} = \left(\mathbf{R}_{\mathrm{T}}^{-1} + \frac{1}{N_0}\mathbf{X}\mathbf{X}^H\right)^{-1} \tag{4.10}$$

$$\mathbf{R}_{\widetilde{\mathbf{H}}} = \mathbf{R}_{\mathrm{T}} - \mathbf{R}_{\mathbf{E}} \tag{4.11}$$

Equation (4.11) is obtained from the orthogonality property of LMMSE estimator [106].

Assume no feedback for the pilot symbols, then the orthogonal pilot symbols, i.e., $\mathbf{X}\mathbf{X}^H = (P_pL/N)\mathbf{I}$ is shown to minimizes the channel estimation MSE. Therefore the covariance matrix of the channel estimation error is given by

$$\mathbf{R}_{\mathbf{E}} = \left(\mathbf{R}_{\mathrm{T}}^{-1} + \frac{P_pL}{N_0N}\mathbf{I}\right)^{-1}\,, \tag{4.12}$$

where P_p is the total power per pilot transmission. Note that $\mathbf{R}_{\mathbf{E}}$ reduces to be $N_0N/(1+P_pL)\mathbf{I}$ when transmit antennas are spatially uncorrelated.

4.2.2 SU-MIMO MRC with Mutual Coupling

Joint effect of mutual coupling and imperfect channel estimation is considered in this section. Similar to Chapter 3, transmitter coupling and matching are taken into account by using coupling matrix $\mathbf{C}_{\mathrm{T}}$ to represent the effective channel matrix $\mathbf{H}_{\mathrm{mc}} = \mathbf{H}\mathbf{C}_{\mathrm{T}}$, which turns the problem into an equivalent form of estimating $\mathbf{H}_{\mathrm{mc}}$. By analogous estimation scheme in (4.7), the LMMSE estimator gives the effective channel estimation and estimation error respectively as

$$\widetilde{\mathbf{H}}_{\mathrm{mc}} = \widetilde{\mathbf{H}}\mathbf{C}_{\mathrm{T}}, \qquad \mathbf{E}_{\mathrm{mc}} = \mathbf{H}_{\mathrm{mc}} - \widetilde{\mathbf{H}}_{\mathrm{mc}} = \mathbf{E}\mathbf{C}_{\mathrm{T}} \tag{4.13}$$

Consider now the application of MRC to channel (3.16), subject to the input power constraint 3.11. The receiver employs a combiner of the form $z = \mathbf{w}^H\widetilde{\mathbf{H}}_{\mathrm{mc}}^H\mathbf{r}$, which gives the instantaneous SNR after post-processing is

$$\gamma(\mathbf{w}) \;=\; \frac{1}{N_0}\frac{\left|\mathbf{w}^H\widetilde{\mathbf{H}}_{\mathrm{mc}}^H(\widetilde{\mathbf{H}}_{\mathrm{mc}} + \mathbf{E}_{\mathrm{mc}})\mathbf{w}\right|^2}{\mathbf{w}^H\widetilde{\mathbf{H}}_{\mathrm{mc}}^H\widetilde{\mathbf{H}}_{\mathrm{mc}}\mathbf{w}} \tag{4.14}$$

We form a beamforming vector of power P_i, $i = 1, 2, 3$, in the same way from any arbitrary complex vector $\mathbf{u}_i \in \mathbb{C}^{N\times 1}$ as in (3.18):

$$\mathbf{w} = \sqrt{P_i}\cdot\frac{\mathbf{u}_i}{\sqrt{(1/2)\mathbf{u}_i^H\mathbf{A}_i\mathbf{u}_i}}\ . \tag{4.15}$$

The instantaneous SNR in the presence of channel estimation error then can be written as

$$\gamma_i^e(\mathbf{u}_i) = \Gamma_i\frac{\left|\mathbf{u}_i^H\widetilde{\mathbf{H}}_{\mathrm{mc}}^H(\widetilde{\mathbf{H}}_{\mathrm{mc}} + \mathbf{E}_{\mathrm{mc}})\mathbf{u}_i\right|^2}{\mathbf{u}_i^H\mathbf{A}_i\mathbf{u}_i\cdot\mathbf{u}_i^H\widetilde{\mathbf{H}}_{\mathrm{mc}}^H\widetilde{\mathbf{H}}_{\mathrm{mc}}\mathbf{u}_i} \tag{4.16}$$

where $\Gamma_i = 2P_i/N_0$ defined previously is the average input SNR with respect to the power P_i.

Similarly, substituting $\mathbf{u}_i = \mathbf{A}_i^{-\frac{1}{2}}\mathbf{y}_i$ with unit-norm vector $\mathbf{y}$, we obtain

$$\gamma_i^e(\mathbf{y}_i) = \Gamma_i \frac{\left|\mathbf{y}_i^H \mathbf{A}_i^{-1/2} \widetilde{\mathbf{H}}_{\mathrm{mc}}^H (\widetilde{\mathbf{H}}_{\mathrm{mc}} + \mathbf{E}_{\mathrm{mc}}) \mathbf{A}_i^{-1/2} \mathbf{y}_i\right|^2}{\mathbf{y}_i^H \mathbf{A}_i^{-1/2} \widetilde{\mathbf{H}}_{\mathrm{mc}}^H \widetilde{\mathbf{H}}_{\mathrm{mc}} \mathbf{A}_i^{-1/2} \mathbf{y}_i} \tag{4.17}$$

We assume that the receiver is not aware of the channel estimation error and sends the channel estimation $\widetilde{\mathbf{H}}_{\mathrm{mc}}$ back to transmitter through a error-free, zero-delay and unlimited feedback link. This widely used assumption (see [18], [80], [83], [106] and references therein) allows the same transmission strategies as for perfect channel estimation on the original structures of transmitter and receiver shown in Figure 4.4. So $\mathbf{y}_i$ is chosen as the eigenvector corresponding to the largest eigenvalue $\widetilde{\Lambda}_{\max,i}$ of $\widetilde{\mathbf{H}}_{\mathrm{mc}}^H \widetilde{\mathbf{H}}_{\mathrm{mc}} \mathbf{A}_i^{-1}$. The SNR is therefore given by

$$\gamma_i^e = \Gamma_i \frac{\left|\widetilde{\Lambda}_{\max,i} + \mathbf{y}_i^H \mathbf{A}_i^{-1/2} \widetilde{\mathbf{H}}_{\mathrm{mc}}^H \mathbf{E}_{\mathrm{mc}} \mathbf{A}_i^{-1/2} \mathbf{y}_i\right|^2}{\widetilde{\Lambda}_{\max,i}} \tag{4.18}$$

$$= \Gamma_i \left|(\widetilde{\Lambda}_{\max,i})^{1/2} + (\widetilde{\Lambda}_{\max,i})^{-1/2} \mathbf{y}_i^H \mathbf{A}_i^{-1/2} \widetilde{\mathbf{H}}_{\mathrm{mc}}^H \mathbf{E}_c \mathbf{A}_i^{-1/2} \mathbf{y}_i\right|^2 \tag{4.19}$$

For perfect channel estimation, no estimation error exist, i.e., $\mathbf{E}_{\mathrm{mc}} = \mathbf{0}$, which implies $\widetilde{\mathbf{H}}_{\mathrm{mc}}^H = \mathbf{H}_{\mathrm{mc}}$ and $\widetilde{\Lambda}_{\max,i} = \Lambda_{\max,i}$, then the transmission strategies are optimal as seen in Section 3.3. Due to the channel estimation error, however, the SU-MIMO MRC systems may not transmit user data along the largest eigenmode of the actual channel and are no longer optimal. Thus, the performance degradation depends on those parameters such as pilot SNR and the number of pilot symbols per transmission block which affect the accuracy of channel estimation.

4.2.3 Numerical Results

In previous section, we analyzed the way of effective channel estimation and presented the MRC transmission schemes in the presence of channel estimation error

for three different power metrics. In this section, we give some numerical examples to illustrate the joint effect of mutual coupling and imperfect channel estimation for SU-MIMO MRC systems.

Once again, we consider a coupled transmit array consisting of $N = 2$ half-wavelength dipoles with inter-element spacing d. Each dipole has radius $10^{-3}\lambda$ where λ is the signal wavelength. We adopt the same transmitter model with coupling matching studied in Section 3.1. We assume the $M = 2$ receive antennas are spaced far enough apart so as to be uncoupled and uncorrelated.

For the power metric P_i, $i = 1, 2, 3$, the performance of SU-MIMO MRC in the presence of channel estimation error is measured by the outage probability

$$P_{\text{out}}(\tau) = \Pr\left\{\gamma_i^e < \tau\right\} \ , \tag{4.20}$$

where γ_i^e is given in (4.19). No closed-form expressions exist yet, Monte-Carlo simulations with one million channel realizations are used to evaluate the behavior of these outage probabilities shown in Figure 4.5.

Figure 4.5 shows the outage probabilities with $N = M = 2$ and transmit antenna spacing $d = 0.2\lambda$ for each of the three input power constraints in the presence of channel estimation error (denoted as *imperfect estimation*). Channels are estimation by the LMMSE method (4.13) by setting pilot SNR=10 dB and $L = 2$ pilot symbols per transmission block. Also shown for comparison are the outage probabilities of i.i.d. fading case and coupling case with different matching in the absence of channel estimation (3.29), we denote them as perfect estimation. From Figure 4.5(a), we can see that no matter the channel estimation is perfect or not, outages for the conventional power metric P_1 with self-matching (3.31) and multiport matching (3.30) are

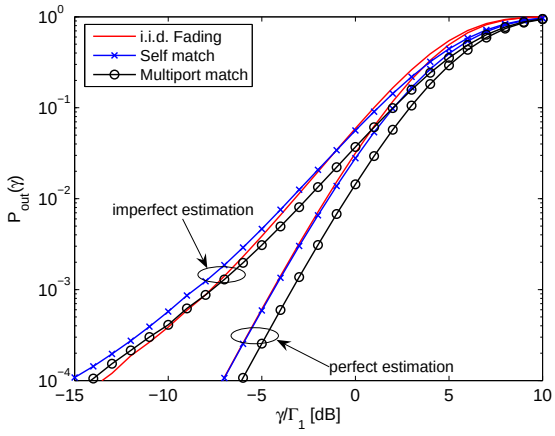

(a) Power measure P_1

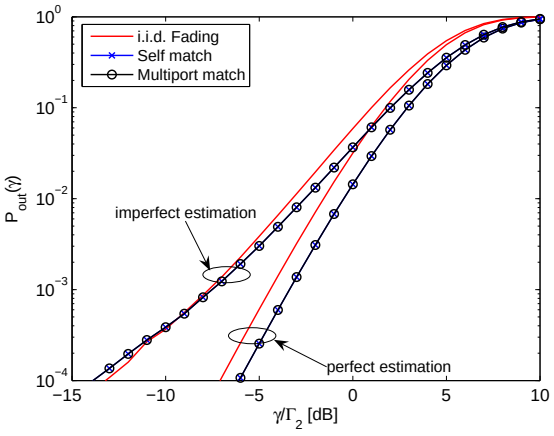

(b) Power measure P_2

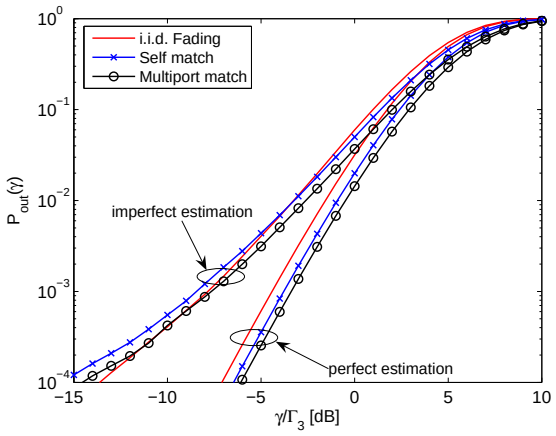

(c) Power measure P_3

Figure 4.5: Outage probabilities vs. normalized SNR with $N = M = 2$, $d = 0.2\lambda$, $P_p/N_0 = 10$ dB and $L = 2$ for different power measures.

close or better than the corresponding i.i.d. case at 1% outage level. This is due to the fact that coupling matrix $\mathbf{C}_{\mathrm{T}}$ tends to whiten the covariance $\mathbf{R}_{\mathrm{T}}$ and increases the array gain at this antenna spacing. Compared with the perfect estimation cases, however, all the three outages with imperfect estimation suffer a $2.1 - 2.3$ dB power

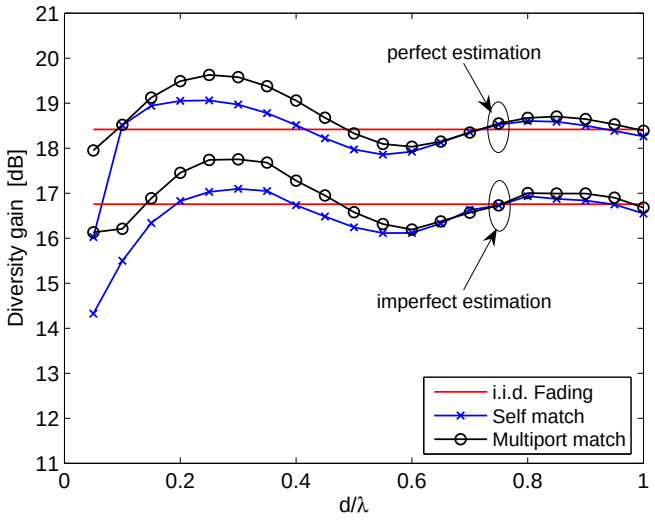

Figure 4.6: Diversity gain vs. antenna spacing d/λ for $N = M = 2$ SU-MIMO MRC system with power measure P_3, $L = 2$ and $P_p/N_0 = 10$ dB.

loss at this outage level. Larger power loss can be seen at even lower outage level, e.g., 0.1% outage. This performance degradations are similar for radiated power P_2 in Figure 4.5(b) and delivered power P_3 in Figure 4.5(c). Another key observation is that multiport matching gives better performance than self-matching for P_1 and P_3, and are not distinguishable for P_2. This can be explained firstly by observing that, given P_1 which though does not correspond to any actual power, coupled antennas are less efficient radiators and so have smaller P_2. Secondly since the self-matching only maximizes power transfer to the isolated antennas, then the delivered power P_3 is not necessarily transferred efficiently to the antennas for small values of d. Finally, P_2 is defined posterior to the matching network, hence performance does not affected by different types of matching networks given P_2.

Further insight can be gained by examining the effect of antenna spacing on

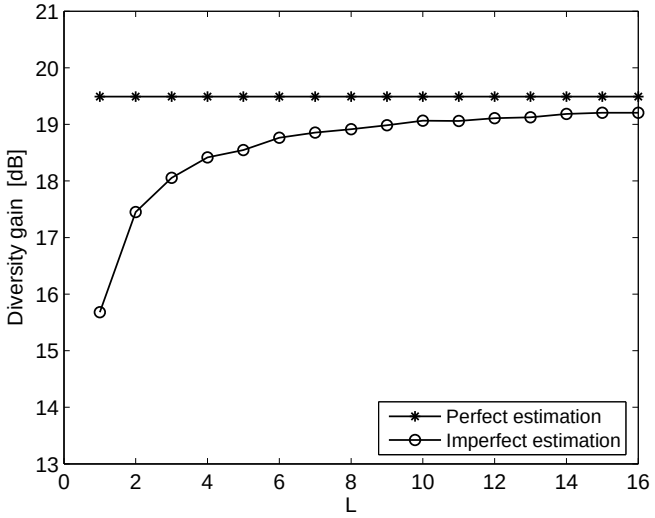

Figure 4.7: Diversity gain vs. number of pilot symbols per transmission block (L) d/λ for $N = M = 2$ SU-MIMO MRC system with power measure P_3, $d = 0.2\lambda$, $P_p/N_0 = 10$ dB and multiport matching.

the diversity gain defined earlier. Figure 4.6 plots the diversity gain versus antenna spacing d/λ for the actual power constraint P_3 with different matching and channel estimation conditions. In this figure, we see that the channel estimation error degrades the diversity gain about 1.7 dB compared with the corresponding case without estimation error. Once again, coupled system (using either self-matching or multiport matching) outperforms the i.i.d. systems for all spacings $0.2\lambda < d < 0.4\lambda$ for both perfect and imperfect channel estimation, with the greatest improvement occurring around $d \approx 0.25\lambda - 0.3\lambda$. No surprise, coupled system using multiport matching achieves a higher diversity gain than that using self-matching. Similar results can be obtained for power measure P_1 and P_2.

Finally, Figures 4.7 and 4.8 plot the dependence of diversity gain on the number of pilot symbols and pilot SNR for the 2×2 SU-MIMO system for power measure

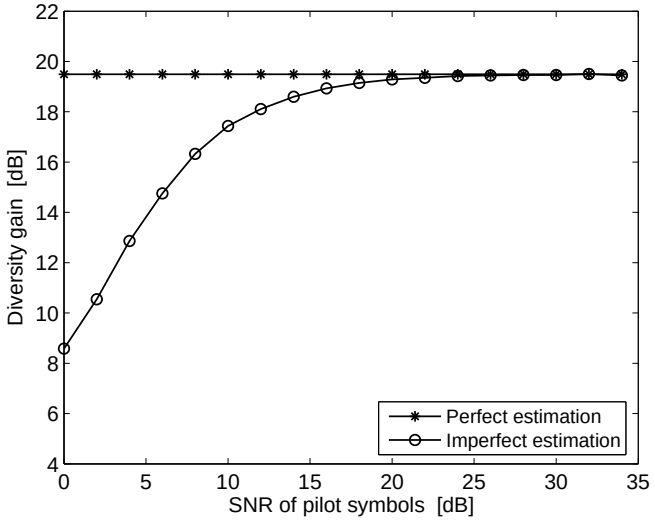

Figure 4.8: Diversity gain vs. pilot SNR P_p/N_0 for $N = M = 2$ SU-MIMO MRC system with power measure P_3, $d = 0.2\lambda$, $L = 2$ and multiport matching.

P_3. WLOG, only the coupled system using multiport matching with antenna spacing $d = 0.2\lambda$ is considered. In Figure 4.7, diversity gain with 10 dB pilot SNR (i.e., with channel estimation error) increases as the number of pilot symbols per transmission block increases, and tends to converge to the case with perfect estimation. From the estimation theory viewpoint, more observation symbols improve the performance of LMMSE estimator. In practice, the number of pilot symbols is limited due to the relative short transmission duration and small transmission bandwidth, then the estimation error always exist. Similarly, the diversity gain can be improved by another means of increasing the SNR of pilot symbols as seen in Figure 4.8. And the diversity gain performance converges to the case with perfect estimation when pilot SNR is greater than 24 dB.

The numerical results above suggest that, regardless of the power measure,

matching and channel estimation conditions, most of the performance benefits of SU-MIMO MRC can be obtained with transmit antennas spaced as close as $0.2 - 0.3\lambda$ apart. In this range, mutual coupling tends to cancel the spatial correlation or/and increases the array gain, so that performance close to (or better than) the i.i.d. case can be obtained even when the antenna elements are strongly coupled. The results also suggest the suboptimal self-matching gives acceptable performance and enjoys the lower design complexity compared with the optimal multiport matching. Finally, imperfect channel estimation degrades the performance and can be compensated by using more pilot symbols and larger pilot SNR when necessary.

4.3 Conclusion

In this chapter, we consider the joint effect of transmitter correlation, mutual coupling, and matching networks and imperfect CSI due to either limited feedback or channel estimation error on the design and performance of SU-MIMO MRC systems. We present codebook design techniques for three different measures of transmitter power which have been proposed in the literature, and we investigate the impact of antenna matching on the performance of these codebooks. Then more realistic model of channel estimation and error using LMMSE estimator is presented. Based on this model, we evaluate the performance loss due to the channel estimation error and consider the parameters which determine the quality of channel estimation. This work extends our earlier study of the impact of mutual coupling on SU-MIMO MRC systems with full CSI (i.e., perfect channel estimation plus unlimited feedback) in Chapter 3. Numerical results suggest the following findings:

First, regardless of the power measure considered and matching network used, most of the performance benefits of SU-MIMO MRC with limited feedback can be obtained with transmit antennas spaced as close as $0.2\lambda - 0.3\lambda$, using as few as $B = 2$ bits feedback.

Second, traditional codebook may degrades the performance in the actual coupled system with self-matching. The performance loss can be dismissed by using multiport matching.

Third, channel estimation error at the receiver degrades the SU-MIMO MRC performance. The performance loss can be reduced by using more pilot symbols per transmission block and/or larger pilot SNR without changing the transmission strategy.

Fourth, When transmit antennas are coupled in a small aperture, matching network allows the antennas spaced as close as $0.2\lambda - 0.3\lambda$ and achieves an acceptable or even better performance compared with the uncoupled and uncorrelated system for all the three power measures.

We conclude that imperfect channel knowledge is at one or both communication ends, the optimal transmission strategies for SU-MIMO MRC with coupling (in Chapter 3) are no longer optimal but are still applicable by using limited feedback technique or LMMSE channel estimation.

Chapter 5

Coordinated Beamforming for MU-MIMO Broadcast Channels

MU-MIMO broadcast systems can significantly improve the downlink throughput by supporting multiple users simultaneously. When receiver noise is uncorrelated and full CSI is available at both ends (or only CSI at receiver plus limited feedback), a jointly designed linear transmit-receive beamforming technique, coordinated beamforming, is suitable for MU-MIMO broadcast channels and is effective to increase the achievable sum-rate and suppress the multiuser interference as seen in Chapter 2. Generally, fading path gain and receiver noise are equally important to determine the output SNR for wireless MIMO systems. Hence when receiver noise and/or signal fading are correlated, the conventional CBF may not be able to acquire the desired SNR and sum-rate, which can be observed by analogy to single-user SIMO receiver [25] and MIMO MRC receiver [27] with correlated fading and noise due to mutual coupling.

Moreover, the statistics of the signal and noise will depend in general on detailed aspects of the receiver design, such as the antenna impedances, matching networks, and amplifiers employed in the receiver RF front-ends. To optimize performance in such scenarios, it is necessary to develop realistic models of these interactions as well as new beamforming techniques that exploit these models to improve performance.

In this chapter, we investigate the effects of receive antenna coupling, matching networks and correlated noise on the design and performance of downlink coordinated beamforming systems. In Section 5.1, we present a new coordinated beamforming technique as well as the limited feedback method for two receivers that is suitable for MIMO broadcast channels with signal and noise correlation at the receiver. In Section 5.2, we present a model for a multi-antenna receiver front-end that characterizes the signal and noise correlation that results from mutual coupling. Finally, in Section 5.3, we present numerical results to evaluate the performance of the proposed beamforming technique to this specific type of signal and noise correlation, and verify its dependence on the properties of the receive array, matching networks, amplifiers, and channel state feedback.

5.1 Coordinated Beamforming

When receive antennas are placed close together, the signal components in each receiver chain may become correlated. In a similar way, recent results have shown that mutual coupling among the receive antennas can also cause the noise in each chain to become correlated (e.g. [58], [71],[25]). In this section, we present a

coordinated beamforming strategy suitable for MIMO broadcast channels with signal and noise correlation at the receiver. The specific form of signal and noise correlation that results from mutual coupling is presented in the next section.

5.1.1 Problem Formulation

Consider a MIMO broadcast channel in which a base station with N transmit antennas sends data to two users with M receive antennas each, as shown in Figure 2.7 with $K = 2$ users. In a rich scattering and frequency-flat Rayleigh fading environment[1], the complex baseband signal detected at the k-th user may be expressed as

$$\mathbf{r}_k = \mathbf{H}_k\mathbf{x} + \mathbf{n}_k \ , \tag{5.1}$$

where $\mathbf{x} = b_1\mathbf{w}_1 + b_2\mathbf{w}_2$ is the transmit signal vector carrying one symbol b_k for the k-th user via the unit-norm beamforming vector $\mathbf{w}_k \in \mathbb{C}^{N\times 1}$, $\mathbf{H}_k \in \mathbb{C}^{M\times N}$ is the channel matrix between the transmitter and the k-th user, $\mathbf{n}_k$ represents noise. We assume the N transmit antennas are spaced far enough apart so as to be essentially uncoupled and uncorrelated, so the columns of $\mathbf{H}_k$ are independent zero-mean circularly-symmetric complex Gaussian vectors with covariance $\mathbf{S}_k$. Hereafter we denote this distribution by $\mathcal{CN}(\mathbf{0}, \mathbf{S}_k)$. The noise is also modeled as Gaussian, $\mathbf{n}_k \sim \mathcal{CN}(\mathbf{0}, \mathbf{T}_k)$. Expressions for $\mathbf{S}_k$ and $\mathbf{T}_k$ are derived in Section 5.2.

The linear multiuser MIMO beamforming scheme studied in [97] and [14] applies a linear combiner $\mathbf{g}_k \in \mathbb{C}^{M\times 1}$ to the received signal at the k-th user to form the

[1]These results extend in a natural way to frequency-selective channels with OFDM, but we will not consider this here.

decision statistics as

$$y_k = \mathbf{g}_k^H \mathbf{r}_k = \mathbf{g}_k^H \mathbf{H}_k \mathbf{w}_k b_k + \mathbf{g}_k^H \mathbf{H}_k \mathbf{w}_l b_l + \mathbf{g}_k^H \mathbf{n}_k \ , \quad (l \neq k) \tag{5.2}$$

where $\mathbf{g}_k^H \mathbf{H}_k \mathbf{w}_k b_k$ is the desired signal and $\mathbf{g}_k^H \mathbf{H}_k \mathbf{w}_l b_l$ is the inter-user interference, $l = 1$ if $k = 2$ and $l = 2$ if $k = 1$ thereafter.

The zero-interference constraints imply

$$\mathbf{g}_1^H \mathbf{H}_1 \mathbf{w}_2 = \mathbf{g}_2^H \mathbf{H}_2 \mathbf{w}_1 = 0 \ , \tag{5.3}$$

in which case the sum-rate of the resulting system is given by

$$C(\mathbf{w}_1, \mathbf{w}_2, \mathbf{g}_1, \mathbf{g}_2) = \log_2(1 + \gamma_1) + \log_2(1 + \gamma_2) \ , \tag{5.4}$$

where $P_k = E[|b_k|^2]$ is the transmit power allotted to user k and

$$\gamma_k = \frac{P_k |\mathbf{g}_k^H \mathbf{H}_k \mathbf{w}_k|^2}{\mathbf{g}_k^H \mathbf{T}_k \mathbf{g}_k} \tag{5.5}$$

is the output SNR of the k-th receiver. The optimization problem is therefore to maximize (6.4) over all unit-norm vectors $\mathbf{w}_1, \mathbf{w}_2 \in \mathbb{C}^{N \times 1}$ and vectors $\mathbf{g}_1, \mathbf{g}_2 \in \mathbb{C}^{M \times 1}$ that satisfy (5.3). Here we assume full CSI ($\mathbf{H}_1$ and $\mathbf{H}_2$) is available at the transmitter, the case of limited feedback is considered below.

5.1.2 Uncorrelated Fading and Noise

For uncorrelated fading ($\mathbf{S}_1 = \mathbf{S}_2 = \mathbf{I}$) and spatially white noise ($\mathbf{T}_1 = \mathbf{T}_2 = N_0\mathbf{I}$), this optimization problem has been studied in [97] and [14]. A brief discussion is given as below (see Section 2.4 for more details).

Each receiver applies MRC combiner of the form

$$\mathbf{g}_1 = \mathbf{H}_1 \mathbf{w}_1 \ , \quad \mathbf{g}_2 = \mathbf{H}_2 \mathbf{w}_2 \ , \tag{5.6}$$

which alters the zero-interference constraints (5.3) as

$$\mathbf{w}_1^H \mathbf{H}_1^H \mathbf{H}_1 \mathbf{w}_2 = \mathbf{w}_2^H \mathbf{H}_2^H \mathbf{H}_2 \mathbf{w}_1 = 0 \ . \tag{5.7}$$

By showing that any beamformers $\mathbf{w}_1$ and $\mathbf{w}_2$ that satisfy (5.7) must be generalized eigenvectors of the matrices

$$\mathbf{F}_1 = \mathbf{H}_1^H \mathbf{H}_1 \ , \quad \mathbf{F}_2 = \mathbf{H}_2^H \mathbf{H}_2 \ , \tag{5.8}$$

Chae *et al.* [14] proposed the following approach to coordinated beamforming.

$$\{\mathbf{w}_1^o, \mathbf{w}_2^o\} \ = \ \arg \max_{\mathbf{w}_1, \mathbf{w}_2 \in \mathcal{W}, \mathbf{w}_1 \neq \mathbf{w}_2} C(\mathbf{w}_1, \mathbf{w}_2, \mathbf{H}_1 \mathbf{w}_1, \mathbf{H}_2 \mathbf{w}_2) \ , \tag{5.9}$$

where $\mathcal{W}$ is the set of unit-norm generalized eigenvectors of $\mathbf{F}_1$ and $\mathbf{F}_2$. Simulations results presented in [14] suggest that this method can achieve a sum-rate close to the sum-capacity of the MIMO broadcast channel when $N = M = 2$.

5.1.3 Correlated Fading and Noise

When signal fading is correlated ($\mathbf{S}_1 \neq \mathbf{I}$ or $\mathbf{S}_2 \neq \mathbf{I}$) but the noise is spatially white, the coordinated beamforming strategy in [14] can still be applied as written, although the resulting average sum-rate will naturally depend on the covariances $\mathbf{S}_1$, $\mathbf{S}_2$. The situation is more complicated when channel noise is correlated. When $\mathbf{T}_1 \neq N_0\mathbf{I}$ or $\mathbf{T}_2 \neq N_0\mathbf{I}$, the strategy in [14] still eliminates multiuser interference in the decision statistics (5.2), but does not generally provide the best sum-rate because it contains no preference for beamformers aligned to directions with minimum channel noise.

To develop a strategy suitable for correlated noise, consider a channel with

non-singular noise covariances $\mathbf{T}_1$ and $\mathbf{T}_2$. Let $\mathbf{T}_k^{1/2}$ denote the Hermitian square-root of $\mathbf{T}_k$. Substituting the change of variables

$$\mathbf{g}_1 = \mathbf{T}_1^{-1/2}\mathbf{u}_1 \ , \quad \mathbf{g}_2 = \mathbf{T}_2^{-1/2}\mathbf{u}_2 \tag{5.10}$$

into (5.2), we obtain the decision statistics

$$y_k = \mathbf{u}_k^H \mathbf{T}_k^{-1/2}\mathbf{H}_k\mathbf{w}_k b_k + \mathbf{u}_k^H \mathbf{T}_k^{-1/2}\mathbf{H}_k\mathbf{w}_l b_l + \mathbf{u}_k^H \mathbf{T}_k^{-1/2}\mathbf{n}_k \ , \quad (l \neq k) \tag{5.11}$$

Observe that choosing vectors $\mathbf{w}_1, \mathbf{w}_2, \mathbf{u}_1, \mathbf{u}_2$ to eliminate multiuser interference and to optimize the resulting sum-rate of the channel (5.11) is mathematically equivalent to the original optimization problem (5.2) with $\mathbf{H}_1$, $\mathbf{H}_2$, $\mathbf{n}_1$ and $\mathbf{n}_2$ replaced by $\hat{\mathbf{H}}_1 = \mathbf{T}_1^{-1/2}\mathbf{H}_1$, $\hat{\mathbf{H}}_2 = \mathbf{T}_2^{-1/2}\mathbf{H}_2$, $\hat{\mathbf{n}}_1 = \mathbf{T}_1^{-1/2}\mathbf{n}_1$ and $\hat{\mathbf{n}}_2 = \mathbf{T}_2^{-1/2}\mathbf{n}_2$, respectively.

Since the new noise vectors $\hat{\mathbf{n}}_1$ and $\hat{\mathbf{n}}_2$ are both $\mathcal{CN}(\mathbf{0}, \mathbf{I})$, we can now apply the beamforming strategy for uncorrelated noise in [14]: If MRC combining is used, then $\mathbf{u}_1 = \hat{\mathbf{H}}_1\mathbf{w}_1$ and $\mathbf{u}_2 = \hat{\mathbf{H}}_2\mathbf{w}_2$, or equivalently

$$\mathbf{g}_1 = \mathbf{T}_1^{-1}\mathbf{H}_1\mathbf{w}_1 \ , \quad \mathbf{g}_2 = \mathbf{T}_2^{-1}\mathbf{H}_2\mathbf{w}_2 \ . \tag{5.12}$$

For these combiners, the zero-interference constraints (5.3) become

$$\mathbf{w}_1^H \mathbf{H}_1^H \mathbf{T}_1^{-1}\mathbf{H}_1\mathbf{w}_2 = \mathbf{w}_2^H \mathbf{H}_2^H \mathbf{T}_2^{-1}\mathbf{H}_2\mathbf{w}_1 = 0 \ . \tag{5.13}$$

For any $M \geq N \geq 2$, we conclude that any beamformers $\mathbf{w}_1$ and $\mathbf{w}_2$ that satisfy (5.13) must be generalized eigenvectors of the matrices

$$\hat{\mathbf{F}}_1 = \mathbf{H}_1^H \mathbf{T}_1^{-1}\mathbf{H}_1 \ , \quad \hat{\mathbf{F}}_2 = \mathbf{H}_2^H \mathbf{T}_2^{-1}\mathbf{H}_2 \ . \tag{5.14}$$

We can now extend the coordinated beamforming strategy in [14] to correlated fading and noise as follows:

$$\{\hat{\mathbf{w}}_1^o, \hat{\mathbf{w}}_2^o\} \ = \ \arg \max_{\mathbf{w}_1, \mathbf{w}_2 \in \hat{\mathcal{W}}, \mathbf{w}_1 \neq \mathbf{w}_2} C(\mathbf{w}_1, \mathbf{w}_2, \mathbf{T}_1^{-1}\mathbf{H}_1\mathbf{w}_1, \mathbf{T}_2^{-1}\mathbf{H}_2\mathbf{w}_2) \ , \tag{5.15}$$

where $\hat{\mathcal{W}}$ is the set of unit-norm generalized eigenvectors of $\hat{\mathbf{F}}_1$ and $\hat{\mathbf{F}}_2$.

Simulations of the performance of this strategy for receiver mutual coupling are given in Section 5.3. We conclude this section with a general observation about the average performance of this beamforming strategy.

Theorem 1 *The expected sum-rate of the coordinated beamforming strategy above,*

$$\bar{C} = \mathsf{E}\left[\max_{\mathbf{w}_1,\mathbf{w}_2\in\hat{\mathcal{W}},\mathbf{w}_1\neq\mathbf{w}_2} C(\mathbf{w}_1,\mathbf{w}_2,\mathbf{T}_1^{-1}\mathbf{H}_1\mathbf{w}_1,\mathbf{T}_2^{-1}\mathbf{H}_2\mathbf{w}_2)\right] ,$$

depends on $\mathbf{S}_1,\mathbf{S}_2,\mathbf{T}_1,\mathbf{T}_2$ *only through the eigenvalues of the "*SNR*" matrices* $\mathbf{S}_1\mathbf{T}_1^{-1}$ *and* $\mathbf{S}_2\mathbf{T}_2^{-1}$.

Proof of the Theorem 1: From (5.4) and (5.5), observe that for $\mathbf{w}_1,\mathbf{w}_2\in\hat{\mathcal{W}},\mathbf{w}_1\neq\mathbf{w}_2$

$$C(\mathbf{w}_1,\mathbf{w}_2,\mathbf{T}_1^{-1}\mathbf{H}_1\mathbf{w}_1,\mathbf{T}_2^{-1}\mathbf{H}_2\mathbf{w}_2) \;=\; \log_2(1+P_1\mathbf{w}_1^H\hat{\mathbf{F}}_1\mathbf{w}_1)+\log_2(1+P_2\mathbf{w}_2^H\hat{\mathbf{F}}_2\mathbf{w}_2)$$

so $\bar{C}$ depends only on the distributions of the independent random matrices $\hat{\mathbf{F}}_1$ and $\hat{\mathbf{F}}_2$ in (5.14). The first channel matrix can be written as $\mathbf{H}_1=\mathbf{S}_1^{1/2}\tilde{\mathbf{H}}_1$, where $\tilde{\mathbf{H}}_1$ is a matrix with independent $\mathcal{CN}(0,1)$ entries, and thus $\hat{\mathbf{F}}_1=\tilde{\mathbf{H}}_1^H\mathbf{S}_1^{1/2}\mathbf{T}_1^{-1}\mathbf{S}_1^{1/2}\tilde{\mathbf{H}}_1$. The eigenvalue decomposition yields

$$\mathbf{S}_1^{1/2}\mathbf{T}_1^{-1}\mathbf{S}_1^{1/2}=\mathbf{U}^H\mathbf{\Lambda}_1\mathbf{U}$$

where $\mathbf{\Lambda}_1$ is a diagonal eigenvalue matrix and $\mathbf{U}$ is an $M\times M$ unitary matrix. Since $\bar{\mathbf{H}}_1=\mathbf{U}\tilde{\mathbf{H}}_1$ and $\tilde{\mathbf{H}}_1$ have the same probability distribution, it follows that $\hat{\mathbf{F}}_1=\bar{\mathbf{H}}_1^H\mathbf{\Lambda}_1\bar{\mathbf{H}}_1$ where $\bar{\mathbf{H}}_1$ is a matrix with independent $\mathcal{CN}(0,1)$ entries. Since $\mathbf{S}_1^{1/2}\mathbf{T}_1^{-1}\mathbf{S}_1^{1/2}$ and $\mathbf{S}_1\mathbf{T}_1^{-1}$ have the same eigenvalues, the distribution of $\hat{\mathbf{F}}_1$ thus depends only on the eigenvalues of $\mathbf{S}_1\mathbf{T}_1^{-1}$. Proceeding in the same way, we can show that the distribution of $\hat{\mathbf{F}}_2$ depends only on the eigenvalues of $\mathbf{S}_2\mathbf{T}_2^{-1}$, which completes the proof.

5.1.4 Limited Feedback

The coordinated beamforming scheme in Section 5.1.3 requires the matrices $\hat{\mathbf{F}}_1$ and $\hat{\mathbf{F}}_2$ to be fed back by the users to the base station. We adopt the simple limited feedback method proposed in [14], in which the entries of the normalized matrices

$$\hat{\mathbf{G}}_k = \frac{\hat{\mathbf{F}}_k}{\mathrm{tr}(\hat{\mathbf{F}}_k)} \ , \quad k = 1, 2$$

are uniformly quantized and fed back to the transmitter. As shown in [14], these matrices are Hermitian, preserve the generalized eigenvectors, and the entries have well-defined ranges. For example, let $g_{ij} = [\hat{\mathbf{G}}_k]$, then we have $g_{11}, \ldots, g_{NN} \in [0, 1]$ with $\sum_{i=1}^{N} g_{ii} = 1$ and $\mathrm{Re}\{g_{ij}\}, \mathrm{Im}\{g_{ij}\} \in [-0.5, 0.5]$ when $i \neq j$. Hence for each $\hat{\mathbf{G}}_k$) (i.e., for each user) only $N - 1$ diagonal real scalars and $N^2 - N$ off diagonal real scalars need to be quantized, which requires a total of $(N^2 - 1)Q$ bits if each real scalar is quantized by Q bits.

As noted in Section 2.4.2, the multiuser interference in (5.2) may not be completely canceled when using quantized version of CSI. Consequently, the following SINRs (5.16) should be used in (5.4) to evaluate the sum-rate in the presence of limited feedback.

$$\gamma_k = \frac{P_k |\mathbf{g}_k^H \mathbf{H}_k \mathbf{w}_k|^2}{P_l |\mathbf{g}_k^H \mathbf{H}_k \mathbf{w}_l|^2 + \mathbf{g}_k^H \mathbf{T}_k \mathbf{g}_k} \ . \tag{5.16}$$

5.2 Receiver Model with Mutual Coupling

We now present a model for a multi-antenna receiver with correlation and mutual coupling. The aim is to derive physical expressions for the correlation matrices $\mathbf{S}_1, \mathbf{S}_2, \mathbf{T}_1, \mathbf{T}_2$ introduced in Section 5.1.3. Since the mechanisms that lead to

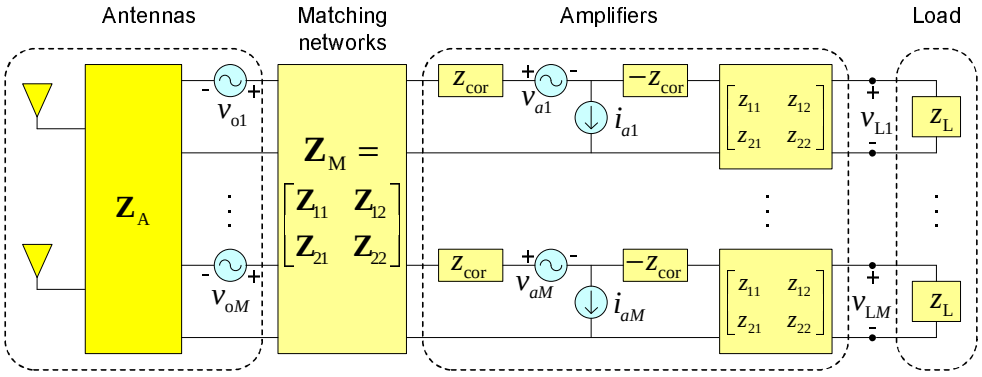

Figure 5.1: Circuit model of an M-antenna receiver with mutual coupling.

correlation in both receivers are similar, throughout this section we focus solely on receiver 1.

We consider the circuit model for an M-antenna receiver introduced in [25], which is illustrated in Figure 5.1. This model includes the impedances of the antenna array, matching network, front-end amplifiers and load, as well as the currents and voltages due to the signal and dominant noise sources.[2] We assume the system is narrowband, so that all impedances are constant over the system bandwidth and all signals can be expressed in complex baseband form.

5.2.1 Antenna Array

The antenna array can be represented as an M-port Thevenin equivalent circuit, as shown in Figure 5.1. The relationship between terminal voltages and currents is then described by an $M \times M$ impedance matrix $\mathbf{Z}_A$. The antenna array converts

[2]For simplicity, the downstream noise in [25, eq. 25] is omitted, so $r_d = 0$.

the incident electromagnetic field into an *open-circuit voltage* $\mathbf{V}_{\mathrm{o}}$ across the antenna terminals. Since this voltage contains both signal and noise components, it can be written as

$$\mathbf{v}_{\mathrm{o}} = \mathbf{H}_{\mathrm{o}}\mathbf{x} + \mathbf{n}_{\mathrm{o}} \ , \tag{5.17}$$

where $\mathbf{H}_{\mathrm{o}}\mathbf{x}$ is the voltage induced by the transmitted signal $\mathbf{x}$ and $\mathbf{n}_{\mathrm{o}}$ represents noise. We assume that the columns of $\mathbf{H}_{\mathrm{o}}$ are independent, $\mathcal{CN}(\mathbf{0}, \mathbf{S}_{\mathrm{o}})$ random vectors. For a uniform linear array, some authors [85, 51, 22, 61] have modeled the open-circuit signal covariance by Clarke's model

$$[\mathbf{S}_{\mathrm{o}}]_{mn} = J_0(2\pi d|m-n|/\lambda) \ , \tag{5.18}$$

where d is the inter-element spacing, λ is the wavelength, and J_0 is the zeroth-order Bessel function of the first kind. Simulations suggest that this model may not be accurate for small d, however, so we estimate this matrix numerically in Section 5.3.

For perfectly conducting antennas, $\mathbf{n}_{\mathrm{o}}$ represents the voltage induced in the array by noise from the surrounding environment. As in [25], we consider here thermal noise from an isotropic distribution of black-body radiators with a uniform temperature T_0. In this case, the noise voltage is $\mathbf{n}_{\mathrm{o}} \sim \mathcal{CN}(\mathbf{0}, \mathbf{T}_{\mathrm{o}})$, where [25]

$$\mathbf{T}_{\mathrm{o}} = 2k_{\mathrm{B}}T_0B(\mathbf{Z}_{\mathrm{A}} + \mathbf{Z}_{\mathrm{A}}^H) \ , \tag{5.19}$$

$k_{\mathrm{B}} = 1.38 \times 10^{-23} J/K$ is Boltzmann's constant and B is the system bandwidth in Hz. In this paper, we take $T_0 = 290$ K, the standard temperature. Note that, in the absence of mutual coupling, $\mathbf{Z}_{\mathrm{A}}$ is diagonal and the noise is spatially white. When coupling is present, however, $\mathbf{Z}_{\mathrm{A}}$ is no longer diagonal and the noise is correlated.

5.2.2 Matching Networks

A matching network is often used to alter the antenna array impedance, usually in order to maximize the power transfer or minimize the noise factor of the amplifiers. This network is usually formed from passive, reactive elements so it is noiseless, lossless and reciprocal. If $\mathbf{v}_1$, $\mathbf{i}_1$, $\mathbf{v}_2$, $\mathbf{i}_2$ denote the voltages and currents at the network input and output, respectively, then the network is described by four $M \times M$ impedance matrices:

$$\mathbf{v}_1 = \mathbf{Z}_{11}\mathbf{i}_1 + \mathbf{Z}_{12}\mathbf{i}_2 \tag{5.20}$$

$$\mathbf{v}_2 = \mathbf{Z}_{21}\mathbf{i}_1 + \mathbf{Z}_{22}\mathbf{i}_2 \ . \tag{5.21}$$

As shown in [42, eq. (2.4)–(2.5)], this network is lossless (i.e. dissipates no power) if the following conditions are satisfied: $\mathbf{Z}_{11} = -\mathbf{Z}_{11}^H$, $\mathbf{Z}_{12} = -\mathbf{Z}_{21}^H$ and $\mathbf{Z}_{22} = -\mathbf{Z}_{22}^H$. The antennas and matching network together constitute a noisy linear network which can be represented as a Thevenin equivalent circuit with open-circuit voltage [42, pg. 13]

$$\mathbf{v}_{\mathrm{o}}' = \mathbf{M}\mathbf{v}_{\mathrm{o}} \ , \qquad \mathbf{M} = \mathbf{Z}_{21}(\mathbf{Z}_{11} + \mathbf{Z}_{\mathrm{A}})^{-1} \ , \tag{5.22}$$

and impedance

$$\mathbf{Z}_{\mathrm{A}}' = \mathbf{Z}_{22} - \mathbf{M}\mathbf{Z}_{12} \ . \tag{5.23}$$

These equations will be applied to some specific matching networks of interest in Section 5.3.

5.2.3 Amplifiers

The matching network is connected to the load through a bank of M identical, uncoupled amplifiers. Each amplifier can be modeled as a linear, noisy two-port

network [25], as shown in Figure 5.1. The internal noise in amplifier k is represented by a random noise voltage $v_{ak} \sim \mathcal{CN}(\mathbf{0}, 4k_{\mathrm{B}}T_0Br_a)$ and an independent noise current $i_{ak} \sim \mathcal{CN}(\mathbf{0}, 4k_{\mathrm{B}}T_0Bg_a)$, where r_a and g_a are the *equivalent noise resistance* and *equivalent noise conductance*, respectively. The parameter $z_{\mathrm{cor}} = r_{\mathrm{cor}} + jx_{\mathrm{cor}}$ is called the *correlation impedance* and models the degree of correlation between the noise observed at the two ports of the amplifier. Note that the noise statistics of an amplifier are completely characterized by the parameters $\{r_a, g_a, z_{\mathrm{cor}}\}$.

When an isolated amplifier is connected to a source of impedance $z_{\mathrm{s}} = r_{\mathrm{s}} + jx_{\mathrm{s}}$, the *noise factor* is defined as the total noise power observed at the output port divided by the noise power contributed by the source alone, which is given by [25]

$$F = 1 + \frac{1}{r_{\mathrm{s}}}\left(r_a + g_a|z_{\mathrm{s}} + z_{\mathrm{cor}}|^2\right) \ .$$

The noise factor is a useful metric because it relates the input and output SNRs of the amplifier. In decibels, this relationship is given by $\mathsf{SNR}_{\mathrm{out}} = \mathsf{SNR}_{\mathrm{in}} - \mathrm{NF}$, where $\mathrm{NF} = 10\log_{10} F$ is the *noise figure*. It can be shown that the minimum value of F is

$$F_{\min} = 1 + 2\left(g_a r_{\mathrm{cor}} + \sqrt{g_a r_a + (g_a r_{\mathrm{cor}})^2}\right) \ , \tag{5.24}$$

which is achieved when $z_{\mathrm{s}} = z_{\mathrm{opt}}$ where

$$z_{\mathrm{opt}} = \sqrt{r_a/g_a + r_{\mathrm{cor}}^2} - jx_{\mathrm{cor}} \ . \tag{5.25}$$

5.2.4 Load

In Section 5.1, we denoted the input to the first user's combiner by $\mathbf{r}_1$ in (5.1). In our model, $\mathbf{r}_1$ is taken to be the voltage $\mathbf{V}_{\mathrm{L}}$ observed across the load in Figure 5.1. We assume that the receiver chains after the amplifiers are uncoupled and each is

electrically isolated from the receiver front-end, so each branch of the load can be modeled by an impedance z_L.

With the assumptions above, the fading covariance in (5.1) was shown in [25] to be given by

$$\mathbf{S}_1 = \mathbf{DCMS}_{\mathrm{o}}\mathbf{M}^H\mathbf{C}^H\mathbf{D}^H \tag{5.26}$$

where $\mathbf{S}_{\mathrm{o}}$ is the open-circuit fading covariance (e.g., 5.18),

$$\mathbf{C} = z_{21}(\mathbf{Z}'_{\mathrm{A}} + z_{11}\mathbf{I})^{-1} , \tag{5.27}$$

$$\mathbf{D} = z_L[(z_L + z_{22})\mathbf{I} - z_{12}\mathbf{C}]^{-1} , \tag{5.28}$$

$\mathbf{I}$ is the $M \times M$ identity matrix, and $\mathbf{M}$ and $\mathbf{Z}'_{\mathrm{A}}$ are defined in (5.22) and (5.23), respectively. Here $\mathbf{M}$ describes the impact of the matching network on the open-circuit fading covariance, and $\mathbf{DC}$ is obtained by using elementary circuit theory to map the fading covariance at the output of the matching network to the corresponding covariance at the load. The noise covariance was shown in [25, eq. (25)] to be

$$\mathbf{T}_1 = (\mathbf{DC})\mathbf{T}_a(\mathbf{DC})^H , \tag{5.29}$$

where

$$\mathbf{T}_a = 4k_BT_0B\left[\frac{1}{2}(\mathbf{Z}'_{\mathrm{A}} + \mathbf{Z}'^H_{\mathrm{A}}) + r_a\mathbf{I} + g_a(\mathbf{A}'_a + z_{\mathrm{cor}}\mathbf{I})(\mathbf{A}'_a + z_{\mathrm{cor}}\mathbf{I})^H\right] , \tag{5.30}$$

k_{B} is Boltzmann's constant, T_0 is the noise temperature of the amplifier and surrounding noise (assumed equal), B is the bandwidth, and $\{r_a, g_a, z_{\mathrm{cor}}\}$ are the amplifier noise parameters. Intuitively, $\mathbf{T}_a$ represents the combined covariance of all noise sources, referred to the output of the matching network.

The covariance $\mathbf{T}_1$ and the analogous covariance $\mathbf{T}_2$ of receiver 2 are the inputs to the coordinated beamforming strategy proposed in Section 5.1.3. Note that

this strategy in general depends on detailed aspects of the receiver design, such as the antenna impedances, matching networks, amplifier parameters and surrounding noise environment. The performance of this strategy, however, can be expressed in a somewhat simpler form. From Theorem 1, we know that the average sum-rate performance of this system depends on $\mathbf{S}_1$ and $\mathbf{T}_1$ only through the eigenvalues of the SNR matrix $\mathbf{S}_1\mathbf{T}_1^{-1}$. When $\mathbf{DC}$ is non-singular, however, then

$$\mathbf{S}_1\mathbf{T}_1^{-1} = (\mathbf{DC})\mathbf{M}\mathbf{S}_{\mathrm{o}}\mathbf{M}^H\mathbf{T}_a^{-1}(\mathbf{DC})^{-1} \ .$$

Since $\mathbf{S}_1\mathbf{T}_1^{-1}$ is related to $\mathbf{M}\mathbf{S}_{\mathrm{o}}\mathbf{M}^H\mathbf{T}_a^{-1}$ by a similarity transformation, they have the same eigenvalues. From Theorem 1, we can therefore take $\mathbf{S}_1\mathbf{T}_1^{-1} = \mathbf{M}\mathbf{S}_{\mathrm{o}}\mathbf{M}^H\mathbf{T}_a^{-1}$ for the purposes of evaluating the average sum-rate performance.

5.3 Numerical Results

In this section, we give numerical examples that illustrate how the coordinated beamforming strategy proposed in Section 5.1.3 performs when applied to mobiles with receiver correlation and mutual coupling, as modeled in Section 5.2. We consider a system with $N = 2$ transmit antennas spaced far enough apart so as to be uncoupled and uncorrelated. We assume the transmitter allocates equal power to each user, so $P_1 = P_2 = P/2$ where P is the total transmit power.

We assume the transmitter sends data to two users with identical receivers. Each receiver employs a uniform linear array of $M = 2$ or 4 half-wavelength dipoles with inter-element spacing d. Each dipole has radius $10^{-3}\lambda$, where λ is the signal wavelength.

The open-circuit fading covariance $\mathbf{S}_{\mathrm{o}}$ was computed as follows. Let $g_m(\phi)$ denote the open-circuit voltage induced in the m-th receive antenna by a vertically-polarized, unit-power plane wave with angle-of-arrival ϕ due to a scatterer located in the antenna far-field. If the received signal consists of a superposition of a large number of plane waves with random phases, which are uniformly distributed in azimuth ϕ, then the signal is approximately Gaussian with mean zero and covariance [71, 25]

$$[\mathbf{S}_{\mathrm{o}}]_{mn} = \frac{1}{2\pi} \int_0^{2\pi} g_m(\phi) g_n^*(\phi) e^{j2\pi \frac{d}{\lambda}(m-n)\cos\phi} \, d\phi \ .$$

For omnidirectional antennas ($g_m(\phi) = 1$), this expression reduces to Clarke's model (5.18). While infinitesimally thin dipoles are often well modeled as omnidirectional, finite-diameter dipoles in an array are not. We therefore calculated the functions $g_m(\phi)$ using the *Numerical Electromagnetics Code* (NEC) [2], a program based on the method of moments. NEC was also used to estimate the antenna impedance $\mathbf{Z}_{\mathrm{A}}$, which should be more accurate than the thin dipole approximations in [6].

We consider the Maxim 2642 SiGe low-noise amplifier [68], which is designed for use in the cellular band. In high-gain mode with $R_{\mathrm{bias}} = 510\ \Omega$ and $f = 900$ MHz, its impedance matrix and noise parameters are given by

$$\begin{bmatrix} z_{11} & z_{12} \\ z_{21} & z_{22} \end{bmatrix} = \begin{bmatrix} 35.7\angle -82.0^\circ & 2.74\angle 91.8^\circ \\ 325\angle -119^\circ & 46.1\angle -23.3^\circ \end{bmatrix} \ \Omega$$
$$r_a = 9.45\ \Omega, \quad g_a = 3.24\ \mathrm{mS}, \quad z_{\mathrm{cor}} = 35.3\angle -114^\circ\ \Omega \tag{5.31}$$

To maximize power transfer from the amplifiers to the load, we assume the load is conjugate matched to the amplifier output impedance, so $z_{\mathrm{L}} = z_{22}^*$.

We consider two matching networks that have been discussed in the literature [59, 71]. In *optimal multiport matching* for minimum noise factor, the network $\mathbf{Z}_{\mathrm{M}}$ in

(5.23) is chosen so that $\mathbf{Z}'_{\mathrm{A}} = z_{\mathrm{opt}}\mathbf{I}$, where z_{opt} is the source impedance (5.25) that minimizes the amplifier noise factor. It is easily verified that a lossless, reciprocal network that implements this match is

$$\mathbf{Z}_{\mathrm{M}}^{\mathrm{mm}} = j \begin{bmatrix} -\mathbf{X}_{\mathrm{A}} & -\sqrt{r_{\mathrm{opt}}}\mathbf{R}_{\mathrm{A}}^{1/2} \\ -\sqrt{r_{\mathrm{opt}}}\mathbf{R}_{\mathrm{A}}^{1/2} & x_{\mathrm{opt}}\mathbf{I} \end{bmatrix} \tag{5.32}$$

where $\mathbf{X}_{\mathrm{A}} = \mathrm{Im}\{\mathbf{Z_A}\}$, $r_{\mathrm{opt}} = \mathrm{Re}\{z_{\mathrm{opt}}\}$, $x_{\mathrm{opt}} = \mathrm{Im}\{z_{\mathrm{opt}}\}$, and $\mathbf{R}_{\mathrm{A}} = (1/2)(\mathbf{Z}_{\mathrm{A}}^H + \mathbf{Z}_{\mathrm{A}})$. From (5.29) and (5.30), we see that this matching network effectively uncouples the antennas, and so the noise covariance in (5.30) reduces to spatially white noise, $\mathbf{T}_a = N_0\mathbf{I}$, where $N_0 = 4k_BT_0BF_{\mathrm{min}}r_{\mathrm{opt}}$.

The optimal multiport match can be difficult to realize in practice. We therefore also consider a simpler, suboptimal type of matching, called self-matching [59, 25], in which a two-port matching network is connected to each single dipole that achieves the minimum noise figure for that antenna in isolation. A reciprocal and passive network that implements this match is

$$\mathbf{Z}_{\mathrm{M}}^{\mathrm{sm}} = j \begin{bmatrix} -\mathbf{X}_{\mathrm{AS}} & -\sqrt{r_{\mathrm{opt}}}\mathbf{R}_{\mathrm{AS}}^{1/2} \\ -\sqrt{r_{\mathrm{opt}}}\mathbf{R}_{\mathrm{AS}}^{1/2} & x_{\mathrm{opt}}\mathbf{I} \end{bmatrix} \tag{5.33}$$

where $\mathbf{Z}_{\mathrm{AS}} = \mathrm{diag}(\mathbf{Z_A})$, $\mathbf{R}_{\mathrm{AS}} = \mathrm{Re}\{\mathbf{Z}_{\mathrm{AS}}\}$ and $\mathbf{X}_{\mathrm{AS}} = \mathrm{Im}\{\mathbf{Z}_{\mathrm{AS}}\}$. Here $\mathrm{diag}(\cdot)$ retains only the diagonal entries of the matrix.

In Figure 5.2, we plot the expected sum-rate (5.4) versus SNR ($= P/N_0$, more precisely is average input SNR) of coordinated beamforming systems for $M = 2$ receive antennas spaced $d = 0.1\lambda$ apart. When optimal multiport matching (5.32) is used, the noise covariances $\mathbf{T}_1$ and $\mathbf{T}_2$ are spatially white and the coordinated beamforming algorithm for uncorrelated noise (CBF-U) in Section 5.1.2 can be applied. When

full CSI is available, this algorithm yields the largest sum-rate in Figure 5.2 for all SNRs. In fact, the sum-rate of this highly coupled system is slightly better than the performance obtained for i.i.d. fading and noise in [14]. Although it may be surprising that a highly coupled system can actually perform slightly better than i.i.d. fading and noise, similar results have been reported for MIMO capacity [93], receive diversity [25] and single-user MIMO MRC [27]. Using the simpler but suboptimal self-match (5.33) with CBF-U leads to a performance loss of roughly 3.6 dB at high SNRs, due to the presence of correlated noise in the receivers. If we compensate for the correlation by applying the new coordinated beamforming algorithm for correlated noise (CBF-C) in Section 5.1.3, the loss is reduced to about 1.8 dB. When self-matching is used, note that both algorithms enforce zero multiuser interference at the receivers; however, CBF-C also exploits the noise correlation present in coupled receivers to further improve performance.

Figure 5.2 also shows the expected sum-rate of these four systems with limited feedback (LF) with $Q = 2$ bits (black lines) or $Q = 4$ bits (red lines), as described in Section 5.1.4. Again we see that CBF-U with multiport matching provides the best performance and is slightly better than the performance obtained for i.i.d. fading and noise in [14]. The performance loss entailed by using self-matching with CBF-U is in the range 3.6-8.0 dB for $Q = 2$ and 3.6-5.0 dB for $Q = 4$. If the new algorithm CBF-C is used with self-matching, however, these losses are reduced to 0.8-1.8 dB for $Q = 2$ and 1.0-1.8 dB for $Q = 4$. For SNRs in the range 0-5 dB, note that all of the limited feedback curves are close to the corresponding full CSI curves, so $Q = 2$ could be used with little loss of performance. The limited feedback systems with $Q = 4$ perform close to full CSI systems for SNRs up to 15 dB. For higher SNRs, a large

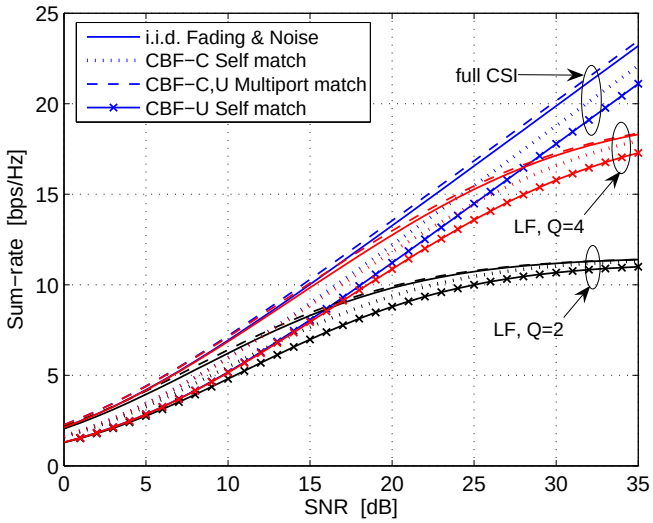

Figure 5.2: Sum rate vs. SNR with $N = M = 2$ and $d = 0.1\lambda$.

gap opens up between the performance of the new algorithm with full CSI and the limited feedback versions, which might be mitigated by choosing a larger Q.

The advantages of larger arrays are illustrated in Figure 5.3, which plots the expected sum-rate of CBF-C (or CBF-U) with multiport matching for $M = 2$ and 4 receive antennas, spaced 0.2λ apart, and different feedback scenarios. For full CSI, the larger array improves the sum-rate by a consistent 4.7 dB relative to the $M = 2$ case. For limited feedback scenarios, however, the improvement decreases as SNR increases, particularly for small Q. Note that similar conclusion can be drawn for the sum-rate performance for self-matching.

We now consider the impact of receive antenna spacing on the expected sum-rate. Figure 5.4 plots the expected sum-rate of the proposed beamforming system for $M = 2$, limited feedback $Q = 2$ or 4, two different SNRs ($P/N_0 = 10$ dB and 20

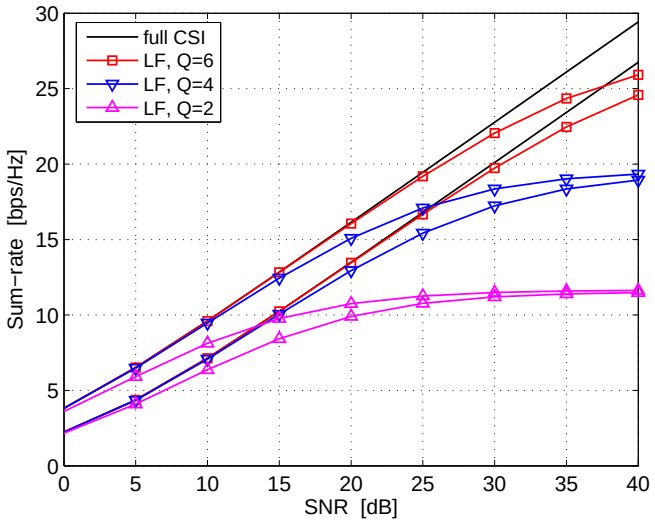

Figure 5.3: Sum-rate for multiport matching vs. SNR with $N = 2$, $M = 2$ or 4 and $d = 0.2\lambda$.

dB). Also shown for comparison is the performance of an i.i.d. system with the same SNRs. Note that sum-rate can be increased by using larger SNR even in the presence of limited feedback. This improvement is significant for larger Q, about 0.5 - 1.5 bps/Hz when SNR = 0 dB and 2.5 - 4.5 bps/Hz when SNR = 20 dB. Regardless of SNR and Q, multiport matching can achieve performance close to the i.i.d. case even in the presence of strong coupling, whereas performance with self-matching tends to degrade for $d < 0.4\lambda$.

Another performance metric of interest in coordinated beamforming is the outage probability:

$$P_k^{\text{out}}(\tau) \;=\; \Pr\{\gamma_k < \tau\} \;, \tag{5.34}$$

where τ is a non-negative threshold and γ_k is defined by (5.5) for full CSI systems and by (5.16) for limited feedback. Since no closed-form formulas exist for the outage

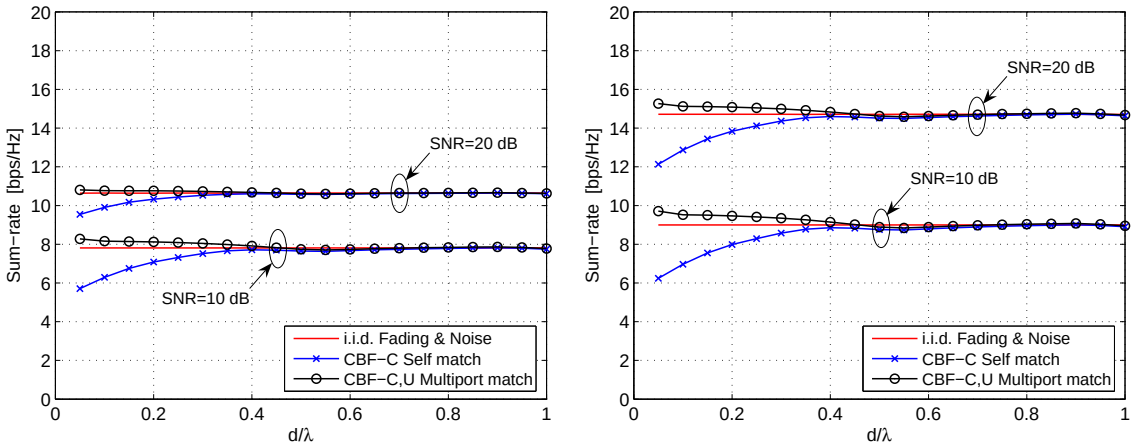

(a) $Q = 2$ (b) $Q = 6$

Figure 5.4: Sum-rate vs. antenna spacing with $N = 2$, $M = 4$ and different feedback scenarios.

probability of coordinated beamforming systems, we will estimate it by Monte Carlo methods.

The outage probabilities versus normalized SNR are shown in Figure 5.5 for coordinated beamforming systems with $M = 2$ antennas spaced $d = 0.1\lambda$ and 0.2λ apart. Also shown for comparison are results for a SU-MIMO MRC system with mutual coupling (black lines) from [28]. Here normalized SNR means that $P_k^{\text{out}}(\tau)$ is plotted versus

$$\bar{\tau}_k = \frac{\tau}{P_k/N_0} = \frac{\tau}{\frac{P}{2N_0}} \ ,$$

where P_k/N_0 is the average input SNR of user k with zero multiuser interference. When antenna spacing is 0.1λ shown in Figure 5.5(a), for full CSI (blue lines), we see that CBF-U (and CBF-C) with multiport matching yields the best outage of all the coordinated beamforming systems considered, and at 1% outage is about 3.7 dB

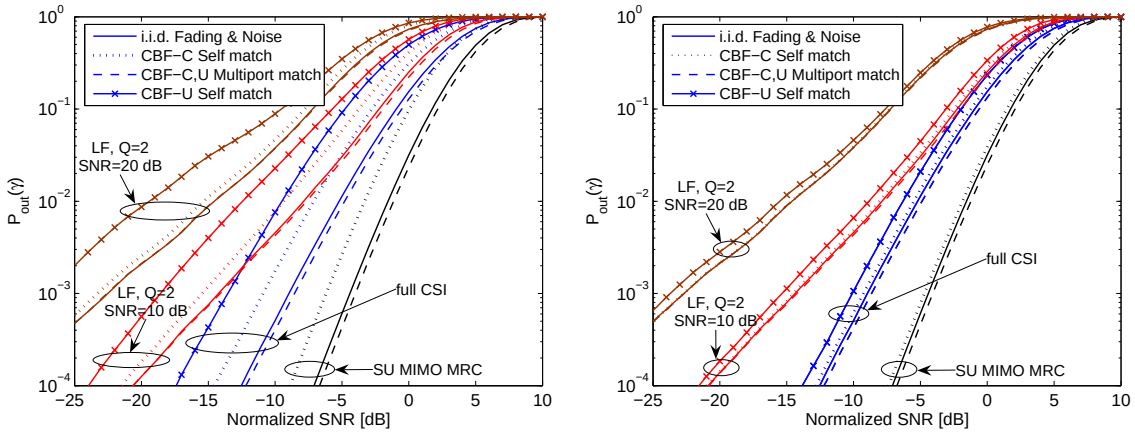

(a) $d = 0.1\lambda$ (b) $d = 0.2\lambda$

Figure 5.5: Outage probability vs. normalized SNR with $N = M = 2$ for different feedback scenarios.

away from the performance of a SU-MIMO MRC system with mutual coupling (black lines). For self-matching, CBF-U suffers a loss of about 5 dB relative to multiport matching at 1% outage. If the new algorithm CBF-C is used with self-matching, this loss is reduced to 2.3 dB. When antenna spacing is increased to 0.2λ shown in Figure 5.5(b), these performance loss using self-matching with full CSI relative to multiport matching at the same outage level are reduced to 1.4 dB for CBF-U and to 0.8 dB for CBF-C. This is intuitive since near this antenna spacing, mutual coupling tends to cancel the correlation for both the fading and noise (e.g., antenna noise and partial amplifier noise, but not for all noise sources).

Figure 5.5 also plots the outage of limited feedback systems with $Q = 2$ bits (red and brown lines). At 1% outage and 0.1λ spacing, the new algorithm CBF-C with self-matching performs within 1.7 dB of CBF-U with multiport matching for $P/N_0 =$

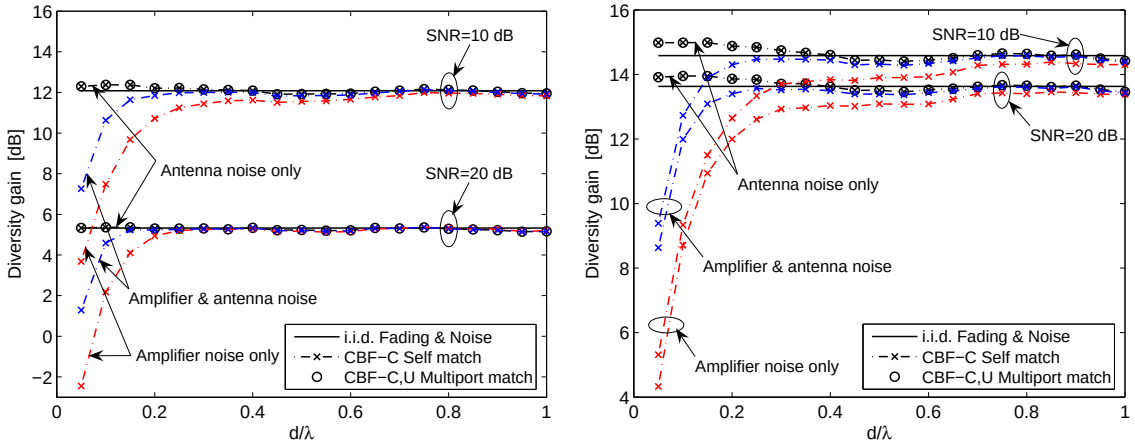

(a) $Q = 2$ (b) $Q = 4$

Figure 5.6: Diversity gain vs. antenna spacing with $N = M = 2$ for different feedback scenarios and noise sources.

10 dB, and within 0.7 dB for $P/N_0 = 20$ dB. However the algorithm CBF-U with self match suffers about 5 dB loss for both SNRs at the same outage level. Once again, the performance loss using self-matching for LF systems is reduced when antenna spacing is 0.2λ. Note that LF systems perform poorly for high SNRs because multiuser interference is not completely canceled and the performance becomes interference limited since

$$\frac{\gamma_k}{\frac{P}{2N_0}} = \frac{|\mathbf{g}_k^H \mathbf{H}_k \mathbf{w}_k|^2}{\frac{P}{2N_0}|\mathbf{g}_k^H \mathbf{H}_k \mathbf{w}_l|^2 + \frac{1}{N_0}\mathbf{g}_k^H \mathbf{T}_k \mathbf{g}_k} \ . \tag{5.35}$$

Further insights can be gained by examining the effect of different noise sources on the diversity gain, which is defined as the difference in SNR between the $M = 2$ and SISO ($M = N = 1$) outage curves at a fixed outage probability. Figure 5.6 shows the diversity gain of CBF-C at 1% outage versus antenna spacing d/λ for $M = 2$, limited feedback $Q = 2$ and 4, and different types of noise and matching conditions.

Note that the diversity gain of CBF-C with self-matching decreases as d/λ decreases in a way that depends on which source of noise is dominant. When antenna noise is dominant (e.g., $r_a = g_a = 0$), the performance of CBF-C with self-matching is exactly the same as multiport matching. On the other hand, when amplifier noise dominates (e.g., $\mathbf{T}_{\mathrm{o}} = \mathbf{0}$) then the diversity gain tends to deteriorate rapidly as d/λ decreases below 0.2. This can be explained by observing that antenna noise and the signal enter the receiver at the same point, so that all subsequent impedances transform the signal and noise in the same way, and so do not affect performance. Amplifier noise is more of a problem because noise at the input terminal of amplifier 1 can be transferred via mutual coupling to antenna 2 and become amplified by amplifier 2. Finally, observe that CBF-C (or CBF-U) with multiport matching can achieve a diversity gain close to the i.i.d case even when the receive antennas are strongly coupled, regardless of what type of noise dominates. For large d, note that the antennas become less coupled and the performance of both matching networks converges to the i.i.d. case for each type of noise.

5.4 Conclusion

In this chapter, we investigated the effect of receiver correlation, mutual coupling, matching networks, and correlated noise sources on coordinated beamforming systems. We presented a new coordinated beamforming technique for two receivers appropriate for MIMO broadcast channels with signal and noise correlation at the receiver. The numerical examples in the previous section suggest the following findings:

First, when multiport matching is used, coordinated beamforming, CBF-U algorithm in [14], can provide performance close to the i.i.d. case even when the receive antennas are spaced as close as $0.2\lambda - 0.4\lambda$ apart. However, the multiport matching itself is a coupled network and difficult to achieve in practice.

Second, self-matching is suboptimal but simpler compared with multiport matching. With self-matching, the proposed CBF-C algorithm can significantly outperform CBF-U in coupled systems. However, the performance is often significantly worse than multiport matching, particularly in strongly coupled systems.

Third, all of the information needed by the transmitter about the noise environment, antennas, matching networks and amplifiers at receiver k can be lumped into a single matrix $\hat{\mathbf{F}}_k$, which is fed back as CSI to the transmitter. Limited feedback methods can often attain performance comparable to full CSI, although the amount of feedback depends in an essential way on the SNR.

Fourth, performance depends on which noise sources are dominant in the coupled multi-antenna receiver front-end.

We conclude that, even in the presence of strong correlation and mutual coupling at the receiver, most of the benefits of coordinated beamforming can be preserved by using appropriate matching networks and linear beamforming. Moreover, these benefits can be achieved even when feedback is limited.

Chapter 6

Asymmetric Coordinated Beamforming for MU-MIMO Broadcast Channels

In a MIMO broadcast channel as noted earlier, multiuser interference (MUI) deceases the receiver SNR and the overall sum-rate. A linear MIMO beamforming technique can be used to suppress the interference by transmitting data in well designed beamforming directions to multiple receivers. When full channel knowledge is available at the transmitter, the linear non-iterative coordinated beamforming studied in [14] and [30] seeks to jointly optimize the transmit-receive beamforming and enjoys the benefits of zero-interference and higher achievable sum-rate. This coordinated beamforming technique achieves symmetric-rate for each user and does not necessarily achieve optimal sum-rate performance.

In this chapter, we aim to further improve the sum-rate performance of down-

link MU-MIMO coordinated beamforming systems subject to zero-interference constraints. In Section 6.2, we first present a new linear non-iterative symmetric coordinated beamforming (SCBF) scheme suitable for MU-MIMO broadcast channels. In Section 6.3, we relax the symmetry restriction and present an asymmetric coordinated beamforming (ACBF) method. In this method, the first user employs single-user MIMO MRC by sending data along the largest eigenmode, while the second user attempts to maximize his rate of transmission subject to a zero-interference constraint. In Section 6.4, we present a parameterized asymmetric coordinated beamforming (P-ACBF) to achieve a better tradeoff between the rates of two users. We combine these two ACBF strategies with time-division policy to create new, higher sum-rate and symmetric beamforming strategies. Finally, in Section 6.5, we present numerical results to illustrate the performance of all proposed coordinated beamforming strategies and the dependence on the number of transmit and/or receive antennas.

6.1 Problem Formulation

Consider a MIMO broadcast channel in which a base station with N transmit antennas sends data to two users with M receive antennas each, as shown in Figure 6.1. It is well known that the sum-rate capacity of this channel is achieved by "dirty paper" coding, which is non-linear and can be difficult to implement in practice. We will therefore consider the simpler (but suboptimal) linear beamforming scheme in which the base station transmits one symbol to each user via linear beamforming, so that $\mathbf{x} = b_1\mathbf{w}_1 + b_2\mathbf{w}_2$ is transmitted, where b_k is the symbol intended for the k-th user and $\mathbf{w}_k \in \mathbb{C}^{N\times 1}$ is a unit-norm beamformer. We assume a rich scattering environment

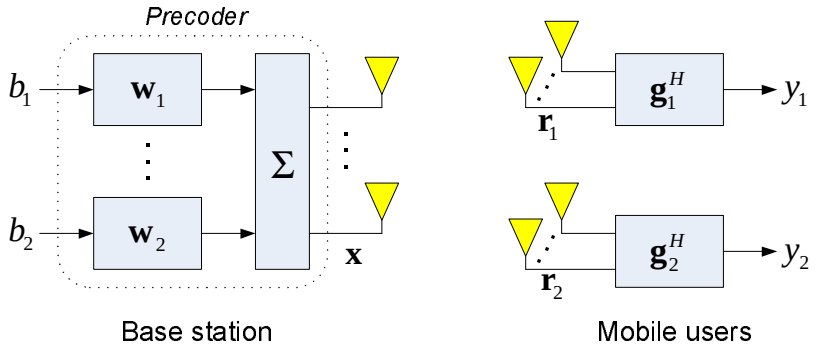

Figure 6.1: A MIMO broadcast channel with coordinated beamforming and two users.

with a delay spread that is small compared to the inverse signal bandwidth, so the complex baseband signal detected at the k-th user may be expressed as

$$\mathbf{r}_k = \mathbf{H}_k\mathbf{x} + \mathbf{n}_k, \tag{6.1}$$

where $\mathbf{H}_k \in \mathbb{C}^{M\times N}$ is the channel matrix between the transmitter and the k-th user, and $\mathbf{n}_k \in \mathbb{C}^{M\times 1}$ represents noise. We assume the N transmit antennas (and M receive antennas) are spaced far enough apart so as to be essentially uncorrelated, so $\mathbf{H}_k$ are independent zero-mean circularly-symmetric complex Gaussian matrices with i.i.d. $\mathcal{CN}(0,1)$ entries. The noise is also modeled as AWGN, $\mathbf{n}_k \sim \mathcal{CN}(\mathbf{0}, N_0\mathbf{I})$.

Applying linear combiner $\mathbf{g}_k \in \mathbb{C}^{M\times 1}$ at the k-th user, the system outputs the decision statistics:

$$y_1 = \mathbf{g}_1^H\mathbf{r}_1 = \mathbf{g}_1^H\mathbf{H}_1\mathbf{w}_1b_1 + \mathbf{g}_1^H\mathbf{H}_1\mathbf{w}_2b_2 + \mathbf{g}_1^H\mathbf{n}_1\ , \tag{6.2-1}$$

$$y_2 = \mathbf{g}_2^H\mathbf{r}_2 = \mathbf{g}_2^H\mathbf{H}_2\mathbf{w}_1b_1 + \mathbf{g}_2^H\mathbf{H}_2\mathbf{w}_2b_2 + \mathbf{g}_2^H\mathbf{n}_2\ . \tag{6.2-2}$$

We want to design linear beamformers $\mathbf{w}_1, \mathbf{w}_2$ and combiners $\mathbf{g}_1, \mathbf{g}_2$ so as to maximize the sum-rate of this system, subject to the constraint that no interference

is present in either decision statistic. The zero-interference constraints imply

$$\mathbf{g}_1^H \mathbf{H}_1 \mathbf{w}_2 = \mathbf{g}_2^H \mathbf{H}_2 \mathbf{w}_1 = 0, \tag{6.3}$$

in which case the sum-rate of the resulting system is given by

$$C(\mathbf{w}_1, \mathbf{w}_2, \mathbf{g}_1, \mathbf{g}_2) = C_1(\mathbf{w}_1, \mathbf{g}_1) + C_2(\mathbf{w}_2, \mathbf{g}_2), \tag{6.4}$$

where $C_k(\mathbf{w}_k, \mathbf{g}_k) = \log_2(1 + \gamma_k)$ is the rate of the k-th user, $P_k = E[|b_k|^2]$ is the transmit power allotted to user k and

$$\gamma_k = \frac{P_k}{N_0} \frac{|\mathbf{g}_k^H \mathbf{H}_k \mathbf{w}_k|^2}{\mathbf{g}_k^H \mathbf{g}_k} \tag{6.5}$$

is the output SNR of the k-th receiver. We assume full channel state information (CSI) is available, so both $\mathbf{H}_1$ and $\mathbf{H}_2$ are known at the transmitter but the k-th user only knows $\mathbf{H}_k$. Note that the receiver CSI (CSIR) can be obtained through pilot-based channel estimation, and transmitter CSI (CSIT) can easily be obtained from the reciprocity of the channel or via feedback for unreciprocal channels. The optimization problem is therefore given by

$$\{\mathbf{w}_1^o, \mathbf{w}_2^o, \mathbf{g}_1^o, \mathbf{g}_2^o\} \;=\; \arg \max_{\substack{\mathbf{w}_1, \mathbf{w}_2 \in \mathbb{C}^{N\times 1},\ \mathbf{g}_1, \mathbf{g}_2 \in \mathbb{C}^{M\times 1} \\ ||\mathbf{w}_1||_2 = ||\mathbf{w}_2||_2 = 1,\ \mathbf{w}_1 \neq \mathbf{w}_2}} C(\mathbf{w}_1, \mathbf{w}_2, \mathbf{g}_1, \mathbf{g}_2)\ . \tag{6.6}$$

Though it is possible to send more data streams to each user and achieve higher throughput, which is beyond the scope of this paper, we restrict ourselves to single data stream per user. Under zero-interference constraints, the broadcast system performs like two parallel single-user MIMO beamforming systems each with full diversity.

6.2 Symmetric Coordinated Beamforming

In this section, we proceed by introducing the traditional coordinated beamforming method studied in [97] and [14]. In this method, each user is equipped with MRC combiner and achieves average symmetric-rate, which is referred as to symmetric coordinated beamforming (SCBF) in this dissertation. We then proposed a new SCBF method in which two transmit beamformers are with the form of maximum-ratio transmission.

6.2.1 Traditional Symmetric Coordinated Beamforming

For $M \geq N = 2$, Wong [97] asserts that the optimal receiver processing can be obtained by MRC of the form $\mathbf{g}_k = \mathbf{H}_k \mathbf{w}_k$ when transmit beamformers $\mathbf{w}_k$ are given. Then the zero-interference constraints (6.3) and SNRs (6.5) can be simplified as

$$\mathbf{w}_1^H \mathbf{H}_1^H \mathbf{H}_1 \mathbf{w}_2 = \mathbf{w}_2^H \mathbf{H}_2^H \mathbf{H}_2 \mathbf{w}_1 = 0 \ , \tag{6.7}$$

$$\gamma_k = (P_k/N_0) \mathbf{w}_k^H \mathbf{H}_k^H \mathbf{H}_k \mathbf{w}_k \ . \tag{6.8}$$

Chae *et al.* [14] extend this work to $M \geq N \geq 2$ case by showing that any beamformers $\mathbf{w}_1$ and $\mathbf{w}_2$ that satisfy (5.7) must be generalized eigenvectors of the matrices

$$\mathbf{F}_1 = \mathbf{H}_1^H \mathbf{H}_1 \ , \quad \mathbf{F}_2 = \mathbf{H}_2^H \mathbf{H}_2 \ . \tag{6.9}$$

Then following approach to coordinated beamforming is proposed in [14]

$$\{\mathbf{w}_1^o, \mathbf{w}_2^o\} \ = \ \arg \max_{\mathbf{w}_1, \mathbf{w}_2 \in \mathcal{W}, \mathbf{w}_1 \neq \mathbf{w}_2} C(\mathbf{w}_1, \mathbf{w}_2, \mathbf{H}_1 \mathbf{w}_1, \mathbf{H}_2 \mathbf{w}_2) \ , \tag{6.10}$$

where $\mathcal{W}$ is the set of unit-norm generalized eigenvectors of $\mathbf{F}_1$ and $\mathbf{F}_2$.

Let $\mathbf{w}_0 = \sum_{j=1,j\neq i}^{N} a_j \mathbf{w}_j$ with scalars $\forall a_j \in \mathbb{C}$, then $\mathbf{w} = \mathbf{w}_0/||\mathbf{w}_0||$ is an arbitrary unit-norm vector in the space $\mathcal{V}_i^{(s)} = \text{span}\{\mathbf{w}_j\}_{j=1,j\neq i}^{N}$ spanned by $N-1$ vectors $\{\mathbf{w}_j\}_{j=1,j\neq i}^{N}$. Both vectors $\mathbf{w}$ and $\mathbf{w}_i \in \mathcal{W}$ satisfy the zero-interference constraints (6.7) that $\mathbf{w}^H \mathbf{F}_k \mathbf{w}_i = 0$ for $k = 1, 2$. If the k-th user selects $\mathbf{w}$ as its beamformer, the resulting SNR is therefore proportional to the following amount

$$\begin{aligned} \mathbf{w}\mathbf{H}_k^H \mathbf{H}_k \mathbf{w} &= \frac{\mathbf{w}_0 \mathbf{H}_k^H \mathbf{H}_k \mathbf{w}_0}{\mathbf{w}_0 \mathbf{w}_0} \\ &= \frac{\sum_{j=1,j\neq i}^{N} |a_j|^2 \mathbf{w}_j^H \mathbf{F}_k \mathbf{w}_j}{\sum_{j=1,j\neq i}^{N} |a_j|^2} \\ &\leq \max_{j,\, j\neq i} \mathbf{w}_j^H \mathbf{F}_k \mathbf{w}_j \end{aligned} \tag{6.11}$$

The last inequality implies that the optimal beamformer for the k-th user is chosen from the set $\mathcal{W}$.

Hence, the optimization problem using larger candidate sets for two beamformers

$$\{\mathbf{w}_1^o, \mathbf{w}_2^o\} = \arg \max_{\substack{\mathbf{w}_1=\mathbf{w}_i\in\mathcal{W},\ \mathbf{w}_2\in\mathcal{V}_i^{(s)} \text{ with } ||\mathbf{w}_2||=1 \\ \text{or } \mathbf{w}_1\in\mathcal{V}_j^{(s)} \text{ with } ||\mathbf{w}_1||=1,\ \mathbf{w}_2=\mathbf{w}_j\in\mathcal{W}}} C(\mathbf{w}_1, \mathbf{w}_2, \mathbf{H}_1\mathbf{w}_1, \mathbf{H}_2\mathbf{w}_2) \tag{6.12}$$

is equivalent to the original one (6.10).

6.2.2 Proposed Symmetric Coordinated Beamforming

Alternatively, beamformers and combiners for linear coordinated beamforming scheme can be designed in the reverse order: given combiners $\mathbf{g}_1$ and $\mathbf{g}_2$, the optimal unit-norm transmit beamforming vectors are with the form of maximum-ration transmission [24],

$$\mathbf{w}_1 = \frac{\mathbf{H}_1^H \mathbf{g}_1}{||\mathbf{H}_1^H \mathbf{g}_1||_2}, \qquad \mathbf{w}_2 = \frac{\mathbf{H}_2^H \mathbf{g}_2}{||\mathbf{H}_2^H \mathbf{g}_2||_2}, \tag{6.13}$$

in which case the instantaneous SNRs (6.5) can be simplified as

$$\gamma_k = \frac{P_k}{N_0} \frac{\mathbf{g}_k^H \mathbf{H}_k \mathbf{H}_k^H \mathbf{g}_k}{\mathbf{g}_k^H \mathbf{g}_k}, \tag{6.14}$$

and the zero-interference constraints (6.3) become

$$\mathbf{g}_1^H \mathbf{H}_1 \mathbf{H}_2^H \mathbf{g}_2 = 0. \tag{6.15}$$

Since the performance do not depend on the norm of these combiners, then $\mathbf{g}_1$ and $\mathbf{g}_2$ can be any pair of left and right singular vectors corresponding to different singular values of $\mathbf{H}_1 \mathbf{H}_2^H$.

Based on this observation, we propose the following approach to coordinated beamforming. First we compute two sets $\mathcal{U} = \{\mathbf{u}_i\}_{i=1}^M$ and $\mathcal{V} = \{\mathbf{v}_i\}_{i=1}^M$ of left and right singular vectors of $\mathbf{H}_1 \mathbf{H}_2^H$, respectively. We then choose the combiners from these two sets respectively so as to maximize the sum-rate when transmit processing (6.13) is used:

$$\{\mathbf{g}_1^o, \mathbf{g}_2^o\} \;=\; \arg \max_{\mathbf{g}_1 = \mathbf{u}_i \in \mathcal{U},\, \mathbf{w}_2 = \mathbf{v}_j \in \mathcal{V},\, i \neq j} C\left(\frac{\mathbf{H}_1^H \mathbf{g}_1}{||\mathbf{H}_1^H \mathbf{g}_1||_2}, \frac{\mathbf{H}_2^H \mathbf{g}_2}{||\mathbf{H}_2^H \mathbf{g}_2||_2}, \mathbf{g}_1, \mathbf{g}_2 \right). \tag{6.16}$$

Note that $\mathbf{u}_i^H \mathbf{H}_1 \mathbf{H}_2^H \mathbf{v}_j = 0$ if $i \neq j$, then $\mathbf{u}_i$ is orthogonal to the space

$$\text{span}\{\mathbf{v}_1, \ldots, \mathbf{v}_{i-1}, \mathbf{v}_{i+1}, \ldots, \mathbf{v}_M\} \,. \tag{6.17}$$

By extending the candidate sets of either $\mathbf{g}_1$ or $\mathbf{g}_2$, the following design therefore improves the performance of sum-rate relative to (6.16):

$$\{\mathbf{g}_1^o, \mathbf{g}_2^o\} \;=\; \arg \max_{\substack{\mathbf{g}_1 = \mathbf{u}_i \in \mathcal{U},\, \mathbf{g}_2 \in \mathcal{V}_i^{(\mathrm{s})} \\ \text{or } \mathbf{g}_1 \in \mathcal{U}_n^{(\mathrm{s})},\, \mathbf{g}_2 = \mathbf{v}_n \in \mathcal{V}}} C\left(\frac{\mathbf{H}_1^H \mathbf{g}_1}{||\mathbf{H}_1^H \mathbf{g}_1||_2}, \frac{\mathbf{H}_2^H \mathbf{g}_2}{||\mathbf{H}_2^H \mathbf{g}_2||_2}, \mathbf{g}_1, \mathbf{g}_2 \right) \,, \tag{6.18}$$

where $\mathcal{V}_i^{(\mathrm{s})} = \text{span}\{\mathbf{v}_j\}_{j=1, j\neq i}^M$ and $\mathcal{U}_n^{(\mathrm{s})} = \text{span}\{\mathbf{u}_m\}_{m=1, m\neq n}^M$ are the subspaces spanned by $M-1$ orthogonal vectors respectively.

Now we consider the problem of finding optimal $\mathbf{g}_2 \in \mathcal{V}_i^{(s)}$ to maximize the sum-rate given $\mathbf{g}_1 = \mathbf{u}_i$ where $\mathbf{u}_i$ is an arbitrary vector in $\mathcal{U}$. Under this assumption, to maximize the sum-rate is equivalent to maximize the SNR γ_2 of user 2 (6.14). Let $\mathbf{a} \in \mathbb{C}^{(M-1)\times 1}$ be arbitrary vector, then $\mathbf{g}_2$ takes the form

$$\mathbf{g}_2 = \mathbf{V}_i \mathbf{a} \tag{6.19}$$

where $\mathbf{V}_i = [\mathbf{v}_1 \dots \mathbf{v}_{i-1}\ \mathbf{v}_{i+1} \dots \mathbf{v}_M]$ denotes the submatrix of $\mathbf{V}$ by deleting the i-th column. Then γ_2 is given by

$$\begin{aligned} \gamma_2 &= \frac{P_2}{N_0} \frac{\mathbf{a}^H \mathbf{V}_i^H \mathbf{H}_2 \mathbf{H}_2^H \mathbf{V}_i \mathbf{a}}{\mathbf{a}^H \mathbf{V}_i^H \mathbf{V}_i \mathbf{a}} \\ &= \frac{P_2}{N_0} \frac{\mathbf{a}^H \mathbf{V}_i^H \mathbf{H}_2 \mathbf{H}_2^H \mathbf{V}_i \mathbf{a}}{\mathbf{a}^H \mathbf{a}} \\ &\leq \frac{P_2}{N_0} \lambda_{\max}(\mathbf{V}_i^H \mathbf{H}_2 \mathbf{H}_2^H \mathbf{V}_i) \end{aligned} \tag{6.20}$$

where $\lambda_{\max}(\mathbf{A})$ returns the largest eigenvalue of matrix $\mathbf{A}$, the second equality is due to the fact that $\mathbf{V}_i^H \mathbf{V}_i = \mathbf{I}$, the last equality can be achieved when $\mathbf{a}$ is the eigenvector corresponding to the largest eigenvalue of $\mathbf{V}_i^H \mathbf{H}_2 \mathbf{H}_2^H \mathbf{V}_i$. We denote this optimal $\mathbf{a}$ as $\mathbf{a}^o$, then the desired combiner for user 2 is $\mathbf{g}_2 = \mathbf{V}_i \mathbf{a}^o$ which maximizes γ_2. Similarly, when $\mathbf{g}_2 = \mathbf{v}_n \in \mathcal{V}$ is given, the desired $\mathbf{g}_1$ can be computed by this subspace optimization method.

Note that both the traditional SCBF (6.10) and the proposed SCBF (6.18) approaches are possible solutions to the constrained optimization problem (6.6). However, they are not necessarily equivalent since they may have different candidate sets for beamformers and combiners. Moreover, they may not be optimal since the beamformers in traditional SCBF and combiners in proposed SCBF are not necessarily optimal under zero-interference constraints.

6.3 Asymmetric Coordinated Beamforming

Both symmetric beamforming strategies in Section 6.2 contain no user preference and therefore achieve symmetric-rate (see Section 6.5 for numerical results). However, it is practical that two users may have different bandwidths and traffic demands, e.g., one is for high-speed internet and the other is for voice or normal traffic. It is therefore necessary to design a linear coordinated beamforming strategy in which one user communicates with base station at a higher rate and the other user at a relatively lower rate. This motivates the design of asymmetric coordinated beamforming by relaxing the symmetry restriction on MU-MIMO coordinated beamforming.

Without loss of generality (WLOG), we assume user 1 is the desired user at a higher rate. The rate (or equivalent the SNR) of user 1 can be maximized by transmitting data along the largest eigenmode of the wireless MIMO channel between base station and user 1. Under zero-interference constraints, user 1 performs equivalently to a SU-MIMO MRC system. Let $\mathbf{H}_1^H\mathbf{H}_1 = \mathbf{T}_1\mathbf{\Lambda}_1\mathbf{T}_1^H$ denote eigenvalue decomposition (EVD) where the diagonal matrix $\mathbf{\Lambda}_1 = \text{diag}(\lambda_1, \ldots, \lambda_N)$ contains the eigenvalues of $\mathbf{H}_1^H\mathbf{H}_1$ in ascending order, i.e., $\lambda_1 \leq \ldots \leq \lambda_N$, and $\mathbf{T} = [\mathbf{t_1} \ldots \mathbf{t_N}]$ is a unitary matrix. Then $\lambda_{\max}\left(\mathbf{H}_1^H\mathbf{H}_1\right) = \lambda_N$, and therefore the beamformer $\mathbf{w}_1 = \mathbf{t}_N$ and combiner $\mathbf{g}_1 = \mathbf{H}_1\mathbf{t}_N$ facilitate user 1 achieving the optimal instantaneous SNR (6.5) as

$$\max_{\mathbf{w}_1} \gamma_1(\mathbf{w}_1, \mathbf{H}_1\mathbf{w}_1) = (P_1/N_0)\lambda_{\max}\left(\mathbf{H}_1^H\mathbf{H}_1\right) \tag{6.21}$$

Assuming beamforming scheme above is applied for user 1, then the zero-interference constraints (6.3) become

$$\mathbf{w}_1^H\mathbf{H}_1^H\mathbf{H}_1\mathbf{w}_2 \;=\; \mathbf{g}_2\mathbf{H}_2\mathbf{w}_1 \;=\; 0. \tag{6.22}$$

Let $\mathbf{a} = [a_1 \dots a_{N-1}]^T \in \mathbb{C}^{(N-1)\times 1}$ be an arbitrary $(N-1)$-dimensional vector and $\mathbf{Q} = [\mathbf{t}_1 \dots \mathbf{t}_{N-1}]$ be the submatrix of $\mathbf{T}_1$ by deleting the last column. Denote $\mathcal{T}_N^{(\mathrm{s})} = \mathrm{span}\{\mathbf{t}_i\}_{i=1}^{N-1}$. Since $\mathbf{t}_i \mathbf{H}_1^H \mathbf{H}_1 \mathbf{t}_j = 0$ when $i \neq j$, then any unit-norm vector

$$\mathbf{w}_2 = \frac{\mathbf{Qa}}{||\mathbf{Qa}||_2} \in \mathcal{T}_N^{(\mathrm{s})} \tag{6.23}$$

may cancel the interference at user 1 caused by user 2 due to the fact that

$$\mathbf{g}_1 \mathbf{H_1} \mathbf{w}_2 = \sum_{i=1}^{N-1} \frac{\mathbf{t}_N^H \mathbf{H_1}^H \mathbf{H}_1 \mathbf{t}_i a_i}{||\mathbf{Qa}||_2} = 0 \ .$$

Therefore the sum-rate is maximized by choosing beamformer $\mathbf{w}_2$ and combiner $\mathbf{g}_2$ for user 2 as follows:

$$\{\mathbf{w}_2^o, \mathbf{g}_2^o\} \ = \ \arg \max_{\substack{\mathbf{w}_2 \in \mathcal{T}_N^{(\mathrm{s})} \text{ with } ||\mathbf{w}||_2 = 1 \\ \mathbf{g}_2 \in (\mathbf{H}_2 \mathbf{t}_N)^{\perp}}} C(\mathbf{t}_N, \mathbf{w}_2, \mathbf{H}_1 \mathbf{t}_N, \mathbf{g}_2) \ , \tag{6.24}$$

where $(\mathbf{A})^{\perp}$ denotes the null space of the space spanned by all the column vectors of matrix $\mathbf{A}$.

Next we begin the design of optimal $\mathbf{w}_2$ and $\mathbf{g}_2$ subject to the zero-interference constraints (6.22) by deriving the candidate set of $\mathbf{g}_2$. Let $\mathbf{H}_2 \mathbf{t}_N = [\mathbf{U}_2^{(1)} \ \mathbf{U}_2^{(0)}] \mathbf{\Sigma}_2 \mathbf{V}_2^H$ denote the singular value decomposition (SVD), where $\mathbf{U}_2^{(1)}$ represents the first left singular vector, $\mathbf{V}_2$ only contains a complex scalar, and $\mathbf{\Sigma}_2 \in \mathbb{C}^{M\times 1}$ is only with the first entry non-zero. Denote $\mathbf{U}_2^{(0)} = [\mathbf{u}_1 \dots \mathbf{u}_{M-1}]$, arbitrary vector $\mathbf{b} \in \mathbb{C}^{(M-1)\times 1}$ and $\mathcal{U}_M^{(\mathrm{s})} = \mathrm{span}\{\mathbf{u}_i\}_{i=1}^{M-1}$. Then arbitrary vector

$$\mathbf{g}_2 = \mathbf{U}_2^{(0)} \mathbf{b} \in \mathcal{U}_M^{(\mathrm{s})} \tag{6.25}$$

may eliminate the interference caused by user 1 at user 2 since

$$\mathbf{g}_2^H \mathbf{H_2} \mathbf{w}_1 = \mathbf{b}^H \left(\mathbf{U}_2^{(0)} \right)^H \mathbf{H_2} \mathbf{t}_N = 0.$$

Therefore the SNR of user 2 (6.5) is given by

$$\begin{aligned}\gamma_2 &= \frac{P_2}{N_0}\frac{\left|\mathbf{b}^H\left(\mathbf{U}_2^{(0)}\right)^H\mathbf{H}_2\mathbf{Q}\mathbf{a}\right|^2}{||\mathbf{Q}\mathbf{a}||_2^2\cdot||\mathbf{U}_2^{(0)}\mathbf{b}||_2^2}\\ &= \frac{P_2}{N_0}\frac{\left|\mathbf{b}^H\left(\mathbf{U}_2^{(0)}\right)^H\mathbf{H}_2\mathbf{Q}\mathbf{a}\right|^2}{\mathbf{a}^H\mathbf{a}\cdot\mathbf{b}^H\mathbf{b}}\\ &\leq \frac{P_2}{N_0}\sigma_{\max}^2\left(\left(\mathbf{U}_2^{(0)}\right)^H\mathbf{H}_2\mathbf{F}\right)\end{aligned} \tag{6.26}$$

where $\sigma_{\max}(\mathbf{A})$ returns the largest singular value of matrix $\mathbf{A}$, the second equality is due to the facts that $\mathbf{Q}^H\mathbf{Q}=\mathbf{I}$ and $\left(\mathbf{U}_2^{(0)}\right)^H\mathbf{U}_2^{(0)}=\mathbf{I}$, the last equality is achieved when optimal coordinate vectors $\mathbf{a}^o$ and $\mathbf{b}^o$ are the right and left singular vectors of matrix $\left(\mathbf{U}_2^{(0)}\right)^H\mathbf{H}_2\mathbf{F}$ associated with the largest singular value, respectively. Therefore the optimal $\mathbf{w}_2$ and $\mathbf{g}_2$ are

$$\mathbf{w}_2^o=\frac{\mathbf{Q}\mathbf{a}^o}{||\mathbf{Q}\mathbf{a}^o||_2},\qquad \mathbf{g}_2^o=\mathbf{U}_2^{(0)}\mathbf{b}^o. \tag{6.27}$$

which achieve the sum-rate of ACBF as

$$\begin{aligned}C_{\text{ACBF}} &= \log_2\left(1+(P_1/N_0)\lambda_{\max}\left(\mathbf{H}_1^H\mathbf{H}_1\right)\right)\\ &\quad+\log_2\left(1+(P_2/N_0)\sigma_{\max}^2\left(\left(\mathbf{U}_2^{(0)}\right)^H\mathbf{H}_2\mathbf{F}\right)\right)\ .\end{aligned} \tag{6.28}$$

Note that rate of user 1 can be increased by allocating more power. It is trivial that this two-user MIMO broadcast system may reduce to be SU-MIMO MRC system when $P_1=P$ and $P_2=0$.

6.4 Sum-rate Maximization with ACBF

In asymmetric coordinated beamforming scheme, user 1 experiences the highest SNR and user 2 maximizes his SNR over the subspaces of beamformer and com-

biner. However, the dimensional limitation of these subspaces may result in performance loss for the rate of user 2 and then the sum-rate. In this section, we first introduce a simple scheme to improve the sum-rate performance of ACBF. After that we consider the sum-rate maximization problem based on the proposed parameterized ACBF scheme. Finally, we derive a simple upper bound of the sum-rate to facilitate the comparison of performance.

6.4.1 Time-Division ACBF (TD-ACBF)

As in Section 6.3, ACBF scheme for each transmission has $K = 2$ options: apply beamformers $\mathbf{w}_1^{(k)}$, $\mathbf{w}_2^{(k)}$ and combiners $\mathbf{g}_1^{(k)}$, $\mathbf{g}_2^{(k)}$, where k=1 or 2, to let the k-th user performs SU-MIMO MRC to achieve the highest rate

$$\max C_k = \log_2 \left(1 + P_k/N_0 \lambda_{\max} \left(\mathbf{H}_k^H \mathbf{H}_k\right)\right) \text{ bps/Hz} .$$

Denote the set of these two options as

$$\mathcal{S} = \left\{\mathbf{w}_1^{(k)}, \mathbf{w}_2^{(k)}, \mathbf{g}_1^{(k)}, \mathbf{g}_2^{(k)}\right\}_{k=1,2} .$$

Then one natural idea is to time sharing these two modes according to the maximum sum-rate criterion:

$$\{\mathbf{w}_1^o, \mathbf{w}_2^o, \mathbf{g}_1^o, \mathbf{g}_2^o\} = \arg \max_{\{\mathbf{w}_1, \mathbf{w}_2, \mathbf{g}_1, \mathbf{g}_2\} \in \mathcal{S}} C(\mathbf{w}_1, \mathbf{w}_2, \mathbf{g}_1, \mathbf{g}_2), \tag{6.29}$$

This time-division asymmetric coordinated beamforming (TD-ACBF) method achieves a higher sum-rate relative to the original ACBF by changing the priorities of two users. Though the computational burden is doubled for each transmission, it is still acceptable since TD-ACBF is a non-iterative algorithm like ACBF and requires

lower complexity and calculation resources. And it is easy for MU-MIMO broadcast systems to switch the beamforming strategy between ACBF and TD-ACBF, which gives the system more freedom and higher reliability.

6.4.2 Time-Division Parameterized ACBF (TD-P-ACBF)

Note that traditional SCBF is solved by generalized eigenvalue decomposition (GEVD) of two user channels while ACBF is solved by eigenvalue decomposition (EVD) of one user channel. Motivated by this observation, we propose a parameterized ACBF (P-ACBF) method to evaluate the tradeoff between the rates of the two users. WLOG, we assume user 1 is the desired user at a higher rate. Now we consider the following generalized eigenvalue problem with parameter $s \in [0,\ 1]$,

$$\mathbf{H}_1^H \mathbf{H}_1 \mathbf{f} = \lambda \left((1-s)\mathbf{I} + s\mathbf{H}_2^H \mathbf{H}_2 \right) \mathbf{f} \tag{6.30}$$

where λ and $\mathbf{f}$ are the generalized eigenvalue and eigenvector, respectively, of matrices

$$\mathbf{F}_1 = \mathbf{H}_1^H \mathbf{H}_1 \ , \quad \mathbf{F}_2' = \left((1-s)\mathbf{I}_N + s\mathbf{F}_2 \right) \ ,$$

where $\mathbf{F}_2 = \mathbf{H}_2^H \mathbf{H}_2$.

Denote $\mathcal{F} = \{\mathbf{f}_i\}_{i=1}^N$ as the set of all unit-norm generalized eigenvectors of matrices $\mathbf{F}_1$ and $\mathbf{F}_2'$ with the order $\mathbf{f}_1^H \mathbf{F}_1 \mathbf{f}_1 \leq \ldots \leq \mathbf{f}_N^H \mathbf{F}_1 \mathbf{f}_N$. For user 1, the beamformer and combiner are chosen such that

$$\mathbf{w}_1 \ = \ \arg \max_{\mathbf{w}_1 \in \mathcal{F}} \mathbf{w}_1^H \mathbf{F}_1 \mathbf{w}_1 \ = \ \mathbf{f}_N \ , \tag{6.31}$$

$$\mathbf{g}_1 \ = \ \mathbf{H}_1 \mathbf{w}_1 \ = \ \mathbf{H}_1 \mathbf{f}_N \tag{6.32}$$

Now we consider the design of $\mathbf{w}_2$ and $\mathbf{g}_2$. Similar to ACBF scheme in Section 6.3, we take the SVD as $\mathbf{H}_2 \mathbf{w}_1 = [\mathbf{U}_2^{(1)}\ \mathbf{U}_2^{(0)}] \mathbf{\Sigma}_2 \mathbf{V}_2^H$, where $\mathbf{U}_2^{(1)}$ represents the

first left singular vector, $\mathbf{V}_2$ is a scalar and $\mathbf{\Sigma}_2$ is a M-dimensional complex vector only with the first entry non-zero. Denote $\mathbf{Q} = [\mathbf{f}_1 \dots \mathbf{f}_{N-1}]$, $\mathbf{U}_2^{(0)} = [\mathbf{u}_1 \dots \mathbf{u}_{M-1}]$, and arbitrary vectors $\mathbf{a} \in \mathbb{C}^{(N-1)\times 1}$ and $\mathbf{b} \in \mathbb{C}^{(M-1)\times 1}$. Then arbitrary unit-norm vector $\mathbf{w}_2$ and vector $\mathbf{g}_2$ formed by

$$\mathbf{w}_2 = \frac{\mathbf{Qa}}{||\mathbf{Qa}||_2}, \quad \mathbf{g}_2 = \mathbf{U}_2^{(0)}\mathbf{b}, \tag{6.33}$$

may cancel the interference due to the facts that

$$\mathbf{f}_i^H \mathbf{R}_1 \mathbf{f}_j \;=\; 0 \quad \text{if } i \neq j \;, \qquad \left(\mathbf{U}_2^{(0)}\right)^H \mathbf{H}_2 \mathbf{w}_1 \;=\; 0.$$

Similar to (6.24), the sum-rate is maximized by choosing beamformer $\mathbf{w}_2$ and combiner $\mathbf{g}_2$ for user 2 as follows:

$$\{\mathbf{w}_2^o, \mathbf{g}_2^o\} \;=\; \arg \max_{\substack{\mathbf{w}_2 \in \mathcal{F}_N^{(\mathrm{s})} \text{ with } ||\mathbf{w}||_2 = 1 \\ \mathbf{g}_2 \in \mathcal{U}_M^{(\mathrm{s})}}} C(\mathbf{t}_N, \mathbf{w}_2, \mathbf{H}_1 \mathbf{t}_N, \mathbf{g}_2) \;, \tag{6.34}$$

where $\mathcal{F}_N^{(\mathrm{s})} = \mathrm{span}\{\mathbf{f}_i\}_{i=1}^{N-1}$ and $\mathcal{U}_M^{(\mathrm{s})} = \mathrm{span}\{\mathbf{u}_i\}_{i=1}^{M-1}$

Then the SNR of user 2 in (6.5) is

$$\begin{aligned} \gamma_2 &= \frac{P_2}{N_0} \frac{\left|\mathbf{b}^H \left(\mathbf{U}_2^{(0)}\right)^H \mathbf{H}_2 \mathbf{Qa}\right|^2}{||\mathbf{Qa}||_2^2 \cdot ||\mathbf{U}_2^{(0)}\mathbf{b}||_2^2} \\ &= \frac{P_2}{N_0} \frac{\left|\mathbf{b}^H \left(\mathbf{U}_2^{(0)}\right)^H \mathbf{H}_2 \mathbf{Qa}\right|^2}{\mathbf{a}^H \mathbf{B} \mathbf{a} \cdot \mathbf{b}^H \mathbf{b}} \end{aligned}$$

where the last equality is due to the fact that $\left(\mathbf{U}_2^{(0)}\right)^H \mathbf{U}_2^{(0)} = \mathbf{I}$, since $\mathbf{Q}$ has full column rank then $\mathbf{B} = \mathbf{Q}^H\mathbf{Q}$ is a positive-definite Hermitian matrix, it has a Hermitian positive-definite square root $\mathbf{B}^{1/2}$. Substituting $\mathbf{t} = \mathbf{B}^{-1/2}\mathbf{a}$, we obtain

$$\begin{aligned} \gamma_2 &= \frac{P_2}{N_0} \frac{\left|\mathbf{b}^H \left(\mathbf{U}_2^{(0)}\right)^H \mathbf{H}_2 \mathbf{Q} \mathbf{B}^{-1/2} \mathbf{t}\right|^2}{\mathbf{t}^H \mathbf{t} \cdot \mathbf{b}^H \mathbf{b}} \\ &\leq \frac{P_2}{N_0} \sigma_{\max}^2 \left(\left(\mathbf{U}_2^{(0)}\right)^H \mathbf{H}_2 \mathbf{Q} \mathbf{B}^{-1/2}\right) \end{aligned} \tag{6.35}$$

where the last equality is achieved when optimal coordinate vectors $\mathbf{t}^o$ and $\mathbf{b}^o$ are the right and left singular vectors, respectively, of the matrix $\left(\mathbf{U}_2^{(0)}\right)^H \mathbf{H}_2\mathbf{Q}\mathbf{B}^{-\frac{1}{2}}$ associated with the largest singular value. Therefore, the beamformer and combiner of user 2 are given by

$$\mathbf{w}_2^o \;=\; \frac{\mathbf{Q}\mathbf{B}^{-\frac{1}{2}}\mathbf{t}^o}{||\mathbf{Q}\mathbf{B}^{-\frac{1}{2}}\mathbf{t}^o||_2}, \quad \mathbf{g}_2^o \;=\; \mathbf{U}_2^{(0)}\mathbf{b}^o \tag{6.36}$$

and achieve the sum-rate of P-ACBF as

$$\begin{aligned} C_{\mathrm{P-ACBF}} \;&=\; \log_2\left(1+(P_1/N_0)\mathbf{f}_N^H\mathbf{H}_1^H\mathbf{H}_1\mathbf{f}_N\right) \\ &\quad +\log_2\left(1+(P_2/N_0)\sigma_{\max}^2\left(\left(\mathbf{U}_2^{(0)}\right)^H\mathbf{H}_2\mathbf{Q}\mathbf{B}^{-1/2}\right)\right) . \end{aligned} \tag{6.37}$$

This P-ACBF algorithm for each transmission has two modes denoted by the set

$$\mathcal{J} = \left\{\mathbf{w}_1^{(k)}, \mathbf{w}_2^{(k)}, \mathbf{g}_1^{(k)}, \mathbf{g}_2^{(k)}\right\}_{k=1,2} ,$$

in which case the k-th has higher priority in the k-th mode. Then similar time-division policy used in TD-ACBF algorithm can be combined with P-ACBF to increase the sum-rate,

$$\{\mathbf{w}_1^o, \mathbf{w}_2^o, \mathbf{g}_1^o, \mathbf{g}_2^o\} \;=\; \arg \max_{\{\mathbf{w}_1,\mathbf{w}_2,\mathbf{g}_1,\mathbf{g}_2\}\in\mathcal{J}} C(\mathbf{w}_1, \mathbf{w}_2, \mathbf{g}_1, \mathbf{g}_2), \tag{6.38}$$

Note that the optimization problem (6.38) is equivalent to (6.29) when $s = 0$ since all the generalized eigenvectors are the same as the eigenvectors of channel for the single-user. The sum-rate performance versus the parameter s is evaluated in Section 6.5. From the numerical simulation, the specific value of s which achieves even higher sum-rate relative to both SCBFs and ACBFs corresponding to specific system configuration N, M is also addressed.

6.4.3 Upper Bound

The SNR in (6.5) of the k-th user can be easily upper bounded by

$$\gamma_k = \frac{P_k}{N_0} \frac{|\mathbf{g}_k^H \mathbf{H}_k \mathbf{w}_k|^2}{\mathbf{g}_k^H \mathbf{g}_k} \leq \frac{P_k}{N_0} \lambda_{\max} \left(\mathbf{H}_k^H \mathbf{H}_k \right) \ . \tag{6.39}$$

Intuitively, the sum-rate in (6.4) is upper bounded by

$$C(\mathbf{w}_1, \mathbf{w}_2, \mathbf{g}_1, \mathbf{g}_2) = \sum_{k=1}^{2} \log_2(1+\gamma_k) \leq \sum_{k=1}^{2} \log_2 \left(1 + (P_k/N_0) \lambda_{\max} \left(\mathbf{H}_k^H \mathbf{H}_k \right) \right) \tag{6.40}$$

with the sum power constraint $P_1 + P_2 = P$.

For some particular channels, this upper bound may be achievable. Denote $\{\mathbf{f}_i\} i = 1^N$ and $\{\mathbf{t}_i\} i = 1^N$ as the set of unit-norm eigenvectors of $\mathbf{H}_1^H \mathbf{H}_1$ and $\mathbf{H}_2^H \mathbf{H}_2$, respectively. Assume $\mathbf{f}_m$ and $\mathbf{t}_n$ are the principle eigenvectors (associated with the largest eigenvalues) of each user channel. If $\mathbf{f}_n \in \text{span}\{\mathbf{t}_i\}_{i=1, i \neq m}^N$ and $\mathbf{t}_m \in \text{span}\{\mathbf{f}_i\}_{i=1, i \neq n}^N$, then beamformers $\mathbf{w}_1 = \mathbf{f}_n$, $\mathbf{w}_2 = \mathbf{t}_m$ and combiners $\mathbf{g}_1 = \mathbf{H}_1 \mathbf{f}_n$, $\mathbf{g}_2 = \mathbf{H}_2 \mathbf{t}_m$ facilitate two users performing like two SU-MIMO MRC systems without interference.

6.5 Numerical Results

In this section, we give numerical examples that illustrate how the symmetric and asymmetric coordinated beamforming strategies proposed in Section 6.2 and Section 6.3 perform. We consider a system with N antennas at transmitter which sends data to two users with identical receivers employed M antennas each. We assume the transmitter allocates power P_k to the k-th user to maximize the sum-rate, where $P = P_1 + P_2$ is the total transmit power. We assume both user channels

undergo uncorrelated Rayleigh block fading. When signal fading is correlated, all the coordinated beamforming strategies can still be applied as written, although the resulting average sum-rate and achievable rate region will naturally depend on the fading covariances. We assume the perfect CSI known at each user is available at the transmitter, then no inter-use interference occurs for all the coordinated beamforming schemes. In this study, we ignore the situations that either partial or no CSI is available at the transmitter or imperfect CSI is at the receiver due to the channel estimation error.

In Figure 6.2, we plot the achievable average rate region of $C_k = \log_2(1+\gamma_k)$, $k = 1, 2$ by different coordinated beamforming strategies for configuration $N = M = 3$ and $N = M = 4$, respectively. Also shown for comparison is the rate region of *time division multiple access (TDMA)* which only serves one user for each transmission and is denoted as Time-Division. All the rate region are plotted at 15 dB SNR (the average input SNR P/N_0). For one channel realization, the rate region contains all the possible rate pairs (C_1, C_2) which are computed by changing the power allocation (P_1, P_2) subject to the total power constraint. For many channel realizations, these single channel rate regions can be averaged to form the achievable average rate region (referred to as rate region for short hereafter). The line-symmetric property of rate region along the line $C_1 = C_2$ for all the schemes except ACBF can be observed in both figures. This is due to the fact that the strategies other than ACBF aim to maximize the sum-rate without user preference.

In both figures, each rate region has three interesting areas near: $\max C_1$, $\max C_2$ and $\max C = \max(C_1 + C_2)$. In the area near $\max C_1$ of Figure 6.2(a), the asymmetric beamforming strategy ACBF (with preference for user 1) and time-

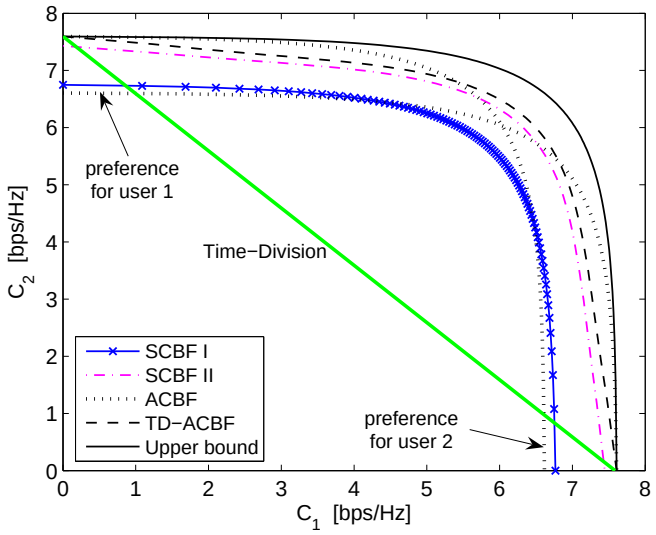

(a) $N = M = 3$

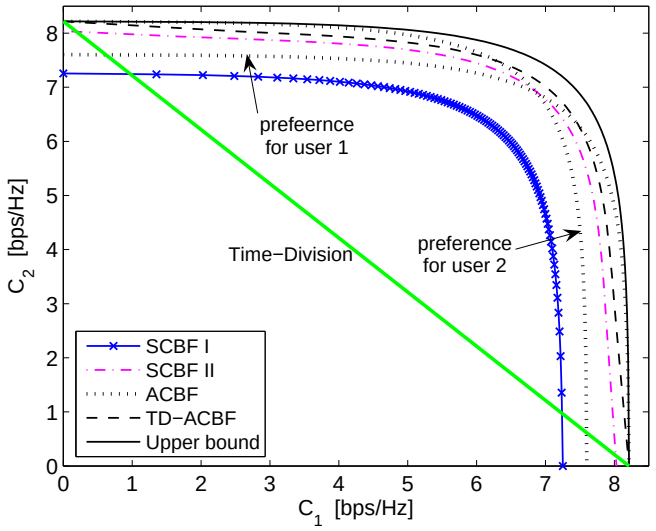

(b) $N = M = 4$

Figure 6.2: Achievable average rate region with SNR=15 dB.

division ACBF converge to the upper bound as P_1 increases and outperform the other three schemes: traditional SCBF (SCBF I), proposed SCBF (SCBF II) and ACBF

with preference for user 2. This result suggests that symmetry property of both SCBF approaches enforces more restriction on the system performance than the asymmetric case which facilitate the convergence to the upper bound. Not surprisingly, the ACBF with preference for user 1 converges much faster than TD-ACBF which reaches the upper bound only near the edge point $C_2 = 0$ with power allocation $(P_1, P_2) = (P, 0)$. The subspace optimization adopted in ACBF (with preference for user 1), TD-ACBF and SCBF II methods enlarges candidate sets of beamformers and/or combiners when $N, M > 2$ and therefore gives better performance than SCBF I. Though ACBF with preference for user 2 also utilizes subspace optimization, it suffers from the user preference and performs the worst. This is due to the fact that zero-interference constraints force the transmission between base station and user 1 offset the dominant eigenmode deeply when transmission between base station and user 2 is dominant. Similar results can be found in the area near $\max C_2$.

The sum-rate performance is also shown in Figure 6.2(a) near the area of $\max C = \max(C_1 + C_2)$. As we expected, TD-ACBF improves the sum-rate relative to the ACBF with user-preference. Sum rate of SCBF II lies in between these two TD-ACBF and ACBF strategies, i.e., about 0.2 bps/Hz worse than TD-ACBF and 0.3 bps/Hz better than ACBF. Though the TD-ACBF is worse than the upper bound about 0.7 bps/Hz, it has improved the sum-rate about 1 bps/Hz compared with the traditional scheme, SCBF I.

Rate region of larger arrays are shown in Figure 6.2(b) for $N = M = 4$. The dimension of the subspaces of the candidate beamformer and/or combiners is increased using larger arrays. The optimization over these subspaces gives more freedom in the system design and improves the performance. In this figure, we can

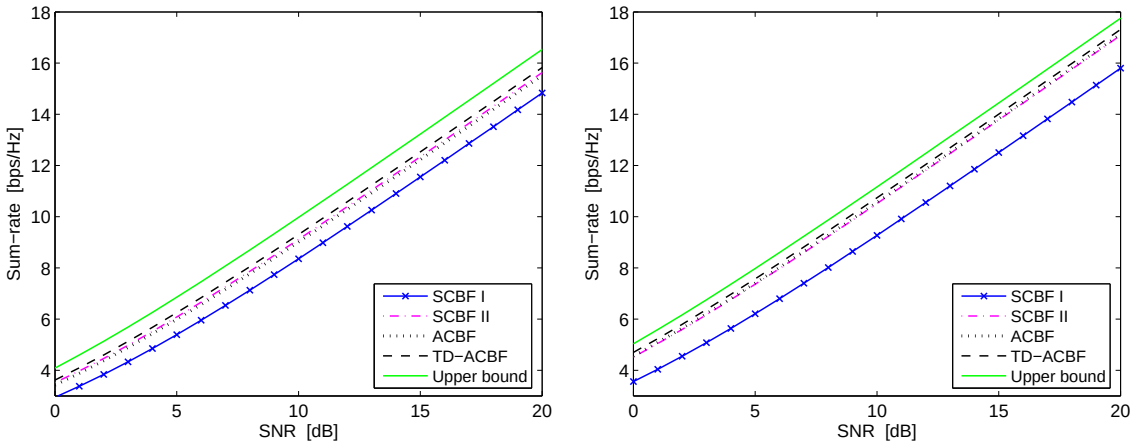

(a) $N = M = 3$ (b) $N = M = 4$

Figure 6.3: Achievable average sum-rate vs. SNR.

see that the SCBF I without subspace optimization performs the worst in all the three areas: near $\max C_1$, near $\max C_2$ and near $\max C$. Another key observation is that the sum-rate improvement of TD-ACBF over SCBF I is increased to 1.5 bps/Hz compared with the 1 bps/Hz improvement for $N = M = 3$ configuration.

Figure 6.3 shows the achievable average sum-rate versus the SNR of four coordinated beamforming schemes as well as the upper bound for two configurations: $N = M = 3$ and $N = M = 4$. In Figure 6.3(a) for $N = M = 3$, TD-ACBF outperforms all the other three coordinated beamforming scheme in the whole range of SNR. And the tradition scheme SCBF I performs the worst compared with the other three schemes based on subspace optimization. Similar phenomena can be seen in Figure 6.3(b) for larger arrays $N = M = 4$. Once again, TD-ACBF increases the performance improvement relative to the SCBF I using larger arrays.

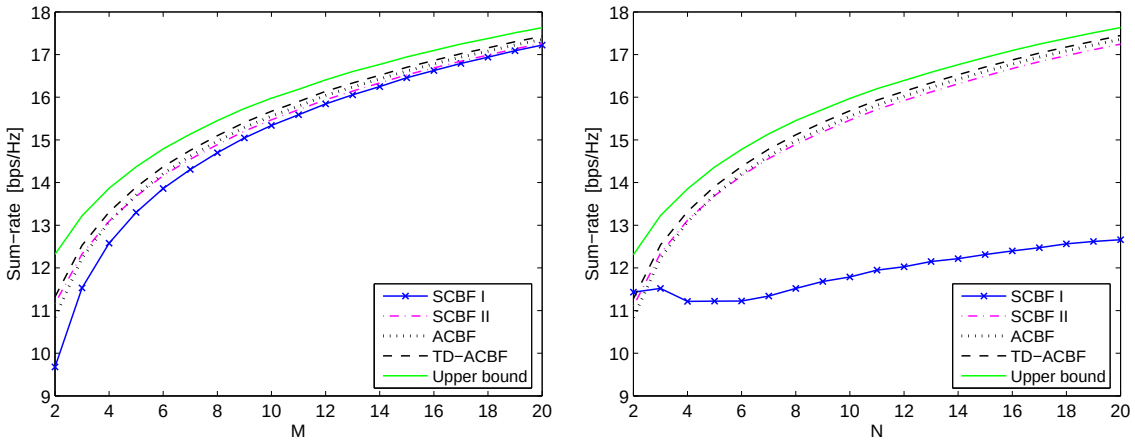

(a) $N = 3$ (b) $M = 3$

Figure 6.4: Achievable average sum-rate vs. (a) number of Tx antennas with $M = 3$ (b) number of Rx antennas with $N = 3$ for SNR $= 15$ dB.

Further insights can be gained by examining the sum-rate performance versus the number of transmit antennas or receive antennas. Figure 6.4(a) plots the sum-rate achieved by two SCBF and two ACBF methods versus the number of receive antennas $M \in [2, 20]$ with $N = 3$ when the SNR is 15 dB. All sum-rates become close to the upper bound as M increases. More precisely, the highest sum-rate is achieved by TD-ACBF which is slightly better than ACBF and SCBF II in the whole range of $2 \leq M \leq 20$. Lowest sum-rate occurs at SCBF I and the performance loss compared with SCBF II is about 1.3 bps/Hz when $M = 2$ and reduces to zero as M increases.

Interesting phenomenon occurs when the number of transmit antennas varies. Figure 6.4(b) plots the sum-rate of all the schemes considered above versus the number of transmit antennas $N \in [2, 20]$ with $M = 3$ when the SNR is 15 dB. From this figure, we can see that TD-ACBF, ACBF and SCBF II have the same trend as those

in Figure 6.4(a). However, SCBF I performs inconsistently and does not converge to SCBF II as N increases. This is due to the less number of candidate beamformers. Note that two beamformers $\mathbf{w}_1$ and $\mathbf{w}_2$ in SCBF I are the generalized eigenvectors of two $N \times N$ Hermitian matrices $\mathbf{F}_1$ and $\mathbf{F}_2$ defined in (6.9). When $N > M$, these two matrices become singular and only have M available generalized eigenvectors (associated with non-zero generalized eigenvalue) can be used as beamformers. This dimensional degradation forces big offsets of beam directions relative to the largest eigenmode for the data transmission and therefore results in a big performance loss. However, the other three schemes, SCBF II, ACBF and TD-ACBF, still can find better beam directions using the beamformers and combiners based on subspace optimization. An interesting phenomenon in this figure is the sum-rate performance when $N = 2$ or 3. When $N = M = 3$, SCBF I performs relatively well and has small performance gaps compared with other schemes though it is still the worst. This is intuitive since both $\mathbf{F}_1$ and $\mathbf{F}_2$ have full rank and their generalized eigenvectors may not suffer big beam direction offsets. When $N = 2$, SCBF I achieves the best performance. This is because $N = 2$ reduces the number of candidate beamformers to 2 and then there is no way to apply the subspace optimization which is key technique for SCBF II, ACBF and TD-ACBF. The optimality of SCBF I when $N = 2$ is demonstrated by Chae *et al.* [12]. In practice, the base station has more freedom to employ more antennas than the mobile units.

The results above suggest that TD-ACBF achieves the best sum-rate performance which is, however, not necessarily the optimal achievable sum-rate. We now consider the sum-rate maximization problem based on TD-P-ACBF. Figure 6.5 plots the achievable average sum-rate of TD-P-ACBF versus parameter $s \in [0, 1]$ when

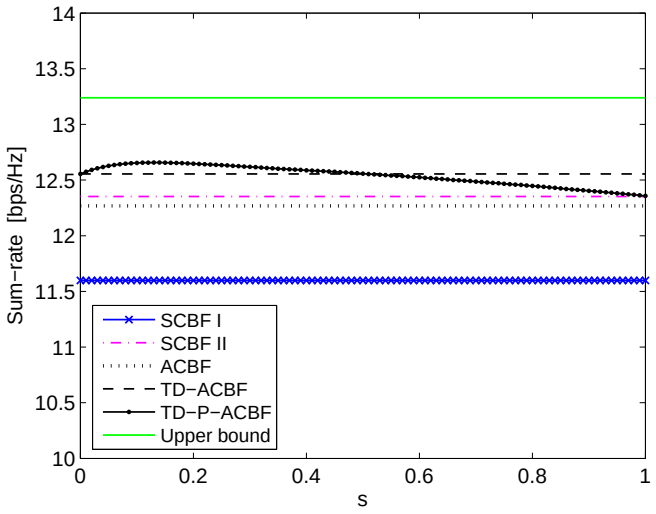

Figure 6.5: Achievable average sum-rate vs. parameter s with $N = M = 3$ and SNR = 15 dB.

$N = M = 3$ and SNR=15 dB. The achievable average sum-rate of SCBF I, SCBF II, ACBF and TD-ACBF are also shown for comparison though there are constant over parameter s. Interesting phenomenon occurs in the range $0 < s < 0.5$ where TD-P-ACBF outperforms all the other schemes. Especially TD-P-ACBF reaches the maximum point at $s = 0.13$ where there is a rate increase of 0.1 bps/Hz compared with TD-ACBF.

Achievable average rate region of TD-P-ACBF with $N = M = 3$ and $s = 0.13$ is plotted in Figure 6.6. And all the other rate regions remain the same as in Figure 6.2(a). We can observe 0.1 bps/Hz sum-rate improvement over TD-ACBF in the area near $\max C$. Note that the optimal value of parameter s may be different for different system configurations. When SNR=15 dB, some experimental value of s which let TD-P-ACBF achieve the highest sum-rate are given in Table 6.1.

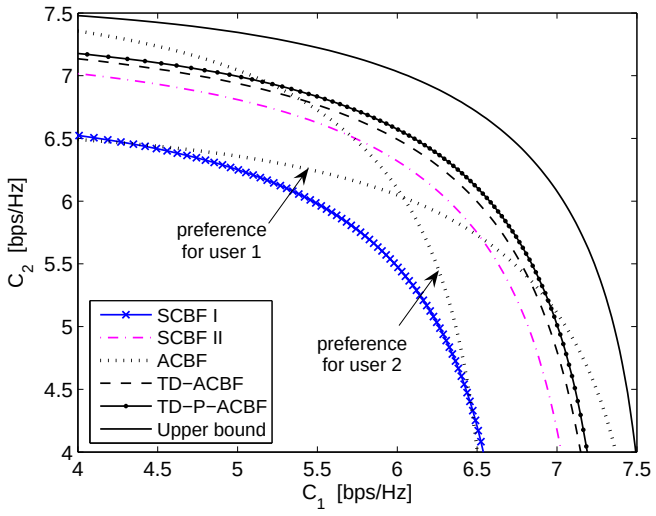

Figure 6.6: Achievable average rate region with $N = M = 3$ and $\mathsf{SNR} = 15$ dB.

Table 6.1: Experimentally optimal value of parameter s for TD-P-ACBF.

(N, M)	(3,3)	(3,4)	(4,3)	(4,4)	$\cdots$
s	0.13	0.09	0.08	0.06	$\cdots$

Note that TD-P-ACBF with the optimal parameter value may not necessarily be the globally optimal approach. Hence it still remains the open problem to find the beamformers and combiners to achieve the globally highest sum-rate subject to the zero-interference constraints.

6.6 Conclusion

In this chapter, we investigated the individual rate and sum-rate performance on downlink coordinated beamforming systems. We presented new symmetric-rate

and asymmetric-rate coordinated beamforming methods for two receivers appropriate for MIMO broadcast channels. We then considered the maximization problem of sum-rate by combining time-division policy with asymmetric coordinated beamforming techniques. Numerical results in the previous section suggest the following findings:

First, when $N > 2$, all the proposed schemes achieve higher sum-rate than the traditional coordinated beamforming with the help of subspace optimization on finding the beamformers and combiners. As the number of either transmit or receive antennas increases, all the proposed schemes achieve sum-rates close to the upper bound. The traditional scheme performs the best when $N = 2$ but suffers a big performance loss when $N > 2$.

Second, the best individual rate is attained when asymmetric coordinated beamforming is used. Then the preferred user can always transmit data along its largest eigenmode like SU-MIMO MRC system. Though the other user may sacrifice its rate, the system still can achieves a relative better sum-rate performance compared with the traditional symmetric scheme and close to the proposed symmetric scheme.

Third, time-division policy can be introduced into ACBF to achieve higher sum-rate by changing user-preference and their individual rates. Sum-rate performance can be further maximized in the proposed parameterized asymmetric strategy with time-division policy and appropriate value of parameter.

We conclude that all the proposed coordinated beamforming schemes can significantly outperform the traditional scheme studied in [14] when the transmitter employs more than two antennas. Moreover, all the proposed methods are non-iterative, linear and interference-canceled like the traditional method, and still enjoy the benefits of coordinated beamforming for MIMO broadcast channels.

Chapter 7

Summary, Conclusions and Future Work

7.1 Summary

MIMO systems have been recognized as a important technique to meet the ever increasing demand for high data-rate and high link-quality in wireless communications. MIMO beamforming is a promising transmission scheme that offers extra gain by exploiting the spatial dimensions in MIMO channels [38] and has been considered as one of the key technique for current and emerging wireless systems [47], [48], [1]. Such promises rely on the key assumptions that the transmitter and receiver know the full channel knowledge and each antenna array has sufficiently large spacings so as to be essentially uncoupled. Real-world MIMO systems are however much more complex and may experience antenna coupling and imperfect channel knowledge as well as multiuser interference.

In this dissertation, we extended the prior studies on MIMO beamforming with ideal assumptions, and considered the design of MIMO beamforming with mutual coupling, limited feedback and coordination. We summarize the main results in Section 7.2 and raise some possible direction of future work in Section 7.3.

7.2 Conclusions

We began our study in Chapter 2 by evaluating the performance of beamforming in two MIMO communication schemes: SU-MIMO MRC and downlink MU-MIMO CBF. In particular, we looked at the outage probability of SU-MIMO MRC and sum-rate of MU-MIMO CBF each with unlimited feedback (full CSI) and limited feedback. For SU-MIMO MRC scheme, larger array can achieve lower outage and higher diversity gain with full CSI or limited feedback with more feedback bits. This improvement however is reduced when the transmitter is correlated. Similar advantage of larger array can be found in MU-MIMO CBF scheme with full CSI to obtain higher sum-rate relative to small array or SISO system. When the feedback is limited, MU-MIMO CBF suffers from the multiuser interference but may use more feedback bits to improve the performance. The default assumption that both transmit array and receive array are uncoupled motivated the study of mutual coupling effect in subsequent chapters.

In Chapter 3, we introduced a model for compact diversity transmitter and then investigated the impact of transmitter correlation, mutual coupling and matching networks on SU-MIMO MRC system with full CSI. We presented optimal transmission strategies for three input power metrics as well as formulas for the resulting

outage probabilities. It was shown that regardless of the power measure considered and matching networks used, most of the performance benefits of SU-MIMO MRC can be obtained when transmit antennas are strongly coupled.

In Chapter 4, we relaxed the full CSI assumption used in Chapter 3 and considered the following effects on SU-MIMO MRC system with mutual coupling: (1) CSIR with limited feedback and (2) imperfect channel estimation at receiver with unlimited feedback. By observing the codebook design of transmit beamformers with transmitter correlation only in Chapter 2, we were able to extend existing design principles to the coupled system subject to three different power measures. For the second scenario, a pilot-based LMMSE channel estimator was used to evaluate the performance in the presence of channel estimation error and the way to reduce the estimation error.

In Chapter 5, we studied the effects of receive antenna coupling, matching networks and correlated noise on the design and performance of downlink MU-MIMO CBF system. New CBF algorithm with full CSI as well as the limited feedback design suitable for correlated fading and noise was proposed and examined on a more realistic model for multi-antenna receiver front-end that characterizes the signal and noise correlation that results from mutual coupling. The properties of the receive array, matching networks, amplifiers, noise sources and channel state feedback were shown to affect the performance.

In Chapter 6, we aimed to improve the sum-rate of downlink MU-MIMO CBF from a communication perspective with the ideal assumption that antennas are uncoupled and both fading and noise are uncorrelated. By observing the symmetry property of traditional and proposed symmetric coordinated beamforming methods, we pro-

pose new asymmetric-rate coordinated beamforming strategies which improve both the individual rates of each user and the sum-rate subject to zero-interference constraints. These asymmetric-rate strategies can also be combined using time-division to create new, higher-rate symmetric beamforming strategies.

7.3 Future Work

Several interesting problems raised during this study and some related topics are worth to be addressed in future research. First, from a communication theory perspective, we may recommend

(1) *Mutual Coupling Effects on Other MIMO Beamforming Systems*

In single-user closed-loop MIMO beamforming systems, transmit beamforming techniques such as selection diversity transmission (SDT), equal gain transmission (EGT), and maximum ratio transmission (MRT), and receive combining techniques such as selection diversity combining (SDC), equal gain combining (EGC), and maximum ratio combining (MRC) have been used to obtain the diversity advantage (see [62], [90], [88], [63], [70] and references therein). Unit-norm beamformers $\mathbf{w}$ and combiners $\mathbf{g}$ can be any complex vectors in MRT and MRC, and have entries with equal absolute value in EQT and EQC (i.e., $|w_i| = 1/\sqrt{N}$, $i = 1, \ldots, M$ and $|g_j| = 1/\sqrt{M}$, $j = 1, \ldots, M$), and are constrained to be columns of identity matrix in SDT and SDC[1]. Compared with the SU-MIMO MRC using MRT-MRC studied in this dissertation, other eight combined techniques have relative lower complexity but non-optimal

[1]They can be extended to antenna selection (AS) which selects a subset of antennas during each transmission. When the subset is limited to one antenna, antenna selection reduces to SDT and/or SDC.

performance. Then it would be an interesting topic to investigate the mutual coupling effects on these closed-loop MIMO beamforming techniques as well as their quantized versions (limited feedback).

The open-loop MIMO beamforming systems in the presence of mutual coupling has been deeply studied such as receive antenna selection [99] and [100], and optimal MRC receiver [25], but is not completed yet.

The study of these beamforming techniques can be parallelly applied to multiuser MIMO systems.

(2) *Mutual Coupling Effects on MIMO Spatial Multiplexing Systems*

Spatial multiplexing (SM or SMX) is another transmission technique in MIMO wireless systems to transmit multiple data streams simultaneously and has been adopted in may wireless communication standards [44], [47], [48], [1]. Some specific MIMO spatial multiplexing technique such as Vertical-Bell Laboratories -Layered -Space-Time (V-BLAST) [96] with mutual coupling is studied in [22]. However, the design of more general MIMO spatial multiplexing for SU-MIMO or MU-MIMO in the presence of mutual coupling is still unsolved.

(3) *Optimality of Coordinated Beamforming for downlink MU-MIMO Systems*

TD-P-ACBF in Chapter 6 can maximize the sum-rate performance with appropriate value of parameter, however, is not necessarily globally optimal. To prove the optimality of TD-P-ACBF or to find the globally optimal beamformers and combiners still remain the open problems.

(4) *Multiuser Diversity in Downlink MU-MIMO CBF*

Prior work and our study on coordinated beamforming for MIMO broadcast channels only support two active users [97], [14] and Chapter 6 and therefore achieve

small multiuser diversity [43]. Two basic approaches can be used to improve the downlink multiuser diversity. One is to select two active users from a large number of users by scheduling. Traditional CBF with scheduling is studied in [14] but the proposed SCBF and ACBF are still lack of user scheduler. The other approach is to design a new coordinated beamforming strategy to support more than two active users simultaneously[2]. Note that traditional CBF cannot suppress the interference for more than two users based on generalized eigenvalue decomposition. The proposed coordinated beamforming schemes seem to have freedom to design beamformers and combiners for more than two users subject to zero interference constraints, which is worth to be addressed in the future.

Second, from a radio frequency perspective, we may recommend

(1) *Other Configuration of Antenna Array*

The coupled antenna array studied in Chapter 3, 4 and 5 is assumed to be uniform linear array (ULA). The compact uniform circular array (UCA) [49], [46] is another interesting array configuration in which we would apply the insights developed in this dissertation.

(2) *Experimental verification*

The numerical examples of antenna coupling in Chapter 3, 4 and 5 considered an idealized model for thin-wire omnidirectional dipole antennas and simply assumed 2-dimensional signal fading. The practical dipole antennas are much more complex [6] and the coupling among the feed lines[3] should be also taken into account. Hence, experimental work using either numerical simulation software[4] or real test-bed would

[2]Scheduling may be also added here for extra improvement.

[3]The feed line in RF systems is the physical cabling that carries the RF signal to and/or from the antenna.

[4]Such as NEC [2], Ansoft HFSS [4], Zeland IE3D [104], etc.

be an additional verification of our study.

(3) *Modern Antennas*

In modern telecommunications, patch antennas such as Planar Inverted F Antenna (PIFA) are commonly used in cellular handsets with built-in antennas and recommended for 4G terminals [82]. It would be more realistic to extend the insights of this dissertation to the compact PIFA antenna array based on the prior studies and experiments of PIFA antennas with mutual coupling [9], [19].

Bibliography

[1] 3GPP TS 36.213 v8.6.0, 3GPP; Technical Specification Group Radio Access Network; Evolved Universal Terrestrial Radio Access (E-UTRA); Physical layer procedures (Release 8), Mar. 2009.

[2] A. Voors, 4nec2, NEC based antenna modeler and optimizer. [Online]. Available: http://home.ict.nl/∼arivoors/

[3] V. A. Aalo, "Performance of maximal-ratio diversity systems in a correlated Nakagami-fading environment," *IEEE Trans. Commun.*, vol. 43, pp. 2360-2369, Aug. 1995.

[4] Ansoft HFSS^{TM}: 3D Full-wave Electromagnetic Field Simulation. [Online]. Available: http://www.ansoft.com/products/hf/hfss/

[5] P. Almers, E. Bonek, A. Burr, *et al.*, "Survey of channel and radio propagation models for wireless MIMO systems," *EURASIP J. Wireless Commun. and Netw.*, vol. 2007, 2007.

[6] C. B. Balanis, *Antenna Theory: Analysis and Design,* 2nd ed. New York: Wiley, 1997.

[7] E. Biglieri, R. Calderbank, A. Constantinides, A. Goldsmith, A. Paulraj, and H. V. Poor, "MIMO Wireless Communications," Cambridge: University Press, 2007.

[8] M. Biguesh and A. B. Gershman, "Training-based MIMO channel estimation: a study of estimator tradeoffs and optimal training signals," *IEEE Trans. Signal Process.*, vol. 54, pp. 884–893, Mar. 2006.

[9] D. W. Browne, M. Manteghi, M. P. Fitz, and Y. Rahmat-Samii, "Experiments With Compact Antenna Arrays for MIMO Radio Communications," *IEEE Trans. Antenna Propga.*, vol. 54, pp. 3239–3250, Nov. 2006.

[10] D. G. Brennan, "Linear diversity combining techniques," in *Proc. IRE*, vol. 47, pp. 1075–1102, Jun. 1959.

[11] G. Caire and S. Shamai (Shitz), "On the achievable throughput of a multi-antenna Gaussian broadcast channel," *IEEE Trans. Inf. Theory*, vol. 43, pp. 1691–1706, Jul. 2003.

[12] C.-B. Chae and R. W. Heath Jr., "On the optimality of linear multiuser MIMO beamforming for a two-user two-input multiple-output broadcast system," *IEEE Signal Process. Lett.*, vol. 16, pp. 117-120, Feb. 2009.

[13] C.-B. Chae, R. W. Heath Jr., and D. Mazzarese, "Achievable sum rate bounds of zero-forcing based linear multi-user MIMO systems," in *Proc. 44th Allerton Conf. Commun., Control, Comput.*, pp. 1134–1140, Sep. 2006.

[14] C.-B. Chae, D. Mazzarese, N. Jindal and R. W. Heath Jr.,"Coordinated beam-

forming with limited feedback in the MIMO broadcast channel," *IEEE J. Sel. Areas Commun.*, vol. 26, no. 8, pp. 1505–1515, Oct. 2008.

[15] C.-B. Chae, D. Mazzarese, T. Inoue, and R. W. Heath Jr., "Coordinated beamforming for the multiuser MIMO broadcast channel with limited feedforward," *IEEE Trans. Signal Process.*, vol. 56, pp. 6044–6056, Dec. 2008.

[16] S. Chandran, "Adaptive Antenna Arrays: Trends and Applications," Springer, Jul. 2007.

[17] K. Chang, "RF and microwave wireless systems," 1st ed. New York: Wiley, 2000.

[18] Y. Chen and C. Tellambura, "Performance analysis of maximal ratio transmission with imperfect channel estimation," *IEEE Commun. Lett.*, vol. 9, pp. 322–324, Apr. 2005.

[19] C.-Y. Chiu, C.-H. Cheng, R. D. Murch, and C. R. Rowell, "Reduction of mutual coupling between closely-packed antenna elements," *IEEE Trans. Antennas Propga.*, vol. 55, pp. 1732–1738, Jun. 2007.

[20] L.-U. Choi, R. D. Murch, "A transmit preprocessing technique for multiuser MIMO systems using a decomposition approach," *IEEE Trans. Wireless Commun.*, vol. 3, pp. 20–24, Jan. 2004.

[21] R. H. Clarke, "A statistical theory of mobile-radio reception," *Bell Syst. Tech. J.* , vol. 47, pp. 957–1000, Jul. 1968.

[22] B. Clerckx, D. Vanhoenacker-Janvier, C. Oestges, and L. Vandendorpe, "Mutual coupling effects on the channel capacity and the space-time processing of MIMO

communication systems," in *Proc. 2003 IEEE Int. Conf. Commun. (ICC'03)*, Anchorage, AK, vol. 4, pp. 2638–2642.

[23] T. M. Cover and J. A. Thomas, "Elements of Information Theory," 2nd ed. Hoboken, NJ: Wiley, 2006.

[24] P. A. Dighe, R. K. Mallik and S. S. Jamuar, "Analysis of transmit-receive diversity in Rayleigh fading," in *Proc. 2001 IEEE Global Commun. Conf. (GLOBECOM'01)*, San Antonio, TX, pp. 1132–1136.

[25] C. P. Domizioli, B. L. Hughes, K. G. Gard and G. Lazzi, "Receive diversity revisited: correlation, coupling and noise," in *Proc. 2007 IEEE Global Commun. Conf. (GLOBECOM'07)*, Washington DC, pp. 3601–3606.

[26] C. P. Domizioli, B. L. Hughes, K. .G. Gard, and G. Lazzi, "Optimal front-end design for MIMO receivers," in *Proc. 2008 IEEE Global Commun. Conf. (GLOBECOM'08)*, New Orleans, LA.

[27] C. P. Domizioli and B. L. Hughes, "Front-end design for compact MIMO receivers: a communication theory perspective," in preparation.

[28] Y. Dong, B. L. Hughes and G. Lazzi, "The impact of mutual coupling on MIMO maximum-ratio combining," in *Proc. IEEE Global Commun. Conf. (GLOBECOM'07)*, Washington DC, pp. 4516–4521.

[29] Y. Dong, B. L. Hughes and G. Lazzi, "Mutual Coupling Effects in MIMO MRC Systems with Limited Feedback," in *Proc. 2008 IEEE Global Commun. Conf. (GLOBECOM'08)*, New Orleans, LA.

[30] Y. Dong, C. P. Domizioli, and B. L. Hughes, "Effects of mutual coupling and noise correlation on downlink coordinated beamforming with limited feedback," *EURASIP J. Advances Signal Process.*, vol. 2009, 2009.

[31] Y. Dong, and B. L. Hughes, "Impact of mutual coupling on MIMO MRC Systems with channel estimation," in preparation.

[32] Y. Dong, and B. L. Hughes, "Asymmetric coordinated beamforming for MIMO broadcast channels," in preparation.

[33] B. Farhang-Boroujeny, Q. Spencer, and A. L. Swindlehurst, "Layering techniques for space-time communications in multi-user networks," in *Proc. 2003 IEEE 58th Veh. Technol. Conf. (VTC'03-Fall))*, Orlando, FL, vol. 2, pp. 1339–1342.

[34] G. J. Foschini and M. J. Gans, "On limits of wireless communications in a fading environment when using multiple antennas," *Wireless Personal Commun.*, vol. 6, pp. 311–335, 1998.

[35] M. J. Gans, "The effect of Gaussian error in maximal ratio combiners," *IEEE Trans. Commun. Tech.*, vol. COM-19, no. 4, pp. 492–500, Aug. 1971.

[36] M. J. Gans, "Channel capacity between antenna arrays C Part I: Sky noise dominates," *IEEE Trans. Commun.*, vol. 54, pp. 1586–1592, Sep. 2006.

[37] M. J. Gans, "Channel capacity between antenna arrays C Part II: Amplifier noise dominates," *IEEE Trans. Commun.*, vol. 54, pp. 1983–1992, Nov. 2006.

[38] A. B. Gershman and N. D. Sidiropoulos, Eds., "Space-Time Processing for

MIOM Communications," Chichester, West Sussex, England: John Wiley and Sons, 2005.

[39] D. Gesbert, H. Holcskei, D. A. Gore, and A. J. Paulraj, "Outdoor MIMO wireless channels: Models and performance prediction," *IEEE Trans. Commun.*, vol. 50, pp. 1926–1934, Dec. 2002.

[40] A. Goldsmith, S. A. Jafar, N. Jindal, and S. Vishwanath, "Capacity limites of MIMO channels," *IEEE J. Sel. Areas Commun.*, vol. 21, no. 5, pp. 684–702, Jun. 2003.

[41] B. Hassibi, and B. M. Hochwald, "How much training is needed in multiple-antenna wireless links?" *IEEE Trans. Inf. Theory*, vol. 49, pp. 951–963, Apr. 2003.

[42] H. A. Haus and R. B. Adler, *Circuit Theory of Linear Noisy Networks*, New York: Wiley, 1959.

[43] R. W. Heath, Jr., M. Airy, and A. J. Paulraj, "Multiuser diversity for MIMO wireless systems with linear receivers," in *Proc. 2001 35th Asilomar Conf. Signals, Syst., Computers (ACSSC'01)*, Pacific Grove, CA, vol. 2, pp. 1194–1199.

[44] H. Holma and A. Toskala, Eds., "WCDMA for UMTS: Radio Access for Third Generation Mobile Communications," 2nd ed. New York: Wiley, 2002.

[45] H. Holma and A. Toskala, Eds., "HSDPA/HSUPA for UMTS: Radio Access for Third Generation Mobile Communications," New York: Wiley, 2006.

[46] Z. Huang, C. A. Balanis, and C. R. Birtcher, "Mutual coupling compensation in UCAs: Simulations and experiment," *IEEE Trans. Antennas Propag.*, vol. 54, pp. 3082–3086, Nov. 2006.

[47] IEEE P802.11n/D1.0: Draft Amendment to Wireless LAN Media Access Control (MAC) and Physical Layer (PHY) Specifications: Enhancements for Higher Throughput, Mar. 2006.

[48] IEEE Std. 802.16e-2005, IEEE Standard for LAN/MAN, Part 16: Air Interface for Fixed and Mobile Broadband Wireless Access Systems, Feb. 2006. [Online]. Available: http://standards.ieee.org/getieee802/download/802.16e-2005.pdf

[49] P. Ioannides and C. A. Balanis, "Mutual coupling is adaptive circular arrays," in *Proc. 2004 IEEE Antennas Propag. Soc. Int. Symp.*, Monterey, CA, vol. 1, pp. 403–406.

[50] R. Janaswamy, "Radioware Propagation and Smart Antennas for Wireless Communications," Norwell, MA: Kluwer Academic Publishers, 2001.

[51] R. Janaswamy, "Effect of element mutual coupling on the capacity of fixed length linear arrays," *IEEE Antennas Wireless Propag. Lett.*, vol. 1, pp. 157–160, 2002.

[52] M. Jankiraman, *Space-time Codes and MIMO Systems*, Artech House, 2004.

[53] N. Jindal, W. Rhee, S. Vishwanath, S. A. Jafar, and A. Goldsmith, "Sum power iterative water-filling for multi-antenna Gaussian broadcast channels," *IEEE Trans. Inf. Theory*, vol. 51, pp. 1570–1580, Apr. 2005.

[54] M. Kang and M.-S. Alouini, "Largest eigenvalue of complex Wishart matrices and performance analysis of MIMO MRC systems," *IEEE J. Sel. Areas Commun.*, vol. 21, no. 3, pp. 418–426, Apr. 2003.

[55] M. Kang and M.-S. Alouini, "Impact of correlation on the capacity of MIMO channels," in *Proc. 2003 IEEE Int. Conf. Commun. (ICC'03)*, Anchorage, AK, vol. 4, pp. 2623–2627.

[56] J. P. Kermoal, L. Schumacher, K. I. Pedersen, P. E. Mogensen, and F. Frederiksen, "A stochastic MIMO radio channel model with experimental validation," *IEEE J. Sel. Areas Commun.*, vol. 20, no. 6, pp. 1211–1226, Aug. 2002.

[57] C. G. Khatri, "Distribution of the largest or the smallest characteristic root under null hyperthesis concerning complex multivariate normal populations," *Ann. Math. Stat.*, vol. 35, pp. 1807–1810, Dec. 1964.

[58] S. Krusevac, P. B. Rapajic, and R. A. Kennedy, "The method for MIMO channel capacity estimation in the presence of spatially correlated noise," in *Proc. 2004 IEEE Int. Symp. Spread Spectr. Tech. Applicat. (ISSSTA'04)*, Sydney, Australia, pp. 511-514.

[59] B. K. Lau, J. B. Andersen, G. Kristensson and A. F. Molisch, "Impact of matching network on bandwidth of compact antenna arrays," *IEEE Trans. Antennas Propag.*, vol. 54, pp. 3225–3238, Nov. 2006.

[60] W. C. Y. Lee, "Mutual coupling effect on maximum-ratio diversity combiners and application to mobile radio," *IEEE Trans. Commun. Technol.*, vol. COM-18, pp. 779–791, Dec. 1970.

[61] X. Li and Z.-P. Nie, "Mutual coupling effect on the performance of MIMO wireless channels," *IEEE Antennas Wireless Propag. Lett.*, vol. 3, pp. 344–347, 2004.

[62] T. K. Y. Lo, "Maximum ratio transmission," *IEEE Trans. Commun.*, vol. 47, pp. 1458–1461, Oct. 1999.

[63] D. J. Love, R. W. Heath, Jr., "Equal transmission in multiple-input multiple-output wireless systems," *IEEE Trans. Commun.*, vol. 51, pp. 1102–1110, Jul. 2003.

[64] D. J. Love, R. W. Heath, Jr. and T. Strohmer, "Grassmannian beamforming for multiple-input multiple-output wireless systems," *IEEE Trans. Inf. Theory*, vol. 49, pp. 2735–2747, Oct. 2003.

[65] D. J. Love and R. W. Heath, Jr., "Limited Feedback Diversity Techniques for Correlated Channels," *IEEE Trans. Veh. Technol.*, vol. 55, no. 2, pp. 718–722, Mar. 2006.

[66] D.J. Love, R. W. Heath, Jr., V. K. N. Lau, D. Gesbert, B. D. Rao, and M. Andrews, "An overview of limited feedback in wireless communication systems," *IEEE J. Sel. Areas Commun.*, vol. 26, no. 8, pp. 1341–1365, Oct. 2008.

[67] A. Maaref and S. Aissa, "Spectral efficiency limitations of maximum ratio transmission in the presence of channel estimation errors," in *Proc. 2005 IEEE 62nd Veh. Technol. Conf. (VTC'05-Fall)*, Dallas, TX, vol. 1, pp. 502–506.

[68] Maxim 2642/2643 LNAs. Data sheet. [Online]. Available: http://datasheets.maxim-ic.com/en/ds/MAX2642-MAX2643.pdf

[69] M. R. McKay, A. J. Grant, and I. B. Collings, "Largest eigenvalue statistics of double-correlated complex Wishart matrices and MIMO-MRC," in *Proc. 2006 IEEE Int. Conf. Acoust., Speech, Signal Process. (ICASSP'06)*, Toulouse, France, vol. 4, pp. IV-1–4.

[70] A. F. Molisch, M. Z. Win, and J. H. Winters, "Reduced-complexity transmit /receive-diversity systems," *IEEE Trans. Signal Process.*, vol. 51, pp. 2729–2738, Nov. 2003.

[71] M. L. Morris, M. A. Jensen, "Improved network analysis of coupled antenna diversity performance," *IEEE Trans. Wireless Commun.*, vol. 4, no. 4, pp. 1928-1934, Jul. 2005.

[72] K. K. Mukkavilli, A. Sabharwal, E. Erkip and B. Aazhang, "On beamforming with finite rate feedback in multiple-antenna systems," *IEEE Trans. Inf. Theory*, vol. 49, pp. 2562–2579, Oct. 2003.

[73] A. Narula, M. J. Lopez, M. D. Trott, and G. W. Wornell, "Efficient use of side information in mulitiple-antenna data transmission over fading channels," *IEEE J. Sel. Areas Commun.*, vol. 16, no. 8, pp. 1423–1436, Oct. 1998.

[74] M. Ozcelik, N. Herdin, W. Weichselberger, J. Wallace, and E. Bonek, "Deficiencies of Kronecker's MIMO radio channel model," *Electron. Lett.*, vol. 39, pp. 1209–1210, Aug. 2005.

[75] M. Ozcelik, N. Czink, and E. Bonek, "What makes a good MIMO channel model?" in *Proc. 2005 IEEE 61st Veh. Tech. Conf. (VTC'05-Spring)*, Stockholm, Sweden, vol. 1, pp. 156–160.

[76] Z. Pan, K.-K. Wong, and T.-S. Ng, "Generalized multiuser orthogonal space-divition mltiplexing," *IEEE Trans. Wireless Commun.*, vol. 3, pp. 1969–1973, Nov. 2004.

[77] C. B. Peel, B. M. Hochwald, and A. L. Swindlehurst, "A vector-pertubation technique for near capacity multiantenna multiuser communication - part I: channel inversion and regularization," *IEEE Trans. Commun.*, vol. 53, pp. 195–202, Jan. 2005.

[78] D. M. Pozar, "Microwave Engineering," 3rd ed. New York: Wiley, 2005.

[79] J. Roh, and B. D. Rao, "Transmit beamforming in multiple-antenna aystems with finite rate feedback: a VQ-based approach," *IEEE Trans. Info. Theory*, vol. 52, pp. 1101–1112, Mar. 2006.

[80] X. Rui, R. Jin, and J. Geng, "Performance analysis of MIMO MRC systems in the presence of self-interference and co-channel interference," *IEEE Signal Process. Lett.*, vol. 14, pp. 801–803, Nov. 2007.

[81] H. Sampath and A. Paulraj, "Linear precoding for space-time coded systems with known fading correlation," *IEEE Commun. Letters*, vol. 6, pp. 239–241, Jun. 2002.

[82] D. A. Sanchez-Hernandez, "Multiband Integrated Antennas for 4G Terminals," Norwood, MA: Artech House, 2008.

[83] K. Seung, "Performance analysis of MIMO-MRC systems with channel estimation error in the presence of cochannel interference," *IEEE Signal Process. Lett.*, vol. 15, pp. 445–448, 2008.

[84] Q. Spencer, A. L. Swindlehurst, and M. Haardt, "Zero-forcing methods for downlink spatial multiplexing in multiuser MIMO channels," *IEEE Trans. Sig. Process.*, vol. 52, pp.462–471, Feb. 2004.

[85] T. Svantesson and A. Ranheim, "Mutual coupling effects on the capacity of multielement antenna systems," in *Proc. 2001 IEEE Int. Conf. Acoust., Speech, Signal Process. (ICASSP'01)*, Salt Lake City, UT, vol. 4, pp. 2485–2488.

[86] C. T. Tai, "Coupled antennas," in *Proc. IRE*, vol. 36, pp. 487–500, Apr. 1948.

[87] I. E. Telatar, "Capacity of multi-antenna Gaussian channels," *European Trans. Telecommun.*, vol. 10, pp. 585–595, Nov. 1999.

[88] S. Thoen, L. Van der Perre, B. Gyselinckx, and M. Engels, "Performance analysis of combined transmit-SC/receive-MRC," *IEEE Trans. Commun.*, vol. 49, pp. 5–8, Jan. 2001.

[89] Y. Tokgoz and B. D. Rao, "The effect of imperfect channel estimation on the performance of maximum ratio combining in the presence of cochannel interference," *IEEE Trans. Veh. Tech.*, vol. 55, no. 5, pp. 1527–1534, Sep. 2006.

[90] C.-H. Tse, K.-W. Yip, and T.-S. Ng, "Performance tradeoffs between maximum ratio trnsmission and switched-transmit diversity," in *Proc. 2000 IEEE Int. Symp. Personal Indoor Mobile Radio Commun. (PIMRC'00)*, London, UK, vol. 2, pp. 1485–1489.

[91] G. L. Turin, "The characteristic function of Hermitian quadratic forms in complex normal variable," *Biometrika*, vol. 47, pp. 199–201, Jun. 1960.

[92] C. Waldschmidt, S. Schulteis, and W. Wiesbeck, "Complete RF system model for analysis of compact MIMO arrays," *IEEE Trans. Veh. Technol.*, vol. 53, no. 3, pp. 579–586, May 2004.

[93] J. W. Wallace and M. A. Jensen, "Mutual coupling in MIMO wireless systems: a rigorous network theory analysis," *IEEE Trans. Wireless Commun.*, vol. 3, no. 4, pp. 1317–1325, Jul. 2004.

[94] H. Weingarten, Y. Steinberg, and S. Shamai (Shitz), "The capacity region of the Gaussion multiple-input multiple-output broadcast channel," *IEEE Trans. Inf. Theory*, vol. 52, pp. 3936–3964, Sep. 2006.

[95] J. H. Winters, "On the capacity of radio communication systems with diversity in a Rayleigh fading environment," *IEEE J. Sel. Area Commun.*, vol. SAC-5, pp. 871-878, Jun. 1987.

[96] P. W. Wolniansky, G. J. Foschini, G. D. Golden, and R. A. Valenzuela, "V-BLAST: An architecture for realizing very high data rates over the rich-scattering wireless channel," in *Proc. 1998 Int. Symp. Signals, Syst., Electron. (ISSSE'98)*, pp. 295–300.

[97] K.-K. Wong,"Maximizing the sum-rate and minimizing the sum-power of a broadcast 2-user 2-input multiple-output antenna system using a generalized zeroforcing approach," *IEEE Trans. Wireless Commun.*, vol. 5, pp. 3406–3412, Dec. 2006.

[98] P. Xia and G. B. Giannakis, "Design and analysis of transmit-beamforming based

on limited-rate feedback," *IEEE Trans. Signal Process.*, vol. 54, pp. 1853–1863, May 2006.

[99] Z. Xu, S. Sfar, and R. S. Blum, "On the importance of modeling the mutual coupling for antenna selection for closely-spaced arrays," in *Proc. 2006 Conf. Inf. Sci. Syst. (CISS'06)*, Princeton, NJ, pp. 1351–1355.

[100] Y. Yang, R. S. Blum, and Sa. Sfar, "Antenna selection for MIMO systems with closely spaced antennas," *EURASIP J. Wireless Commun. and Netw.*, vol. 2009, 2009.

[101] T. Yoo and A. Goldsmith, "On the optimality of multiantenna broadcast scheduling using zero-forcing beamforming," *IEEE J. Sel. Areas Commun.*, vol. 24, pp. 528–541, Mar. 2006.

[102] T. Yoo and A. Goldsmith, "Capacity and power allocation for fading MIMO channels with channel estimation error," *IEEE Trans. Inf. Theory*, vol. 52, pp. 2203–2214, May 2006

[103] A. Zanella, M. Chiani and M. Win, "Performance of MIMO MRC in correlated Rayleigh fading environments," in *Proc. 2005 IEEE 61st Veh. Tech. Conf. (VTC'05-Spring)*, Stockholm, Sweden, vol. 3, pp. 1633–1637.

[104] Zeland IE3D: MoM-Based EM Simulator. [Online] Available: http://www.zeland.com/ie3d.htm

[105] S. Zhou, Z. Wang, and G. B. Giannakis, "Quantifying the power loss when transmit beamforming relies on finite-rate feedback," *IEEE Trans. Wireless Commun.*, vol. 4, no. 4, pp. 1948–1957 Jul. 2005.

[106] X. Zhou, T. A. Lamahewa, P. Sadeghi, and S. Durrani, "Capacity of MIMO systems: impact of spatial correlation with channel estimation errors," in *Proc. 2008 IEEE Int. Conf. Commun. Syst. (ICCS'08)*, Princeton, NJ, pp. 817–822.